

This item was submitted to Loughborough's Institutional Repository (<https://dspace.lboro.ac.uk/>) by the author and is made available under the following Creative Commons Licence conditions.



CC creative commons
COMMONS DEED

Attribution-NonCommercial-NoDerivs 2.5

You are free:

- to copy, distribute, display, and perform the work

Under the following conditions:

 **Attribution.** You must attribute the work in the manner specified by the author or licensor.

 **Noncommercial.** You may not use this work for commercial purposes.

 **No Derivative Works.** You may not alter, transform, or build upon this work.

- For any reuse or distribution, you must make clear to others the license terms of this work.
- Any of these conditions can be waived if you get permission from the copyright holder.

Your fair use and other rights are in no way affected by the above.

This is a human-readable summary of the [Legal Code \(the full license\)](#).

[Disclaimer](#) 

For the full text of this licence, please go to:
<http://creativecommons.org/licenses/by-nc-nd/2.5/>

Superlattice electrodynamics as a source of Terahertz radiation

P. A. Dakers

A Doctoral Thesis submitted in partial fulfillment of the requirements
for the award of
Doctor of Philosophy
of
Loughborough University

August 2012

©P. A. Dakers 2012

Abstract

Charge-carriers propagating in superlattices exhibit the related phenomena known as negative differential conductivity and Bloch oscillation. This behaviour may be utilised for the generation of tunable electromagnetic radiation. In this work, the dependence of the drift velocity and displacement of charge-carriers on external, applied electric fields is investigated. The theory is extended to incorporate a different miniband structure, with the aim of modelling a superlattice made from graphene. I predict that, for a chosen set of electric field parameters, a semiconductor superlattice will emit radiation in the terahertz range. I create an original mathematical framework within which to calculate the charge-carrier behaviour in a triangular miniband structure, while incorporating an arbitrary variable to account for the effects of corrugation or disorder, and predict the appearance of conductivity multistability. This may be of interest to further work done on the use of graphene for superlattice device construction.

Acknowledgements

I am immensely grateful for the continued support and eternal patience of my supervisor Professor Kusmartsev. Thank you, Feo. Thank you to Dr. Sasha Balanov, for his approachability and constructive comments. To my colleagues and friends in department, thank you, for both fruitful, interesting discussions, and for distraction from the work when it was needed. Thanks in particular to Dr. Rich Wilson, for putting up with my endless questions about LaTeX, amongst other things, and to Satpal “Sunny” Matharu and Paul “Pinky” Holland, for many exchanges of ideas and great conversations about physics. Much love and gratitude to my parents, always only a phone call away, thank you for being so steadfast. To my wonderful girlfriend Yvette, thank you for your support, especially for pushing me when I became lazy!

Most of all, this work is dedicated to Dr. F. A. “Tony” Winzor, truly the finest teacher a person could ask for. Without him, this thesis could never, and would never, have been written.

Contents

1	Superlattice electrodynamics	9
1.1	Band and miniband theory	10
1.1.1	Band Theory in Solid State Physics	10
1.1.2	Superlattices and miniband formation	10
1.2	Miniband structure	13
1.2.1	The tight-binding approximation	13
1.3	Superlattice electrodynamics - static bias	18
1.3.1	Bloch oscillation	18
1.3.2	Emitted radiation	21
1.3.3	Terahertz radiation	22
1.4	Dissipation - Scattering	24
1.4.1	Boltzmann transport equation	24
1.4.1.1	Introduction and background	24
1.4.1.2	Derivation of the Boltzmann transport equation	25
1.4.1.3	Diffusion	26
1.4.1.4	External fields	26
1.4.1.5	Scattering	27
1.4.1.6	Electrical Conductivity	29
1.4.1.7	Fermi surface and distribution function . . .	31
1.4.2	Drift velocity	33

1.4.2.1	Origin of path integral formulation	35
1.4.2.2	Esaki-Tsu result	37
1.4.3	Sawtooth model	39
1.5	Bloch oscillations as sources of radiation, typical values	45
1.6	Non-static electrical bias	46
1.6.1	Single AC field	46
1.6.2	Super Bloch oscillations	49
2	Graphene, a novel material	51
2.1	Introduction, properties of graphene	52
2.1.1	Introduction to graphene	52
2.1.2	The graphene construct	53
2.1.3	Graphene's links to quantum electrodynamics	56
2.1.4	Phenomenon of frequency multiplication in graphene	57
2.1.5	Minimum conductivity and the Klein paradox	58
2.2	Tight-binding model, derivation of linear band structure	60
2.2.1	Basis Vectors and the Reciprocal Lattice	60
2.2.2	Atomic Orbitals	61
2.2.3	Tight-binding calculation	63
2.2.4	Linearity near the Dirac points	68
3	Graphene superlattice	72
3.1	Modelling miniband structure of graphene superlattice	74
3.1.1	Infinite Fourier series	74
3.1.2	Heaviside representation	79
3.1.3	Approximation method	82
4	Suggestions and further work	90
A	Mathematics	93
A.1	Calculation of $\frac{\partial^2 E(k)}{\partial k^2}$ for Fourier series model	94

A.2 Full integration	94
A.2.1 Integrating term 1 using rule (i)	94
A.2.2 Integrating term 2 using rule (ii)	95
A.2.3 Integrating term 4 using rule (iii)	96
A.2.4 Integrating term 5 using rule (iv)	96
A.3 Final calculation of v_d for Heaviside model	97

List of Figures

1.1	Bulk semiconductor superlattice; associated periodic quantum well/barrier structure	12
1.2	Bloch oscillation as a consequence of narrow Brillouin zone . .	20
1.3	Depiction of location of Terahertz region in the electromagnetic spectrum	22
1.4	Response of Fermi sea to external field	32
1.5	Displacement of distribution function at finite temperature due to external field	33
1.6	Esaki-Tsu results for effect of static bias on charge-carrier drift velocity, demonstrating NDV in a semiconductor superlattice	39
1.7	Surface plot demonstrating effect of applied field strength on trajectory in a dissipative system characterised by constant scattering time	43
1.8	Demonstration of dissipative effects inducing transport, and prediction of special cases of localisation	44
1.9	Harmonic driving field	48
1.10	Displacement-time plot demonstrating appearance of Super Bloch oscillations for given AC field strength and frequency .	50
2.1	Graphene substructure of two interlocking, triangular sublattices	54

2.2	Dirac cones evident within graphene's dispersion relation . .	55
2.3	Klein tunneling in graphene via Andreev reflection	60
2.4	Orbital hybridisation in graphene	62
2.5	Tight-binding result of 3D dispersion relation of graphene . .	69
2.6	Top-down surface plot displaying hexagonal reciprocal lattice arrangement of Dirac points	70
3.1	Energy-momentum relation of a superlattice constructed us- ing monolayer graphene	73
3.2	Energy-momentum relation of a superlattice constructed us- ing monolayer graphene	74
3.3	Triangular wave generated by infinite Fourier series	75
3.4	First and second derivatives of linear energy-momentum rela- tion of graphene superlattice	77
3.5	Appearance of infinite conductivity in the limit of totally linear miniband	79
3.6	Approximated band structure and appearance of miniband gap	83
3.7	Effect of interval width on drift velocity - field characteristics .	88
3.8	Appearance of infinite conductivity in the limit of vanishing interval width	89

Chapter 1

Superlattice electrodynamics

1.1 Band and miniband theory

1.1.1 Band Theory in Solid State Physics

Band theory describes the effect of a lattice on electronic energy levels in a bulk or macroscopic system. Instead of having discrete energies, as they would when considered on an individual basis, the available energy states form bands. Consider two identical atoms, with identical energy spectra, being brought closer together. The Coulomb interaction between the two causes the each of the energy levels of both atoms to divide into two narrowly separated levels.

In a bulk system, such as a crystal lattice, the interactions between all N atoms present force the energy spectra of the individual atoms to split into N discrete levels, each very close in energy to its neighbours. For large systems (large N) each of these groups of divided energy levels can be considered continuous (the continuum limit). The components of this new spectrum are known as bands. The lattice periodicity helps determine the nature of the bands.

1.1.2 Superlattices and miniband formation

A novel type of artificial crystal structure was proposed in 1970 by Leo Esaki and Raphael Tsu[1], as a candidate for observation of a new electrodynamic phenomenon. The term "superlattice" is used to describe an array of two, or more, periodically arranged materials to form a new system with different

electronic behaviour.

One-dimensional superlattices have been studied extensively since the veritable explosion of interest in Esaki and Tsu's seminal paper. The most common superlattice systems resemble stacks of two different semiconducting materials, periodic along what is called the "superlattice axis".

It is this layering arrangement that brings about the formation of electron "minibands", and the manner in which they are layered can create different types of superlattice[2]. It is within the mathematical description of these minibands that the electrodynamic transport properties of superlattices may be investigated.

Consider a superlattice constructed using two semiconductor materials, simply denoted 1 and 2 (a typical superlattice may consist of GaAs and $\text{Al}_x\text{Ga}_{1-x}\text{As}$ as materials 1 and 2, respectively). The two materials have different band widths. As a consequence, when arranged in a layered, periodic manner, the chemical potential will vary with location inside the resulting superlattice. This way, it is possible to generate a potential landscape that can be described as a series of quantum wells, separated by barriers, whose height and thickness are characteristic of the semiconductors used to make the superlattice. What a charge carrier now experiences is a new superperiodicity: the effective lattice constant of the superlattice system. This can be much larger than the original lattice constants of either semiconductor, and is simply the sum of the barrier and well widths, which are in turn directly dependent on the layer thicknesses.

Since the lattice period of the superlattice is greater than that of a typical crystal, its Brillouin zones are correspondingly narrower. In this way, it is

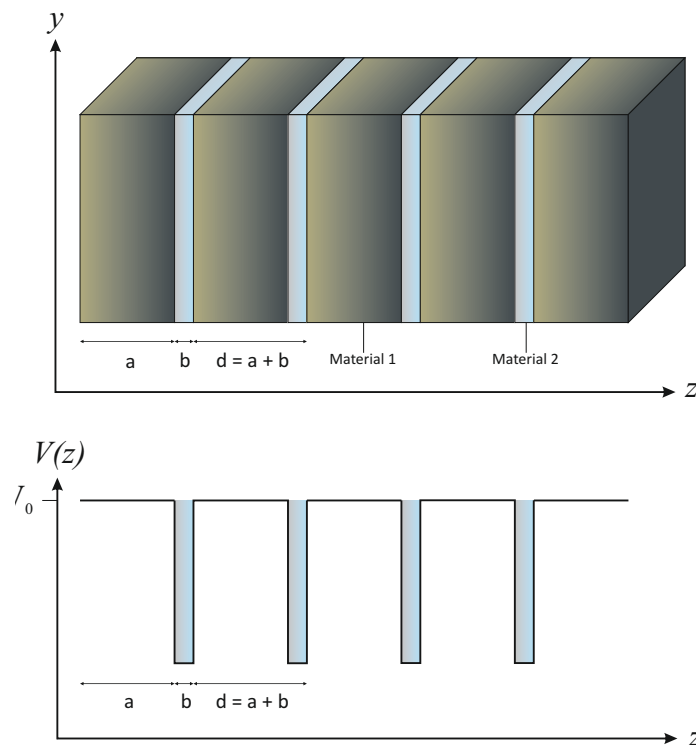


Figure 1.1: Depicted above is a schematic of a bulk, one-dimensional superlattice and its corresponding potential landscape. Note how the variation of chemical potential generates a series of quantum wells separated by thin barriers.

evident how superlattices exhibit novel electronic substructures known as minizones and minibands.

Between respective quantum wells, the wavefunctions of charge-carriers within the superlattice are coupled via the mechanism of quantum tunnelling. The strength of this coupling depends on the height and width of the potential barrier separating the wells. In the limit of very high or very thick barriers, the superlattice can be modelled by considering isolated wavefunctions in each well, with a very small (but finite) probability of interwell tunnelling. However, in the case of stronger coupling, interwell interaction causes the

splitting of energy levels in neighbouring wells into new minibands, in a way similar to band formation as described above. Under conditions that will be elaborated upon later in this work, it is valid to describe the dynamics of the charge-carriers in the superlattice within a quasiclassical framework.

1.2 Miniband structure

1.2.1 The tight-binding approximation

Calculating the band structure of a bulk system is a very important aspect of solid state physics, and it can prove extremely difficult. There exist different methods for doing so analytically, such as the free electron model, the KKR model (also known as the muffin-tin potential), Green's function methods, and the tight-binding approximation. These are all useful, and applicable, in their own ways.

The tight-binding approximation starts building a model of a crystal lattice in the limit of widely spaced atoms with weakly interacting electronic orbitals. This approximation remains valid for atoms with closely bound electrons that have little or no interaction with other atomic potentials. In contrast, the free electron model most accurately describes materials whose orbitals overlap significantly, and whose valence electrons are not bound in an orbital. The free electron model then is a good choice for modelling metals, where interatomic distance is small.

It is straightforward to utilise the tight-binding model for calculation of the

band structure of electrons moving in a periodic potential. This is relevant because it will now be used to derive the miniband structure of a superlattice.

Consider an electron located inside a finite, periodic potential (a crystal lattice). In order to find the energy levels relevant to this system, it is necessary to solve the appropriate Schrödinger equation. The approximation used to formulate the wavefunction of the electron in this crystal is called the tight binding approximation. The wavefunction then is a linear combination of the effect of the potentials from all atoms in the crystal upon the electron, and can be written as[4, 5]:

$$\psi_{\mathbf{k}}(\mathbf{r}) = \sum_j c_{\mathbf{k}j} \phi(\mathbf{r} - \mathbf{r}_j)$$

which is a sum taken over all j atoms in the lattice. The atomic orbitals are denoted by $\phi(\mathbf{r} - \mathbf{r}_j)$, where \mathbf{r}_j is the distance to the lattice point under consideration. It is assumed that there is one lattice site per unit cell. These are Bloch functions, where the coefficients $c_{\mathbf{k}j} = |A|^2 e^{i\mathbf{k}\cdot\mathbf{r}_j}$ denote plane waves, and A is a normalisation constant. This can be proved by considering a translation from one lattice point to another; a vector denoted \mathbf{t} . A Bloch function must be periodic over the whole system, and therefore the wavefunction should be similarly periodic. If there are N atoms in the crystal, then the coefficients are $c_{\mathbf{k}j} = \frac{1}{\sqrt{N}} e^{i\mathbf{k}\cdot\mathbf{r}_j}$ and the wavefunction at the second lattice point is given by

$$\psi_{\mathbf{k}}(\mathbf{r} + \mathbf{t}) = \frac{1}{\sqrt{N}} \sum_j e^{i\mathbf{k}\cdot\mathbf{r}_j} \phi(\mathbf{r} + \mathbf{t} - \mathbf{r}_j)$$

taking the factor $e^{i\mathbf{k}\cdot\mathbf{t}}$ outside the sum allows us to write

$$\psi_{\mathbf{k}}(\mathbf{r} + \mathbf{t}) = \frac{e^{i\mathbf{k}\cdot\mathbf{t}}}{\sqrt{N}} \sum_j e^{i\mathbf{k}\cdot(\mathbf{r}_j - \mathbf{t})} \phi(\mathbf{r} - (\mathbf{r}_j - \mathbf{t})) \quad (1.1)$$

$$= e^{i\mathbf{k}\cdot\mathbf{t}} \psi_{\mathbf{k}}(\mathbf{r}) \quad (1.2)$$

which satisfies the criterion for being a Bloch function. The normalisation condition requires

$$\int |\psi|^2 d^3r = 1$$

which allows us to write

$$\int \psi^* \psi d^3r = |A|^2 \int \sum_m e^{-i\mathbf{k}\cdot\mathbf{r}_m} \phi^*(\mathbf{r} - \mathbf{r}_m) \sum_j e^{i\mathbf{k}\cdot\mathbf{r}_j} \phi(\mathbf{r} - \mathbf{r}_j) d^3r \quad (1.3)$$

$$= |A|^2 \int \sum_m \sum_j e^{i\mathbf{k}\cdot(\mathbf{r}_j - \mathbf{r}_m)} \phi^*(\mathbf{r} - \mathbf{r}_m) \phi(\mathbf{r} - \mathbf{r}_j) d^3r \quad (1.4)$$

where m is an index denoting the destination lattice site after translation by the vector \mathbf{t} . The above integral is true if $j = m$. Replacing all m with j , we calculate the probability of finding the electron at any particular lattice site j in a system of N lattice sites to be

$$P = \sum_j \int \phi^* \phi d^3r = \frac{1}{N}$$

We can now write the atomic wavefunctions fully:

$$\psi_{\mathbf{k}}(\mathbf{r}) = \frac{1}{\sqrt{N}} \sum_j e^{i\mathbf{k}\cdot\mathbf{r}_j} \phi(\mathbf{r} - \mathbf{r}_j)$$

The next stage involves using the variational method to calculate the lowest energy eigenstate of the electron. We know that

$$E_{\mathbf{k}} = \langle \psi_{\mathbf{k}} | \hat{H} | \psi_{\mathbf{k}} \rangle \quad (1.5)$$

$$\psi = \sum_{\mathbf{k}} c_{\mathbf{k}j} \phi \quad (1.6)$$

The variational principle states that the ground state energy, E_0 , is always less than or equal to the expectation value of the Hamiltonian \hat{H} calculated with any trial wavefunction. The expectation value of \hat{H} using a trial wavefunction ψ_{tr} is

$$\langle \psi_{tr} | \hat{H} | \psi_{tr} \rangle = \frac{\int \psi_{tr}^* \hat{H} \psi_{tr} dt}{\int \psi_{tr}^* \psi_{tr} dt} \quad (1.7)$$

Since the eigenfunctions of the Hamiltonian form a complete basis, the trial wavefunction can be expressed as a linear combination of these eigenfunctions:

$$\psi_{tr} = \sum_n c_n \psi_n$$

where

$$\sum_n |c_n|^2 = 1$$

Remembering that the true eigenfunctions ψ_n are orthogonal and normalised, it follows that the trial wavefunctions ψ_{tr} are also. This implies that the denominator in equation (1.7) is equal to unity. Let us now calculate the expectation value of the Hamiltonian:

$$\langle \psi_{tr} | \hat{H} | \psi_{tr} \rangle = \int \left(\sum_n c_n^* \psi_n^* \right) \hat{H} \left(\sum_m c_m \psi_m \right) dt \quad (1.8)$$

$$= \sum_{n,m} c_n^* c_m \int \psi_n^* \hat{H} \psi_m dt \quad (1.9)$$

$$= \sum_{n,m} c_n^* c_m E_m \delta_{nm} = \sum_n |c_n|^2 E_n \quad (1.10)$$

and since $E_n \geq E_0$ for all n , $\langle \psi_{tr} | \hat{H} | \psi_{tr} \rangle \geq E_0$. Therefore, using the variational principle, we can calculate $E_{\mathbf{k}}$ as follows:

$$E_{\mathbf{k}} = \langle \psi_{\mathbf{k}} | \hat{H} | \psi_{\mathbf{k}} \rangle \quad (1.11)$$

$$= \int \frac{1}{\sqrt{N}} \sum_m e^{-i\mathbf{k} \cdot \mathbf{r}_m} \phi^*(\mathbf{r} - \mathbf{r}_m) \hat{H} \frac{1}{\sqrt{N}} \sum_j e^{i\mathbf{k} \cdot \mathbf{r}_j} \phi(\mathbf{r} - \mathbf{r}_j) d^3r \quad (1.12)$$

Using a substitution $\mathbf{a}_m = \mathbf{r}_m - \mathbf{r}$, the above can be rewritten:

$$E_{\mathbf{k}} = \frac{1}{N} \sum_{m,j} e^{i\mathbf{k} \cdot (\mathbf{r}_j - \mathbf{r}_m)} \int \phi^*(\mathbf{r} - \mathbf{r}_m + \mathbf{r}_j) \hat{H} \phi(\mathbf{r} - \mathbf{r}_m + \mathbf{r}_j) d^3r \quad (1.13)$$

$$= \frac{1}{N} \sum_m e^{-i\mathbf{k} \cdot \mathbf{a}_m} \int \phi^*(\mathbf{r} - \mathbf{a}_m) \hat{H} \phi(\mathbf{r}) d^3r. \quad (1.14)$$

Now we neglect all integrals higher than first order (i.e. $m > 1$) and consider only nearest neighbours. The two remaining integrals are

$$\begin{aligned} -\alpha &= \int \phi^*(\mathbf{r}) \hat{H} \phi(\mathbf{r}) d^3r \\ -\gamma &= \int \phi^*(\mathbf{r}) \hat{H} \phi(\mathbf{r}) d^3r \end{aligned} \quad (1.15)$$

It is now possible to write the following:

$$\langle \psi_{\mathbf{k}} | \hat{H} | \psi_{\mathbf{k}} \rangle = E_{\mathbf{k}} = -\alpha - \gamma \sum_m e^{-i\mathbf{k} \cdot \mathbf{a}_m}$$

where γ is the overlap energy and \mathbf{a} is the interatomic distance. For a simple cubic lattice, the vector describing the displacement of the six nearest neighbours from a lattice point situated at the origin is:

$$\rho = (\pm a, 0, 0); (0, \pm a, 0); (0, 0, \pm a)$$

substituting this into the above result for the energy eigenstates we get

$$E_{\mathbf{k}} = -\alpha - \gamma(\cos(k_x a) + \cos(-k_x a) + \cos(k_y a) + \cos(-k_y a)) \quad (1.16)$$

$$\begin{aligned} &+ \cos(k_z a) + \cos(-k_z a)) \\ &= -\alpha - 2\gamma(\cos k_x a + \cos k_y a + \cos k_z a) \end{aligned} \quad (1.17)$$

Since $-1 \leq \cos ka \leq 1$, then the range of values that the energy can take is $-\alpha - 6\gamma \geq E_{\mathbf{k}} \geq -\alpha + 6\gamma$. As a result, we can say that the energy value is confined within a band, of "width" 12γ . It is very important to note that this tells us that the weaker the overlap energy, the narrower the band. For $|ka| \ll 1$, equation (1.17) can be Taylor expanded to second order:

$$E_{\mathbf{k}} \approx -\alpha - 6\gamma + \gamma k^2 a^2$$

and the effective mass of the quasiparticle moving through the band can be calculated using $\frac{1}{m_*} = \frac{1}{\hbar^2} \frac{\partial^2 E(\mathbf{k})}{\partial \mathbf{k}^2}$ giving

$$m_* = \frac{\hbar^2}{2\gamma a^2}$$

This implies that the lower the overlap energy, the greater the effective mass of the quasiparticle. Let us consider the one dimensional case, along the z -axis. The energy-momentum relation along this axis is given by $E_{\mathbf{k}} = -\alpha - 2\gamma \cos k_z a$, and its extrema are

$$E_{\mathbf{k}} = \begin{cases} -\alpha + 2\gamma \\ -\alpha - 2\gamma \end{cases}$$

which implies a band width of 4γ . Let us define the amplitude of the sinusoidal band to be $\frac{\Delta}{2} = \frac{4\gamma}{2} = 2\gamma$ which is half of the band width Δ . For simplicity, let us redefine the reference point of $E_{\mathbf{k}}$ in the following way:

$$E_{\mathbf{k}} - \alpha = 2\gamma(1 - \cos k_z a) = \epsilon_{\mathbf{k}}$$

where

$$\epsilon_{\mathbf{k}} = 2\gamma(1 - \cos k_z a) \quad (1.18)$$

$$= \frac{\Delta}{2}(1 - \cos k_z a) \quad (1.19)$$

This derivation can be directly applied to a charge-carrier moving through the periodic potential that constitutes a superlattice system. Under the constraints that the miniband transport framework requires for validity, it is trivial to replace the interatomic distance a with the effective period of the superlattice d ; and the band width Δ with Δ_{SL} , the miniband width, yielding the energy $E(k)$ of a charge-carrier with quasimomentum k in a superlattice miniband

$$E(k) = \frac{\Delta_{SL}}{2}(1 - \cos kd). \quad (1.20)$$

The Boltzmann transport approach is used in a recent paper[6] to analyse transient electron behaviour in a semiconductor superlattice.

1.3 Superlattice electrodynamics - static bias

1.3.1 Bloch oscillation

Knowing that the energy spectrum of an electron in the lowest miniband of a semiconductor superlattice is given by $E(k) = \frac{\Delta}{2}(1 - \cos kd)$ (omitting the

SL subscript for simplicity); under an applied electric field $\mathbf{F} = F_0\mathbf{z}$, where the superlattice axis is parallel to \mathbf{z} , we solve Newton's equation $\frac{dk}{dt} = \frac{eF_0}{\hbar}$ to find the quasimomentum $k(t)$ as a function of time. We get $k(t) = \frac{eF_0t}{\hbar}$, which, after using the kinetic equation $\frac{1}{\hbar} \frac{dE}{dk} = v_g(t)$ to calculate the group velocity, we know the group velocity as a function of time:

$$v_g(t) = \frac{\Delta d}{2\hbar} \sin \frac{eF_0d}{\hbar} t.$$

This allows the calculation of the displacement of the electron in real space, by integrating the group velocity with respect to time to get

$$x(t) = -\frac{\Delta}{2eF_0} \cos w_b t.$$

This equation describes an electron oscillating in space with the frequency known as the Bloch frequency, given by $w_b = \frac{eF_0d}{\hbar}$ (see Figure 1.2 for illustration). It is important to note that the Bloch frequency is directly proportional to both the magnitude of the electric field F_0 applied to the superlattice, and the superlattice's effective period d ; while the amplitude of the motion is inversely proportional to the size of the electric field. From this, it follows that increasing the electric field strength will lead to stricter electron confinement, as the amplitude will tend to zero with increasing F_0 . At (a) in Figure 1.2, time $t = 0$, the particle has zero momentum and energy as the external electric field is "switched on". After undergoing acceleration due to the electric field, the particle reaches its top speed at the inflection point (b). From here the particle begins to decelerate until it reaches zero velocity at point (c). As the particle is forced to remain in this miniband, the only way to gain momentum is to continue propagating along the miniband. As a result, its velocity changes sign and the particle begins moving backward in space, equivalently "appearing" at point (d) using the reduced zone scheme description of the miniband structure. It is important to note that the electric field in this case is static, and that either the system is assumed dissipationless or that the scattering time is greater than the period of Bloch oscillation.

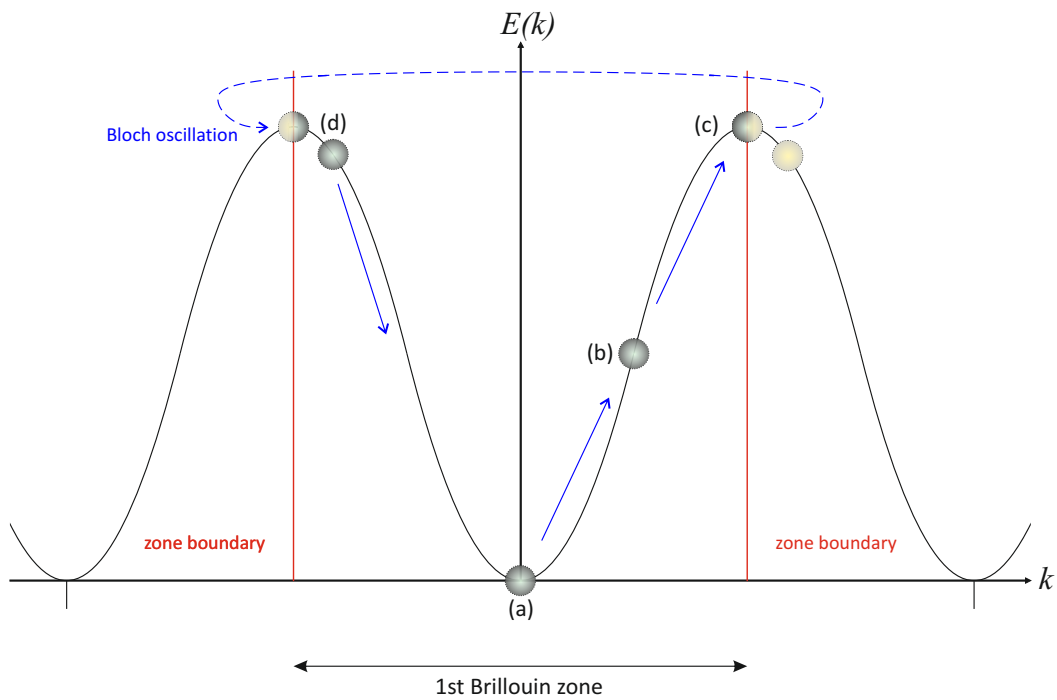


Figure 1.2: A charge-carrier undergoes Bloch oscillation in the first miniband. The group velocity of the charge-carrier is directly proportional to the gradient of its energy-momentum relation for a given value of quasimomentum.

Bloch oscillation is a quantum mechanical effect, and it appears to constitute something similar to a Bragg scattering event at the edge of the Brillouin zone. Later, we will examine the energy landscape under more complex fields.

In such basic terms, scattering processes have not been taken into account: this derivation is only valid for an effectively dissipationless system. This can be rectified when investigating transport properties under such frameworks as the balance equation approach[7, 8], or by the probabilistic approach used by Esaki and Tsu. The latter approach will be explored in greater detail and used as the basis of calculation of drift velocity throughout this thesis.

1.3.2 Emitted radiation

Inducing Bloch oscillations in a superlattice is a way of using an applied field to generate radiation of frequency $\omega_{emit} = \omega_b$, the power of which can be calculated using the Larmor formula

$$P(t) = \frac{e^2}{6\pi\epsilon c^3} \left(\frac{dv_g(t)}{dt} \right)^2,$$

where $v_g(t)$ is the time-dependent group (or instantaneous) velocity of an oscillating charge.

$$\left(\frac{dv_g(t)}{dt} \right)^2 = \left(\frac{d \left(v_0 \sin \frac{eF_0 d}{\hbar} t \right)}{dt} \right)^2 = (v_0 \omega_b \cos \omega_b t)^2,$$

where $v_0 = \frac{\Delta d}{2\hbar}$. Therefore the instantaneous power of emitted radiation is

$$P(t) = \frac{e^2}{6\pi\epsilon c^3} \left(\frac{\Delta d}{2\hbar} \right)^2 \omega_b^2 \cos^2 \omega_b t,$$

where $\omega_b = eF_0 d / \hbar$. This predicts that the power of emitted radiation from a superlattice, whose charge-carriers are undergoing Bloch oscillation due to an applied static bias, is proportional to the strength of the applied field squared. It is worth noting that the power is similarly proportional to the miniband width and superlattice period. Let us calculate the average power emitted from the superlattice:

$$P_{av} = \frac{1}{T} \int_0^T P(t) dt = A \frac{1}{T} \int_0^T \cos^2 \omega_b t dt \quad (1.21)$$

$$= \frac{A}{T} \left(\frac{2\omega_b T + \sin 2\omega_b T}{4\omega_b} \right) \quad (1.22)$$

where

$$A = \frac{e^2}{6\pi\epsilon c^3} \left(\frac{\Delta d}{2\hbar} \right)^2 \omega_b^2$$

for simplicity. Averaging over one period $T = 2\pi/\omega_b$, the average power is given by:

$$P_{av} = \frac{A}{2} = \frac{e^2}{12\pi\epsilon c^3} \left(\frac{\Delta d}{2\hbar} \right)^2 \omega_b^2$$

For a superlattice primarily constructed from GaAs, typical values are $\Delta \approx 0.03\text{eV}$ and $d \approx 100\text{\AA}$. For a Bloch frequency $\omega_b \sim 10\text{THz}$ the average radiation power is $P_{av} \sim 1\text{eVs}^{-1}$. This is in agreement with extrapolation of experimental results in [3].

1.3.3 Terahertz radiation

There exists in the electromagnetic spectrum a region, between the far infrared and microwave regions. The range of this "gap" roughly spans the orders 11 to 14, or 0.1 to 100 terahertz. Up until recently, interest in this region of the spectrum has been stunted by the difficulty in finding methods to generate and detect such frequencies of useful amplitude.

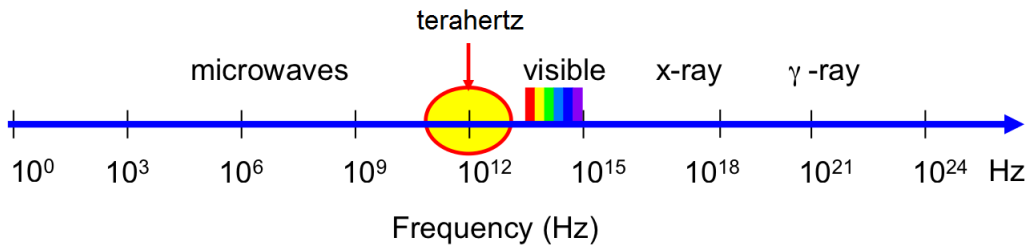


Figure 1.3: Approximate region of the electromagnetic spectrum that constitutes the "terahertz gap".

Terahertz radiation is non-ionising. It can pass through such materials as clothes, brickwork, paper and cardboard, ceramics, plastics and wood. It is being investigated for its use in quality assurance, with such scope of application that it includes detecting engineering flaws in space shuttle compo-

nents. Terahertz body scanners are currently being used in airports worldwide as a major part of the security infrastructure, as they prove adept at detecting explosives or otherwise dangerous chemicals, plastic firearms, ceramics knives, and other weaponry[15]. The frequency of terahertz radiation matches with biomolecular vibrations. Coupled with their ability to penetrate several millimetres into skin tissue and lack of ionising-related damage, terahertz waves may prove invaluable in a broad medical context, for such things as detection of skin cancer, and imaging and cavity detection in dentistry. Other uses include submillimetre astronomical research interests, high-altitude telecommunications, manufacture process monitoring, and many aspects of spectroscopy[16].

Research interest[9, 10] in this so called "terahertz gap" has been reinvigorated, in part, by advances in branches of physics and electronics, since two candidates in particular have been found for possible use for terahertz emission and detection - arrays of Josephson junctions[11, 12], and semiconductor superlattices[13, 14]. Recent advancements include the production of a chip capable of transmitting 1.5 gigabits per second[17], and a publication[18] by researchers from the Tokyo IoT claiming a new record had been set for wireless data transmission using terahertz waves, proposing their use as a new bandwidth for communications.

Bloch oscillations, whereby a charge-carrier spatially oscillates due to quantum mechanical confinement as described earlier, can occur in superlattices. Since any accelerating charge will radiate electromagnetic waves, the power of which is given by the nonrelativistic Larmor formula. It follows that if it is possible to tune the Bloch oscillations taking place in any way, this will translate to tunability of the emitted radiation.

This presumption forms the basis of this research. I will examine how applying electrical fields to superlattice systems can facilitate tunability of electromagnetic radiation, with possible application to emission of terahertz radiation.

1.4 Dissipation - Scattering

So far we have dealt only with situations in which the electrons have not interacted with their environment; there has been no dissipation of energy. In reality, electrical systems are not dissipationless. They lose energy through a process known as scattering, whereby the charge-carriers moving through the system collide or interact with the atoms constituting the material. In this way, the charge-carriers' group velocities will change as they undergo scattering events. Scattering can be accounted for and included in the following approaches[4].

1.4.1 Boltzmann transport equation

1.4.1.1 Introduction and background

Under equilibrium conditions, (fermionic) charge carriers in a material are distributed in energy and momenta, probabilistically weighted and governed by the well known Fermi-Dirac distribution function:

$$f_{\mathbf{k}}^0 = \frac{1}{e^{\frac{\epsilon_{\mathbf{k}} - \mu}{k_B T}} + 1} \quad (1.23)$$

where $\epsilon_{\mathbf{k}}$ is the energy of a particle with momentum \mathbf{k} , μ is the chemical potential, k_B is Boltzmann's constant and T is the temperature. In order to study transport properties of materials, this concept needs to be extended to non-equilibrium situations.

The behaviour of charge carriers present in a material is affected by applying external fields or temperature gradients. Such situations are studied in non-equilibrium statistical mechanics, and in order to be studied with rigour, a transport equation needs to be set up which takes into account the statistical distribution of each particle. Specifically, the situations to be studied are ones in which particles are accelerated by external influences and undergo scattering processes, during which they lose or transfer their acquired energy. An equation which considers all of these conditions can be set up, and is called the Boltzmann transport equation. It can be used to derive such transport properties as thermal, electrical, and Hall conductivity.

1.4.1.2 Derivation of the Boltzmann transport equation

Let us define a quantity, or distribution, $f_{\mathbf{k}}(\mathbf{r})$, which details the local density of charge carriers with momentum \mathbf{k} in the region \mathbf{r} . Firstly, we assume that we are dealing with a set of non-interacting particles. This means we can use the single particle distribution function with no approximations. We must assume that $f_{\mathbf{k}}(\mathbf{r})$ varies with time, in three fundamental ways.

1.4.1.3 Diffusion

Charge carriers enter and exit region \mathbf{r} . If $v_{\mathbf{k}}$ is the group velocity of a charge carrier with momentum \mathbf{k} , then in a time interval t it will travel a distance $\mathbf{v}_{\mathbf{k}}t$. Since the particles in the material are governed by Hamiltonian dynamics, Liouville's theorem (the phase space distribution function is constant along trajectories of the system, that is, the density of points in vicinity of an arbitrary point travelling in phase space is time independent) applies, and we can say that the number of charge carriers in the vicinity of \mathbf{r} at time t is equal to the number of charge carriers in vicinity of $\mathbf{r} - \mathbf{v}_{\mathbf{k}}t$ at time $t = 0$:

$$f_{\mathbf{k}}(\mathbf{r}, t) = f_{\mathbf{k}}(\mathbf{r} - \mathbf{v}_{\mathbf{k}}t, 0) \quad (1.24)$$

This means that the rate of change of the distribution due to diffusion is

$$\left. \frac{\partial f_{\mathbf{k}}}{\partial t} \right|_{\text{diff}} = -\mathbf{v}_{\mathbf{k}} \frac{\partial f_{\mathbf{k}}}{\partial \mathbf{r}} = -\mathbf{v}_{\mathbf{k}} \cdot \nabla f_{\mathbf{k}} \quad (1.25)$$

1.4.1.4 External fields

External, or applied, fields will change the momenta of charge carriers at a rate given by the equation of motion

$$\frac{\partial \mathbf{k}}{\partial t} = \frac{e}{\hbar} \left(\mathbf{E} + \frac{1}{c} \mathbf{v}_{\mathbf{k}} \times \mathbf{H} \right). \quad (1.26)$$

We can look at this as the velocity of the charge carrier in k space, so via analogy with equation (1.24)

$$f_{\mathbf{k}}(\mathbf{r}, t) = f_{\mathbf{k} - t \frac{\partial \mathbf{k}}{\partial t}}(\mathbf{r}, t) \quad (1.27)$$

therefore the applied fields change the distribution at the rate

$$\left. \frac{\partial f_{\mathbf{k}}}{\partial t} \right|_{\text{fields}} = -\frac{\partial \mathbf{k}}{\partial t} \frac{\partial f_{\mathbf{k}}}{\partial \mathbf{k}} = -\frac{e}{\hbar} \left(\mathbf{E} + \frac{1}{c} \mathbf{v}_{\mathbf{k}} \times \mathbf{H} \right) \frac{\partial f_{\mathbf{k}}}{\partial \mathbf{k}} \quad (1.28)$$

1.4.1.5 Scattering

For the purposes of this derivation we will consider only the effects of the simplest type of scattering process, elastic scattering. If a particle scatters elastically, its kinetic energy is conserved, only its direction of motion is altered. The rate of change of the distribution given the occurrence of this scattering is given by

$$\left. \frac{\partial f_{\mathbf{k}}}{\partial t} \right|_{coll} = \int \{f_{\mathbf{k}'}(1 - f_{\mathbf{k}}) - f_{\mathbf{k}}(1 - f_{\mathbf{k}'})\} Q(\mathbf{k}, \mathbf{k}') d\mathbf{k}' \quad (1.29)$$

That is, if the momentum of a particle undergoing a collision changes from \mathbf{k} to \mathbf{k}' , the distribution function will decrease. The likelihood of this happening depends on the function $f_{\mathbf{k}}$ itself, on the momentum of the incident charge carrier \mathbf{k} , and on the quantity $(1 - f_{\mathbf{k}'})$, which is a measure of the number of available momentum states \mathbf{k}' the charge carrier can occupy after the collision. The opposite of this process is also a possibility, weighted as $f_{\mathbf{k}'}(1 - f_{\mathbf{k}})$. This needs to be taken into account, as the next step is to sum over all possible final momenta \mathbf{k}' . The quantity $Q(\mathbf{k}, \mathbf{k}')$ destroys the symmetry of these two possibilities by labelling all possible collision situations with a transition probability which depends on the initial and final momenta of any given scattering process. Q then quantifies the rate of transition from an initial momentum \mathbf{k} to a final momentum \mathbf{k}' given that before the collision, \mathbf{k} was occupied and \mathbf{k}' was an available momentum state. Furthermore, Q becomes a common factor in the integrand above as a consequence of a concept directly linked to the principle of the conservation of energy, known as microscopic reversibility, which is a symmetry of this type of electromechanical process.

The Boltzmann transport equation tells us that for a charge carrier located at a given point \mathbf{r} in the system and in any momentum state \mathbf{k} , the net rate of

change of the distribution is zero. That is

$$\left. \frac{\partial f_{\mathbf{k}}}{\partial t} \right|_{\text{diff}} + \left. \frac{\partial f_{\mathbf{k}}}{\partial t} \right|_{\text{fields}} + \left. \frac{\partial f_{\mathbf{k}}}{\partial t} \right|_{\text{coll}} = 0 \quad (1.30)$$

it is important to note that this equation describes a steady state, not an equilibrium state. We label the equilibrium distribution function $f_{\mathbf{k}}^0$, which we recognise as the Fermi-Dirac distribution function. This function holds when the external fields and temperature gradients are not applied to the system. The next assumption to make is that the steady state distribution function does not deviate far from the equilibrium distribution. This allows us to define a distribution $g_{\mathbf{k}}$ such that

$$g_{\mathbf{k}} = f_{\mathbf{k}}(\mathbf{r}) - f_{\mathbf{k}}^0 \quad (1.31)$$

We now need to consider the effects of temperature variance through the system. Assuming the value of the temperature is well defined at all points, we can write

$$g_{\mathbf{k}} = f_{\mathbf{k}}(\mathbf{r}) - f_{\mathbf{k}}^0\{T(\mathbf{r})\} \quad (1.32)$$

We can also state that, since we might expect that across the entire range of possible occupied momentum states \mathbf{k} , the sum of all the differences between the steady state distribution and the equilibrium distribution at each \mathbf{k} is zero, we can write

$$\int d\mathbf{k}(f_{\mathbf{k}}(\mathbf{r}) - f_{\mathbf{k}}^0) = \int d\mathbf{k}g_{\mathbf{k}} = 0 \quad (1.33)$$

Now since we have defined $g_{\mathbf{k}}$ in equation (1.31), we can substitute it along with equations (1.24) and (1.27) into equation (1.30) to rewrite the Boltzmann transport equation as the following

$$-\mathbf{v}_{\mathbf{k}} \frac{\partial f_{\mathbf{k}}}{\partial \mathbf{r}} - \frac{e}{\hbar} (\mathbf{E} + \frac{1}{c} \mathbf{v}_{\mathbf{k}} \times \mathbf{H}) \frac{\partial f_{\mathbf{k}}}{\partial \mathbf{k}} = - \left. \frac{\partial f_{\mathbf{k}}}{\partial t} \right|_{\text{coll}} \quad (1.34)$$

Recalling that $f_{\mathbf{k}} = g_{\mathbf{k}} + f_{\mathbf{k}}^0$, this becomes

$$-\mathbf{v}_{\mathbf{k}} \frac{\partial f_{\mathbf{k}}^0}{\partial T} \nabla T - \frac{e}{\hbar} (\mathbf{E} + \frac{1}{c} \mathbf{v}_{\mathbf{k}} \times \mathbf{H}) \frac{\partial f_{\mathbf{k}}^0}{\partial \mathbf{k}} \quad (1.35)$$

$$= - \left. \frac{\partial f_{\mathbf{k}}}{\partial t} \right|_{\text{coll}} + \mathbf{v}_{\mathbf{k}} \nabla g_{\mathbf{k}} + \frac{e}{\hbar} (\mathbf{E} + \frac{1}{c} \mathbf{v}_{\mathbf{k}} \times \mathbf{H}) \frac{\partial g_{\mathbf{k}}}{\partial \mathbf{k}} \quad (1.36)$$

The group velocity of a charge carrier with energy momentum relation $\epsilon(\mathbf{k})$, via the kinematic principle, is given by

$$\mathbf{v}_{\mathbf{k}} = \frac{1}{\hbar} \frac{\partial \epsilon}{\partial \mathbf{k}} \quad (1.37)$$

where $f_{\mathbf{k}}^0$ denotes the Fermi-Dirac distribution function, therefore the transport equation becomes

$$-\frac{\partial f_{\mathbf{k}}^0}{\partial \epsilon} \mathbf{v}_{\mathbf{k}} \cdot \left\{ \frac{\epsilon(\mathbf{k}) - \mu}{T} \nabla T + e(\mathbf{E} - \frac{1}{e} \nabla \mu) \right\} \quad (1.38)$$

$$= -\frac{\partial f_{\mathbf{k}}}{\partial t} \Big|_{\text{coll}} + \mathbf{v}_{\mathbf{k}} \cdot \nabla g_{\mathbf{k}} + \frac{e}{\hbar c} (\mathbf{v}_{\mathbf{k}} \times \mathbf{H}) \cdot \frac{\partial g_{\mathbf{k}}}{\partial \mathbf{k}} \quad (1.39)$$

where the term $\mathbf{E} \cdot \frac{\partial g_{\mathbf{k}}}{\partial \mathbf{k}}$ has been taken to be zero due to it being proportional to E^2 , causing a deviation from Ohm's law; and the term $\mathbf{v}_{\mathbf{k}} \cdot \mathbf{v}_{\mathbf{k}} \times \mathbf{H} \equiv 0$ disappears identically to zero. This equation is known as the "linearised Boltzmann transport equation", and will be used to calculate the electrical conductivity of a given system under certain circumstances.

1.4.1.6 Electrical Conductivity

In a system whose boundaries extend to infinity in space, in the absence of an applied temperature gradient or magnetic field, equation (1.39) becomes

$$-\frac{\partial f_{\mathbf{k}}^0}{\partial \epsilon} \mathbf{v}_{\mathbf{k}} \cdot e\mathbf{E} = -\frac{\partial f_{\mathbf{k}}}{\partial t} \Big|_{\text{coll}} \quad (1.40)$$

which, by equation (1.29), gives us the following integral equation for $g_{\mathbf{k}}$

$$\begin{aligned} -\frac{\partial f_{\mathbf{k}}^0}{\partial \epsilon} \mathbf{v}_{\mathbf{k}} \cdot e\mathbf{E} &= \int (f_{\mathbf{k}} - f_{\mathbf{k}'}) Q(\mathbf{k}, \mathbf{k}') d\mathbf{k}' \\ &= \int (g_{\mathbf{k}} - g_{\mathbf{k}'}) Q(\mathbf{k}, \mathbf{k}') d\mathbf{k}' \end{aligned} \quad (1.41)$$

Phenomenologically, we can write

$$-\frac{\partial f_{\mathbf{k}}}{\partial t} \Big|_{\text{coll}} = \frac{1}{\tau} g_{\mathbf{k}} \quad (1.42)$$

This is known as the relaxation time approximation. This makes the assumption that the electron distribution after a scattering process occurs does not depend on the non-equilibrium distribution beforehand, and that these collisions do not affect the form of the equilibrium distribution function (in this case, the Fermi-Dirac distribution function). In other words, collisions seek to return the system to its equilibrium configuration. It is assumed that the rate of change of $f_{\mathbf{k}}$ is proportional to the degree that it differs from $f_{\mathbf{k}}^0$. Furthermore, as one might expect, in the absence of an applied electric field \mathbf{E} , $g_{\mathbf{k}}$ would decay to zero as

$$g_{\mathbf{k}}(t) = g_0 e^{-\frac{t}{\tau}} \quad (1.43)$$

Substituting equation (1.42) into (1.40) gives

$$g_{\mathbf{k}} = -\frac{\partial f_{\mathbf{k}}^0}{\partial \epsilon} \tau \mathbf{v}_{\mathbf{k}} e \mathbf{E} \quad (1.44)$$

The next step in calculating the conductivity is to evaluate the current density \mathbf{J} where

$$\mathbf{J} = \int e \mathbf{v}_{\mathbf{k}} f_{\mathbf{k}} d\mathbf{k} = \int e \mathbf{v}_{\mathbf{k}} g_{\mathbf{k}} d\mathbf{k} \quad (1.45)$$

since the integral of $f_{\mathbf{k}}^0 \equiv 0$ (because it is safe to assume that no current flows when the applied field is zero). To transform this integral over a volume of k space into an integral over surfaces of constant energy ϵ , we can use the following formula

$$\int d\mathbf{k} = \frac{1}{4\pi^3} \int d\epsilon \int \frac{1}{\frac{\partial \epsilon}{\partial \mathbf{k}}} dS = \frac{1}{4\pi^3} \int d\epsilon \int \frac{1}{\hbar \mathbf{v}_{\mathbf{k}}} dS \quad (1.46)$$

Current density can now be expressed as

$$\mathbf{J} = \frac{e^2 \tau}{4\pi^3 \hbar} \iint \mathbf{v}_{\mathbf{k}} (\mathbf{v}_{\mathbf{k}} \cdot \mathbf{E}) \left(\frac{\partial f_{\mathbf{k}}^0}{\partial \epsilon} \right) \frac{\partial S}{|\mathbf{v}_{\mathbf{k}}|} d\epsilon \quad (1.47)$$

According to Fermi-Dirac statistics, in a metal, the distribution behaves like a delta function at the Fermi level (the Fermi-Dirac distribution function tends toward a step function centered at the chemical potential, whose negative

gradient therefore tends toward a delta peak). This allows simplification of equation (1.47), since

$$\int -\frac{\partial f_{\mathbf{k}}^0}{\partial \epsilon} d\epsilon \equiv 1 \quad (1.48)$$

the current density becomes

$$\mathbf{J} = \left\{ \frac{e^2 \tau}{4\pi^3 \hbar} \int \frac{\mathbf{v}_{\mathbf{k}} \cdot \mathbf{v}_{\mathbf{k}}}{|\mathbf{v}_{\mathbf{k}}|} dS_F \right\} \cdot \mathbf{E} \quad (1.49)$$

where the term in brackets is the conductivity tensor σ , requiring us to write it in explicit dyadic notation:

$$\sigma = \frac{e^2 \tau}{4\pi^3 \hbar} \int \frac{\mathbf{v}_{\mathbf{k}} \cdot \mathbf{v}_{\mathbf{k}}}{|\mathbf{v}_{\mathbf{k}}|} dS_F. \quad (1.50)$$

If the electrical response to the applied field is parallel to the field, then $\mathbf{v}_{\mathbf{k}} \cdot \mathbf{E} = v_k E$ and the conductivity is now

$$\sigma = \frac{e^2 \tau}{4\pi^3 \hbar} \frac{1}{3} \int v dS_F \quad (1.51)$$

$$\sigma = \frac{e^2}{4\pi^3 \hbar} \frac{1}{3} \int \lambda dS_F \quad (1.52)$$

where $\lambda = v\tau$ is the mean free path of a charge carrier with total velocity v . The factor of $1/3$ comes from the fact that we have only taken into account the velocity contribution along one of the three axes.

1.4.1.7 Fermi surface and distribution function

It can be seen from the kinematic equation $\dot{\mathbf{k}} = -e\hbar^{-1}\mathbf{E}$ that at the moment that the electric field is applied, all the electrons in the Fermi sea are accelerated and gain momentum equal to $e\tau\hbar^{-1}\mathbf{E}$ before they undergo any scattering process. From equation (1.44), we can write

$$f_{\mathbf{k}} = f_{\mathbf{k}}^0 - \frac{\partial f_{\mathbf{k}}^0}{\partial \epsilon} e\tau \mathbf{v}_{\mathbf{k}} \cdot \mathbf{E} = f_{\mathbf{k}}^0 - \frac{\partial f_{\mathbf{k}}^0}{\partial \epsilon} \frac{\partial \epsilon}{\partial \mathbf{k}} \frac{e\tau}{\hbar} \cdot \mathbf{E} \quad (1.53)$$

Applying Taylor's theorem, this becomes

$$f_{\mathbf{k}} = f^0\left(\mathbf{k} - \frac{e\tau}{\hbar}\mathbf{E}\right) \quad (1.54)$$

This equation describes how the entire Fermi surface is displaced by $e\tau\hbar^{-1}\mathbf{E}$ in momentum space. These principles are shown diagrammatically in Figures 1.4 and 1.5.

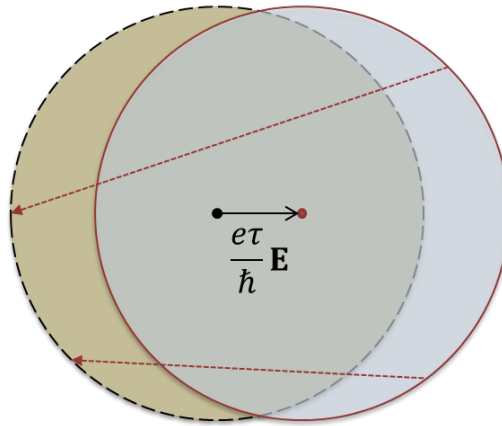


Figure 1.4: Fermi sea of electrons moving in response to the applied electric field \mathbf{E} . This figure is slightly misleading should we forget that the electrons deeper within this sphere, i.e. nearer the bottom of the band, are prevented by Pauli's exclusion principle from being excited by the field or from undergoing scattering processes to lower their energy. In reality, only the electrons nearer the leading edge of the Fermi surface can be scattered, and are scattered to other points on the surface. This is the mechanism by which the Fermi distribution $f_{\mathbf{k}}$ is restored to the equilibrium distribution.

The Boltzmann transport equation allows study of the electrical transport properties of an ensemble of charge-carriers, distributed in momenta and energy via temperature. It makes use of the scattering time approximation, which is used throughout this research.

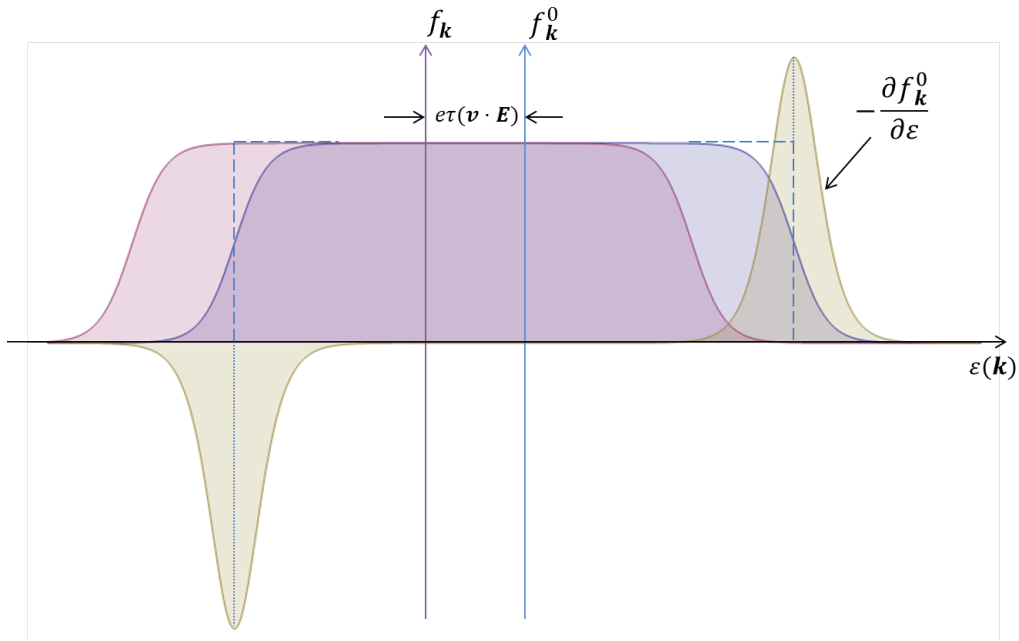


Figure 1.5: The form of the distribution function, and how applying an external electric field \mathbf{E} displaces it. From $g_{\mathbf{k}} = -\frac{\partial f_{\mathbf{k}}^0}{\partial \epsilon} \tau \mathbf{v}_{\mathbf{k}} \cdot e\mathbf{E}$, we can see from the above diagram that $g_{\mathbf{k}}$ is only large near the Fermi surface (with a bit added on to the side where $e\mathbf{v}_{\mathbf{k}} \cdot \mathbf{E} > 0$ and vice-versa) and that it will become a delta peak in the limit of zero temperature.

1.4.2 Drift velocity

Miniband theory states that if the period of a superlattice is shorter than the mean free path of a charge-carrier propagating inside it, then very narrow allowed and forbidden energy bands would form, associated with a series of minizones in the Brillouin zone. Esaki and Tsu pointed out that the combination of miniband formation with the possibility of narrow enough Brillouin zones could allow observation of a quantum mechanical phenomenon known as negative differential conductivity due to the charge-carriers undergoing Bloch oscillation.

In their seminal paper, published in 1970, Esaki and Tsu used a path integral method to calculate the drift velocity of a charge-carrier in the first superlattice miniband under a static bias, while incorporating the effects of probabilistic scattering. In this way it is possible to examine the current-voltage characteristics of the system. Since voltage is directly proportional to the applied bias field, and current is directly proportional to drift velocity, then calculation of drift velocity as a function of applied field will produce a qualitatively identical graph to that of an I-V curve. Let us examine the origins of the scattering theory.

Note that, while the Boltzmann transport equation deals with a collection of particles, we are dealing here with a single electron located initially at the bottom of a miniband. The temperature dependence of its characteristics will be discussed later.

Scattering processes are necessary for conduction to take place. Impurities in the crystal structure can interrupt charge flow by destroying macroscopic lattice periodicity. The major cause of scattering within semiconductor materials however is phonon scattering: that is, thermal vibrations in the lattice give rise to interactions between these phonons and the charge-carriers. In typical semiconductors, scattering events are dominated by electron-phonon interaction. As such, the scattering time is inversely proportional to temperature $\tau \propto \frac{1}{T}$. The scattering time is defined as the average time between two scattering processes, and it is possible to define an effective scattering time τ_{eff} as a combination of elastic (typically due to lattice imperfections and charged impurities in the crystal) and inelastic (electrons interacting with phonons), as follows[19]:

$$\tau_{eff} = \tau_{in} \left(\frac{\tau_{el}}{\tau_{el} + \tau_{in}} \right)^{1/2}$$

Where τ_{in} and τ_{el} are the inelastic and elastic scattering times, respectively.

We will concern ourselves with only the effects of inelastic scattering. Therefore, in the limit of $\tau_{el} \rightarrow \infty$, the effective scattering time $\tau_{eff} = \tau_{in}$. This approximation is valid when dealing with superlattices made from semiconductor materials whose scattering processes are dominated by electron-phonon interaction. We drop the subscript from hereon, for simplicity.

1.4.2.1 Origin of path integral formulation

Esaki and Tsu make use of the scattering time approximation, which asserts that upon undergoing a scattering process, the charge returns to zero momentum; and that the characteristic scattering time of a material is a constant. This assumption is a starting point for the derivation of drift velocity - applied field relations. Let us define the number of *unscattered* electrons at time t within a superlattice miniband as $N(t)$. The probability of any one electron scattering in the infinitesimal time interval dt is $\tau^{-1}dt$, therefore the number of electrons that will undergo scattering in that time interval is given by:

$$\frac{N(t)dt}{\tau}$$

Bearing in mind that $N(t)$ is the number of presently *unscattered* electrons, then after time dt the number of unscattered electrons will be reduced by $\tau^{-1}N(t)dt$, such that

$$N(t + dt) = N(t) - \frac{N(t)dt}{\tau}.$$

Hence the rate at which the number of unscattered electrons changes in time is

$$\begin{aligned} N(t + dt) - N(t) &= -\frac{N(t)dt}{\tau} \\ \frac{dN(t)}{dt} &= \frac{N(t + dt) - N(t)}{dt} = -\frac{N(t)}{\tau}. \end{aligned}$$

This can be rearranged and integrated to calculate the number of unscattered electrons at a given time t , as follows:

$$\begin{aligned}\frac{dN(t)}{N(t)} &= -\frac{dt}{\tau} \\ \int \frac{1}{N(t)} dN &= -\frac{1}{\tau} \int dt \\ \ln N(t) &= -\frac{t}{\tau} + \mathbf{C} \\ \therefore N(t) &= N_0 e^{-\frac{t}{\tau}},\end{aligned}\tag{1.55}$$

where $N_0 = N(t = 0)$ is the number of unscattered electrons at time $t = 0$. Then, the probability P of a single electron scattering in time interval dt can be calculated by dividing the number of electrons that scatter in the same time interval by the total number of electrons:

$$P(t)dt = \frac{1}{N_0} \frac{N(t)dt}{\tau}.$$

Substituting equation (1.55) into the above gives the probability of an electron scattering in time interval dt to be:

$$P(t)dt = \frac{e^{-\frac{t}{\tau}}}{\tau} dt.$$

Under the scattering time approximation, electrons only contribute to net current at a time t (correspondingly, net drift velocity) after undergoing a scattering event at time t . Therefore, we can write

$$v_d(t) = v_g(t)P(t),$$

where v_d is the electron's drift velocity, and v_g is its group velocity. The overall drift velocity of a system is a constant in time; and the total drift velocity of the entire system can be found by integrating the above equation over all

time, as follows:

$$v_d = \int_0^{\infty} v_g(t) P(t) dt$$

$$v_d = \frac{1}{\tau} \int_0^{\infty} v_g(t) e^{-\frac{t}{\tau}} dt. \quad (1.56)$$

Equation (1.56) is the general form for calculating the effect of an applied field on the drift velocity of an electron in a superlattice. This equation constitutes much of the foundation of the research in this thesis.

1.4.2.2 Esaki-Tsu result

Using the well-established kinetic equation and the energy-momentum relation derived earlier, the group velocity of a charge-carrier moving inside the first miniband is calculated as follows. Newton's equation is

$$\frac{dk(t)}{dt} = \frac{eF}{\hbar}$$

where $k(t) = \hbar^{-1}p$ is the quasimomentum of the charge-carrier and F is the magnitude of the electric field applied to the superlattice. The kinetic equation tells us

$$v_g = \frac{1}{\hbar} \frac{dE}{dk}$$

where $E = E(k)$ is the energy-momentum relation of charge-carriers propagating in the first miniband. Differentiating both sides of this equation with respect to t gives

$$\frac{dv_g}{dt} = \frac{1}{\hbar} \frac{d}{dt} \frac{dE}{dk}$$

Rearranging Newton's equation for dt and substituting it into the above yields

$$dv_g = \frac{1}{\hbar} \frac{d}{dk} \frac{eF}{\hbar} \frac{dE}{dk} dt = \frac{eF}{\hbar^2} \frac{d^2E}{dk^2}$$

The velocity change in time increment dt is dv_g . The drift velocity v_d is given by the equation

$$v_d = \int_0^{\infty} e^{-\frac{t}{\tau}} dv_g = \frac{eF}{\hbar^2} \int_0^{\infty} \frac{d^2E}{dk^2} e^{-\frac{t}{\tau}} dt$$

where a more general form of this equation is derived later in this section. Recalling that the energy spectrum of the first miniband was derived earlier to be

$$E(k) = \frac{\Delta}{2} (1 - \cos k(t)d)$$

and differentiating this twice with respect to k and substituting it into the integral for v_d yields

$$v_d = \frac{\Delta eFd^2}{2\hbar^2} \int_0^{\infty} \cos(k(t)d) e^{-\frac{t}{\tau}} dt.$$

Solving the kinetic equation for $k(t)$ gives $k(t) = \frac{eFt}{\hbar} + k_0$, where k_0 is the quasimomentum of the charge-carrier at initial time, which can be set to zero for consideration of a charge-carrier originating from the bottom of the miniband. Substituting this into the integral allows calculation of the drift velocity

$$v_d(F, \tau) = \frac{\Delta eF^2}{2\hbar^2} \int_0^{\infty} \cos \frac{eFdt}{\hbar} e^{-\frac{t}{\tau}} dt = \frac{\Delta d}{2\hbar} \frac{\left(\frac{eFd}{\hbar}\right) \tau}{1 + \left(\frac{eFd}{\hbar}\right)^2 \tau^2}.$$

Let us rewrite this as follows:

$$v_d(F, \tau) = v_0 \frac{\omega_b \tau}{1 + \omega_b^2 \tau^2}$$

which has a maximum of $v_d = v_0$ at $\omega_b \tau = 1$, allowing definition of a "critical field" $F_c = \frac{\hbar}{ed\tau}$ at which the drift velocity peaks, and past which the superlattice exhibits NDV as a result of the onset of Bloch oscillations.

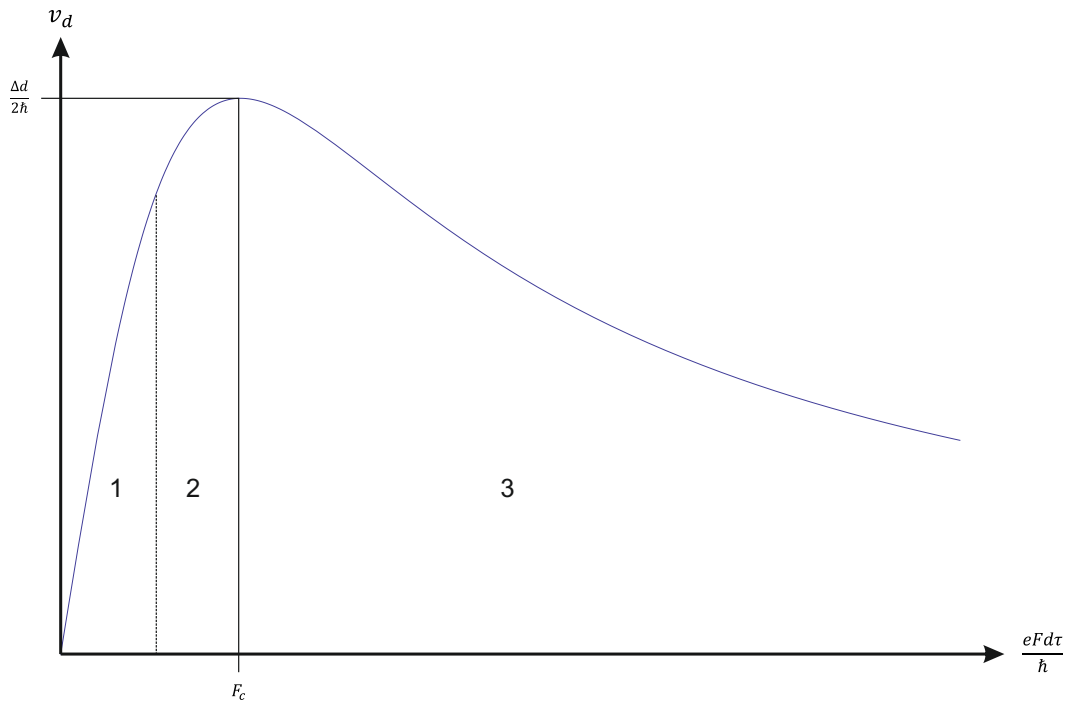


Figure 1.6: Plot showing the dependence of v_d on an applied static field. Region 1 show that, for small field amplitude, the response of the superlattice is essentially ohmic. Inside region 2, the charge-carriers are passing the inflection point in the miniband before undergoing scattering. Negative differential conductivity is exhibited inside region 3, when the charge-carriers manage to begin undergoing one or more Bloch oscillations before scattering. It is evident that a more powerful field leads to greater charge localisation within the superlattice.

1.4.3 Sawtooth model

A scattering event can be assumed to be an inelastic collision in which a small charge-carrier changes direction after interacting with a phonon. The angle of impact will determine the angle at which the charge-carrier will rebound.

The scattering time approximation averages many of these events into the situation in which a charge-carrier impacts upon an ion, and its velocity is reduced to zero.

Let us also assume that a charge-carrier will undergo these scattering events regularly, every τ seconds. In reality, a charge-carrier can only be said to scatter only *most likely* after this amount of time. This simplification will allow an analytical calculation of charge-carrier displacement as a function of time which includes the effect of scattering, as follows.

As calculated previously, the quasimomentum of a charge-carrier in a superlattice miniband evolves linearly with time under a static electric bias:

$$k(t) = \frac{eF_0 t}{\hbar}$$

and the group velocity is proportional to the gradient of the miniband. However, the charge-carrier will undergo a scattering event which returns it to zero momentum, every τ seconds. This means that the quasimomentum evolves in time like a sawtooth wave, with period τ and amplitude $eF_0\tau/\hbar$. The equation for such a sawtooth wave is

$$k(t) = \frac{eF_0\tau}{\hbar} \left(\frac{1}{2} - \frac{1}{\pi} \sum_{n=1}^{\infty} \frac{\sin \frac{2\pi n t}{\tau}}{n} \right)$$

Therefore the group velocity of the charge-carrier is

$$v_g(t) = \frac{\Delta d}{2\hbar} \sin \left[\frac{eF_0\tau d}{\hbar} \left(\frac{1}{2} - \frac{1}{\pi} \sum_{n=1}^{\infty} \frac{\sin \frac{2\pi n t}{\tau}}{n} \right) \right]$$

The infinite summation present in the above equations is convergent:

$$\sum_{n=1}^{\infty} \frac{\sin \frac{2\pi n t}{\tau}}{n} = \frac{i}{2} \left[\log \left(1 - e^{\frac{2i\pi t}{\tau}} \right) - \log \left(1 - e^{-\frac{2i\pi t}{\tau}} \right) \right]$$

It is possible to calculate the displacement analytically

$$x(t) = \int v_g(t) dt \quad (1.57)$$

$$= \int \frac{\Delta d}{2\hbar} \sin \left[\frac{eF_0\tau d}{2\hbar} \left(1 - \frac{i}{\pi} \log \left[1 - e^{-\frac{2i\pi t}{\tau}} \right] + \frac{i}{\pi} \log \left[1 - e^{-\frac{2i\pi t}{\tau}} \right] \right) \right] dt \quad (1.58)$$

$$= -\frac{\Delta}{2eF_0} \cos \left[\frac{eF_0\tau d}{2\hbar} \left(1 - \frac{i}{\pi} \log \left[1 - e^{-\frac{2i\pi t}{\tau}} \right] + \frac{i}{\pi} \log \left[1 - e^{-\frac{2i\pi t}{\tau}} \right] \right) \right] + C \quad (1.59)$$

Where C is to be determined using initial conditions. This is not trivial, as setting the initial displacement to be zero at time $t = 0$ is not totally sufficient. The scattering time approximation dictates that immediately following a scattering event, the charge-carrier returns to zero momentum, hence zero velocity along its axis of motion. Therefore, its displacement will not return to zero every $t = \tau$ seconds as in the equation for displacement calculated above, it must simply repeat its trajectory. Because of this, C must be chosen very carefully in order to fulfill these criteria. Let us express the displacement as follows:

$$x(t) = -\frac{\Delta}{2eF_0} \cos \left[\frac{eF_0\tau d}{2\hbar} \left(1 + \frac{i}{\pi} \log \left[1 - e^{-\frac{2i\pi t}{\tau}} \right] - \frac{i}{\pi} \log \left[1 - e^{-\frac{2i\pi t}{\tau}} \right] \right) \right] + C_0 + C_\tau$$

Where C_0 is determined by the initial condition that $x(t = 0) = 0$:

$$C_0 = -\frac{\Delta}{2eF_0}$$

and where the second quantity C_τ raises the function periodically, by an amount equal to the displacement already gained by the charge-carrier, after every scattering event takes place. This will involve a floor function, with a period equal to the time between scattering events and an amplitude equal to the charge-carrier's displacement travelled in that time.

$$C_\tau = \left\lfloor \frac{t}{\tau} \right\rfloor \frac{\Delta}{2eF_0} \left(1 - \cos \frac{eF_0\tau d}{\hbar} \right)$$

Therefore, in the simple case of a charge-carrier propagating through a one-dimensional superlattice under the influence of a static electrical bias, undergoing scattering processes every $t = \tau$ seconds, the displacement can be expressed analytically as follows:

$$x(t) = \frac{\Delta}{2eF_0} \left\{ 1 - \cos \left[\frac{eF_0\tau d}{2\hbar} \left(1 + \frac{i}{\pi} \log \left[1 - e^{-\frac{2i\pi t}{\tau}} \right] - \frac{i}{\pi} \log \left[1 - e^{\frac{2i\pi t}{\tau}} \right] \right) \right] \right\} \quad (1.60)$$

$$+ \left\lfloor \frac{t}{\tau} \right\rfloor \left(1 - \cos \frac{eF_0\tau d}{\hbar} \right) \quad (1.61)$$

The behaviour of a charge-carrier obeying this equation is illustrated in Figure 1.7.

This simple model has obvious limitations. First, a more physical realisation of scattering processes in a semiconductor is a probabilistic distribution - that is, the particle undergoes scattering *on average* every τ seconds, not exactly every τ seconds. This might have the effect of "blurring" the trajectories in Figure 1.7 due to some scattering events happening earlier or later than in the simple model. Furthermore, the kinetic energy of a particle after scattering is a distribution. The particle may only glance a stationary ion, or it may have its direction completely reversed. This is a shortcoming of the scattering time approximation used throughout this work.

This model has allowed an analytical calculation of the real space trajectories of charge-carriers in a superlattice. It provides a clear illustration of the relation between the gradient of a displacement-time graph inclusive of scattering, and the drift velocity dependence upon field strength. It also predicts total localisation of charge-carriers in a superlattice miniband, when the product $F_0\tau$ corresponds to an even integer multiple of π (when $\frac{eF_0\tau d}{\hbar} = 2n\pi$, where $n = 1, 2, \dots$). It is essential to point out that this prediction is based on

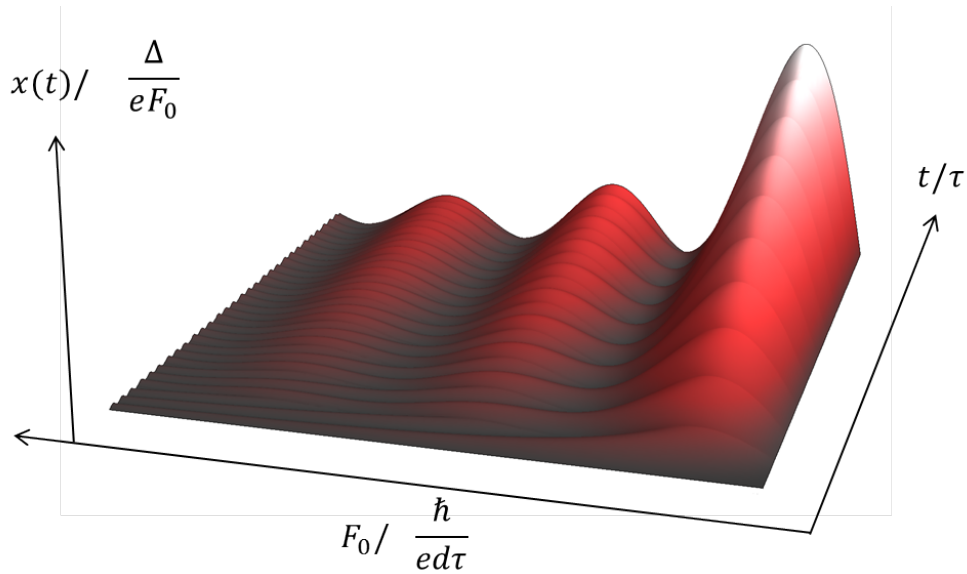


Figure 1.7: This surface plot illustrates how the displacement of a charge-carrier experiencing a static electric field, and undergoing periodic scattering processes, changes in time. As the strength of the field increases, the charge-carrier begins to propagate through the superlattice. Its average velocity reaches a peak, corresponding to the maximal gradient of $x(t)$ versus t . After this, the average displacement goes back to zero. At this point, the charge-carrier has undergone exactly one Bloch oscillation and has scattered upon reaching the bottom of the miniband. Therefore, it has returned to its original position in real space and scattered. The next troughs correspond to the particle scattering after exactly two and three Bloch oscillations, respectively.

the oversimplified model of scattering used to preserve analyticity in this calculation, and that the troughs seen in Figure 1.7 are artefacts of this oversimplification as compared to the results predicted by the Esaki-Tsu model.

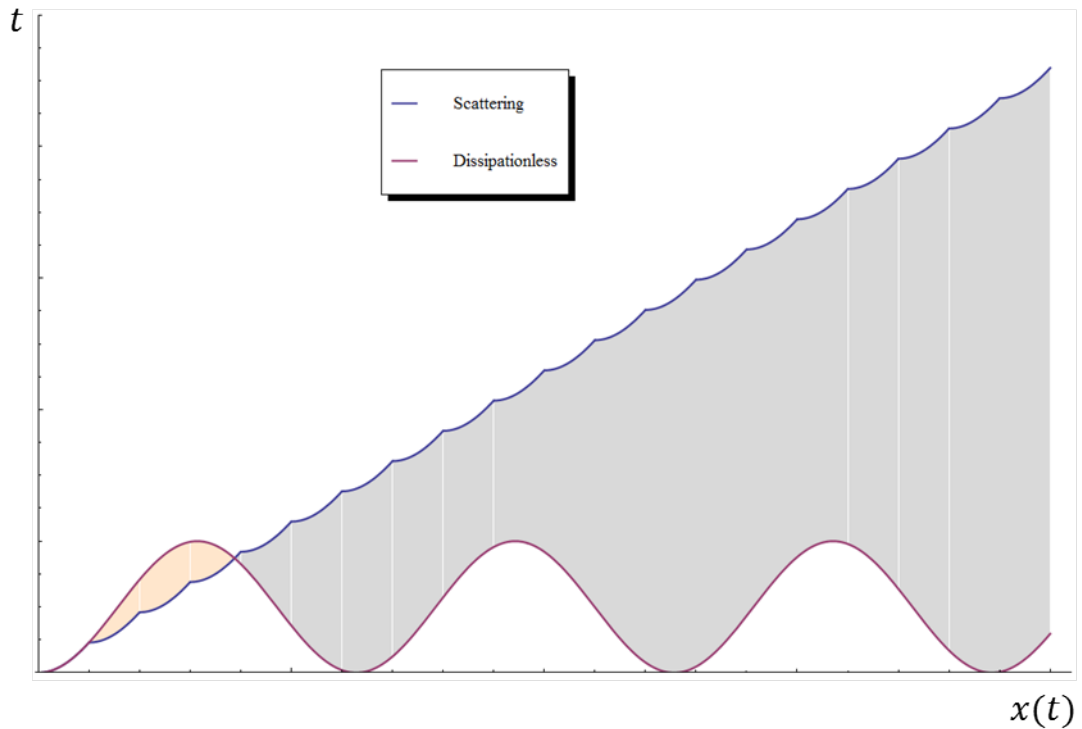


Figure 1.8: A trajectory plot of displacement against time, displaying the difference in the trajectories of a charge-carrier propagating without experiencing dissipation, and one which undergoes scattering every $t = \tau$ seconds. This diagram demonstrates clearly that dissipation can induce macroscopic transport. Note that while the instantaneous gradient of either trajectory curve is the group velocity, the *average* gradient is the drift velocity. In these cases, the drift velocity is zero for dissipationless systems, whereas in systems exhibiting dissipation, it is usually finite. The specifics of the latter are discussed in greater detail in this section.

1.5 Bloch oscillations as sources of radiation, typical values

When a charge-carrier is localised in a superlattice, it is constantly accelerating. As a result, it will emit radiation at that frequency, known as the Bloch frequency. Our sawtooth-momentum model predicts total charge localisation when

$$\frac{eF_0\tau d}{2\pi\hbar} = n; \quad n \in \mathbb{N}^+$$

In a typical semiconductor superlattice largely constructed from GaAs, the typical scattering time at room temperature is $\tau \approx 10^{-12}$ s. Scattering effects in such a material are dominated by phonons, and therefore the relation between scattering time and temperature (as mentioned earlier) is

$$\tau \propto \frac{1}{T}$$

which provides a degree of tunability to the scattering time (and therefore, the regions of localisation). Using $\sigma = ne\mu$ and $\sigma = ne^2\tau m_{\text{eff}}^{-1}$ where σ is the conductivity, μ the mobility, and n the number density of charge-carriers, we can calculate the scattering time for gallium arsenide to be $\tau = 3.24$ ps. Therefore, the sawtooth model predicts that electrons in a superlattice will undergo extended periods of Bloch oscillation at integer multiples of roughly 20THz (assuming a critical field F_c of 10^3 V cm⁻¹). 1

1.6 Non-static electrical bias

1.6.1 Single AC field

The purpose of this research is to investigate how applying electric fields to a superlattice mitigates tunability of the resulting $I - V$ curve. The next logical step is to calculate the drift velocity's dependence upon an applied DC field accompanied by an AC driving field:

$$\mathbf{F}(t) = F_0 + F_1 \cos(\omega_1 t + \phi)$$

where ϕ is the initial phase of the driving field F_1 . The equation used to calculate the drift velocity in this case is derived using the balance equation approach by Ignatov and Renk[21] and is given below:

$$v_d = \frac{1}{T} \int_T v_g(t) dt \quad (1.62)$$

where the group velocity is calculated using

$$v_g(t) = \frac{1}{\tau} \int_{-\infty}^{t_1} e^{-(t-t_1)/\tau} \sin \left[\frac{e}{\hbar} \int_{t_1}^t \mathbf{F}(t_2) dt_2 \right]. \quad (1.63)$$

In this way, the effect that the phase of the driving field has on the motion of the particle is taken into account. Using the Jacobi-Anger expansions

$$e^{\pm i\alpha \sin \theta} = \sum_{n=-\infty}^{\infty} J_n(\alpha) e^{\pm in\theta} \quad (1.64)$$

$$e^{\pm i\alpha \cos \theta} = \sum_{n=-\infty}^{\infty} (\pm i)^n J_n(\alpha) e^{in\theta} \quad (1.65)$$

along with the result for the time-averaging integral calculated by Ignatov *et al.*[22] and the Fourier series expansion

$$J_0(Z \sin \alpha) = J_0^2(Z/2) + 2 \sum_{n=1}^{\infty} J_n^2(Z/2) \cos(2n\alpha)$$

allows the group velocity to be expressed in an integrable form and substituted into the adapted form of the equation for drift velocity, yielding

$$v_d = v_0 \sum_{n=-\infty}^{\infty} J_n^2(\omega'/\omega_1) \frac{(\omega_b + n\omega)\tau}{1 + (\omega_b + n\omega)^2\tau^2}. \quad (1.66)$$

This function is plotted in Figure 1.9 in dimensionless units, for a range of AC field strengths $F_1 = 0..10$ and frequencies $\omega = 0..20$. Looking at Figure 1.9, we can elaborate on two interesting emergent behaviours. First, as the frequency of the applied AC field increases and approaches the Bloch frequency ω_b , the initial slope of the $v_d(F_0)$ curve decreases at a rate proportional to F_1 while the peak drift velocity occurs for greater values of F_0 . This means that, while $\omega < \omega_b$, the superlattice only enters its active region under the application more intense static fields, but as ω approaches ω_b , the electrons become increasingly localised in a region of F_0 which is proportional to F_1 . This behaviour is demonstrated by the fifth graph in Figure 1.9, where the drift velocity becomes zero for several combinations of F_0, F_1 and ω , for a given τ . If an electron is localised under application of a DC field of strength $F_0 \approx 7F_c$ and AC field of strength $F_1 = 10F_c$, then, assuming that the miniband gap is sufficiently large to prevent Zener tunnelling, the electron will oscillate spatially with a frequency $17\hbar^{-1}edF_c$ (where $F_c = \hbar/ed\tau$ denotes the critical field strength - the value of static field strength at which the drift velocity is maximum when $F_1 = 0$). This corresponds to a frequency of roughly 5THz. This value can be increased by increasing the strength of the applied AC field, F_1 , to extend the region of electron localisation and force the electrons to oscillate at a higher frequency, or decreased by decreasing F_0 . In this way, it is theoretically possible to tune the superlattice to emit radiation of a particular frequency. Second, as the AC field frequency increases beyond ω_b , the superlattice begins to allow electron flow for given multiple values of F_0 , as can be seen in the sixth graph. This implies that the superlattice has entered a domain where it has multiple active regions between regions

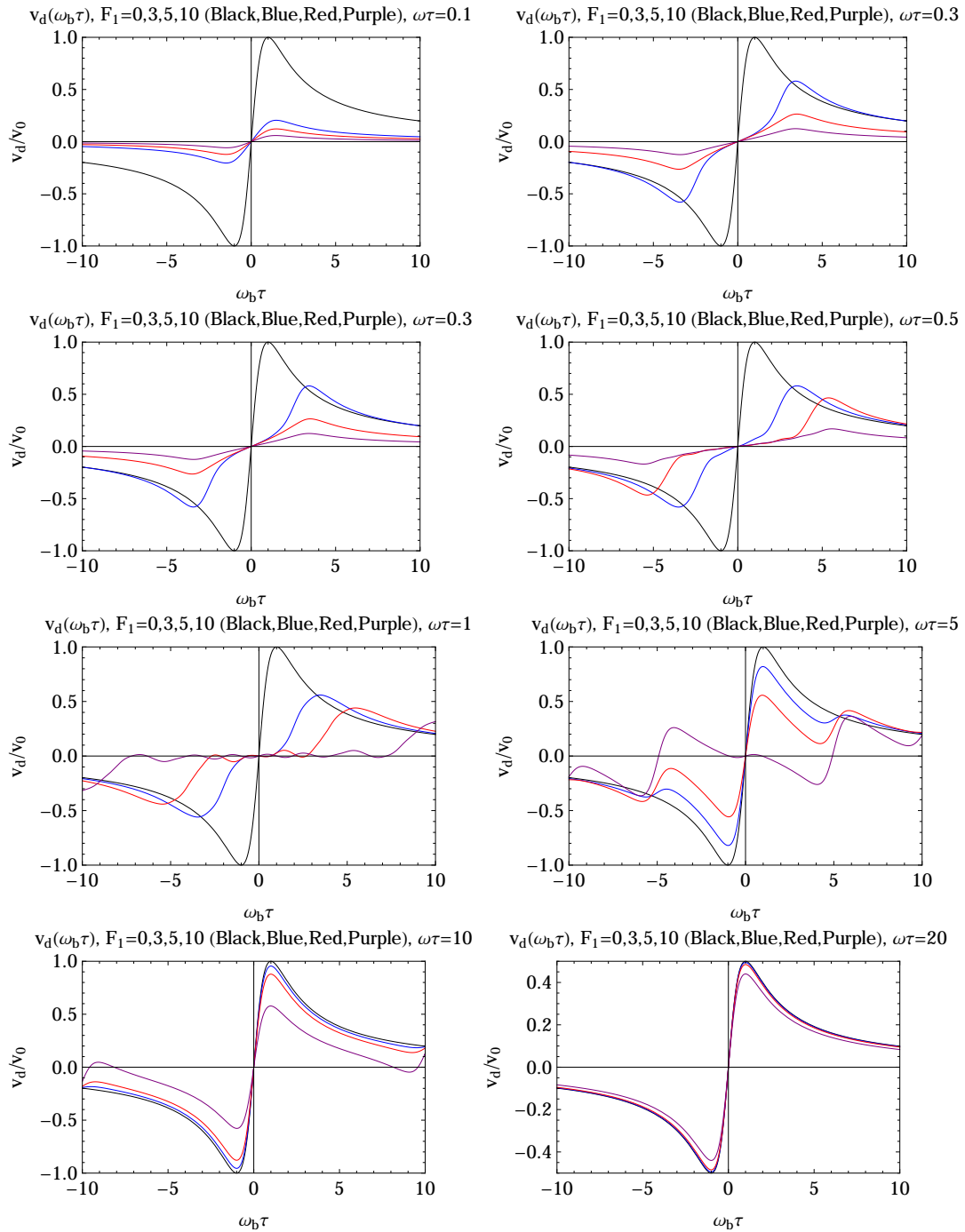


Figure 1.9: Graphs illustrating the effect that applying a harmonic driving field to a superlattice in addition to a static field. The black lines on each graph corresponds to the static field only case. Of particular interest here is the fifth graph in the series, showing a high degree of charge localisation.

of relatively Ohmic behaviour; the size of these regions depends on F_1 and ω . Combined with the appearance of negative conductivity occurring for positive values of F_0 , this switching behaviour could be of interest for novel circuit design. Finally, as the AC field frequency becomes much larger than ω_b , the Ohmic regions between active regions become smaller, and the $v_d(F_0)$ characteristics converge on the DC only behaviour, effectively destroying the useful electronic behaviour.

1.6.2 Super Bloch oscillations

The group velocity of a particle can be thought of as its instantaneous velocity, its infinitesimal rate of change of displacement. Therefore, for time periods shorter than the scattering time τ , it is possible to examine the dependence of the charge-carrier's real space displacement when under the influence of these applied electric fields.

$$x(t) = \int v_g(t) dt = v_0 \sum_n J_n \left(\frac{\omega'_b}{\omega_1} \right) \int \sin [(\omega_b + n\omega_1)t] dt \quad (1.67)$$

$$= -v_0 \sum_n J_n \left(\frac{\omega'_b}{\omega_1} \right) \frac{\cos(\omega_b + n\omega_1)t}{\omega_b + n\omega_1} + C \quad (1.68)$$

where C should be chosen such that $x(t=0) = 0$ in order to define the initial displacement of the charge-carrier to be zero:

$$C = -v_0 \sum_n \frac{J_n \left(\frac{\omega'_b}{\omega_1} \right)}{\omega_b + n\omega_1}$$

A Super Bloch oscillation is, effectively, a normal Bloch oscillation scaled up in amplitude and period. It follows that, if an electron undergoes Bloch oscillations at, say, 200THz, and the SBO has a time period $T_{SBO} = 20T_{BO}$, then

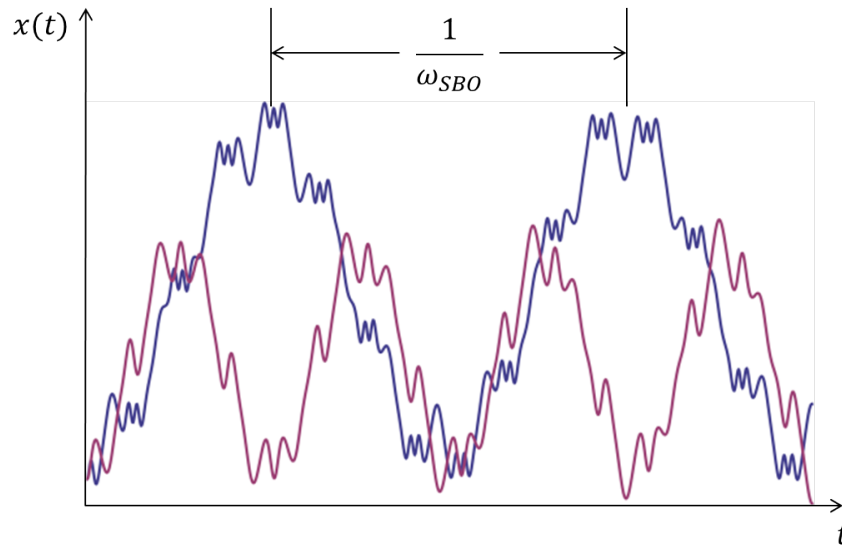


Figure 1.10: Appearance of so called “Super Bloch” oscillations, with an effective period dependent on the difference between the Bloch frequency and the frequency of the applied AC field. Above are plotted displacement-time curves for .

the electron will also oscillate macroscopically in space with a frequency of 10THz.

As $\frac{\omega_b}{\omega_1} \rightarrow n$, the period of the Super Bloch oscillation goes to infinity. That is, as the applied field frequency approaches an integer multiple of the Bloch frequency, the scaling factor between the BO and the SBO begins to increase. In this way it is possible to tune the strength and frequency of an applied AC field along with the strength of the DC field, in order for SBOs of required frequency manifest.

A problem with SBOs is that the characteristic scattering time must scale with the period of the SBO in order to preserve its coherence. This would require a larger effective superlattice period, or a longer characteristic scattering time. The latter might be achieved by lowering the operating temperature.

Chapter 2

Graphene, a novel material

2.1 Introduction, properties of graphene

2.1.1 Introduction to graphene

There exist several allotropes of carbon in the world, two of which are diamond and graphite. These two materials consist solely of carbon atoms, bonded together in a crystal lattice structure. Diamond's lattice structure is isometric-hexoctahedral, whereas graphite consists of planes of hexagonally arranged atoms, stacked one on top of the other, the layers bound together by weak Van der Waals forces. It is thanks to the weakness of these forces that graphite is an effective writing implement - layers of carbon are very easily, with little force, "peeled" from the graphite crystal onto paper.

Graphene is the name given to a single, isolated layer of graphite - a monatomically thin layer of benzene rings. The term was perhaps first used by Mouras, et al. [23], but has been theorised (or at least, touched upon) since 1946[24], in a paper that examined the properties of a single layer of graphite using the tight-binding approximation.

Over recent years, there have been a vast number of papers published and experiments conducted to further examine this new material - mainly thanks to the intensive research of Geim, Novoselov et al., at the University of Manchester [25, 26]. It was there that the first graphene was created and isolated successfully, and was discovered to be stable and maintain its crystallinity even at room temperature.

Graphene has been shown[27, 28] to contain charge carriers which have a very high mobility, and which travel on almost perfectly ballistic trajectories

through the lattice. The speed with which these charge carriers move is one three-hundredth of that of light, and they seem to exhibit zero effective mass. (The term “zero effective mass” here denotes a parameter that describes how a charge carrier responds to applied forces at particular wavevectors. The fact that this parameter goes to zero in the case of graphene’s quasiparticles implies that their velocity remains constant.) In this situation, these particles can only be accurately described by a Dirac-like equation. It is this property of graphene which, in many ways, forms links between condensed matter physics and quantum electrodynamics, even on the scale of a laboratory desktop.

2.1.2 The graphene construct

Graphene’s crystal lattice is actually made up of two symmetrical triangular sublattices, which overlap one another to form the hexagonal lattice we see. The figure below (2.1) shows the components of the graphene lattice, denoted sublattices A and B.

Note that the lattice site of one sublattice is in the centre of a triangle defined by the other sublattice, and that the lattice is invariant under 120° rotation. That being the case, there are therefore two carbon atoms per unit cell. The Brillouin zone is constructed as shown in Figure 2.2; and close to the K (and K’) points, where the energy bands are formed by quantum mechanical “hopping” of the charge carriers between sublattices, the electronic band structure ceases to be familiarly parabolic and becomes linear.

It is in these regions that the charge carriers have zero effective mass, due to their linear dispersion relation given by

$$E(\underline{k}) = \hbar v_F k \quad (2.1)$$

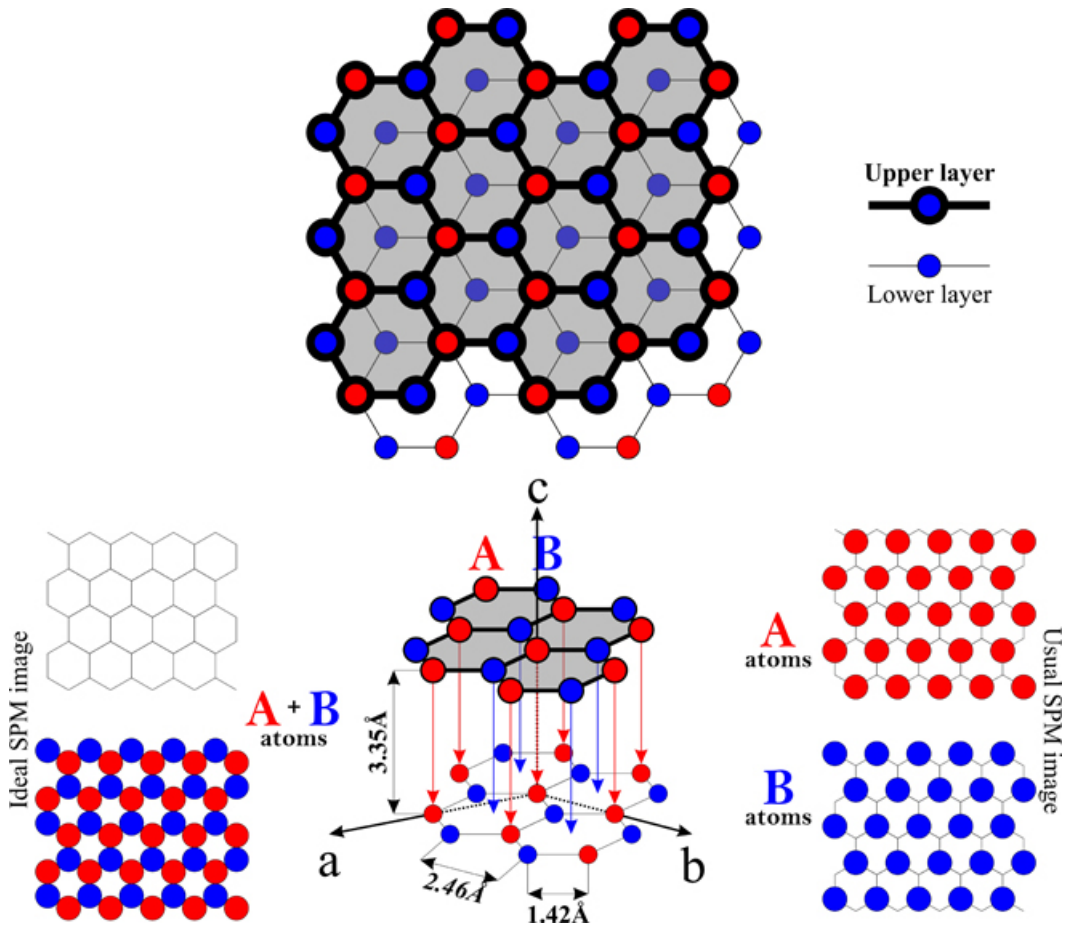


Figure 2.1: This diagram[29] clarifies how the hexagonal lattice is, more fundamentally, two symmetrical, interlocking sublattices[34, 35, 36]. It is this crystal symmetry between the sublattices from which graphene's linear dispersion characteristics arise.

It is also significant that at the K and K' points, there is no energy gap whatsoever between the conduction and valence bands. This means that graphene is a gapless semiconductor; and its quasiparticles are described formally by the following equation[37]:

$$\hat{H}_0 = -i\hbar v_F \sigma \nabla \quad (2.2)$$

where $\sigma = (\sigma_x, \sigma_y)$ are the Pauli spin matrices and v_F is the Fermi velocity, mentioned earlier to be approximately $c/300$.

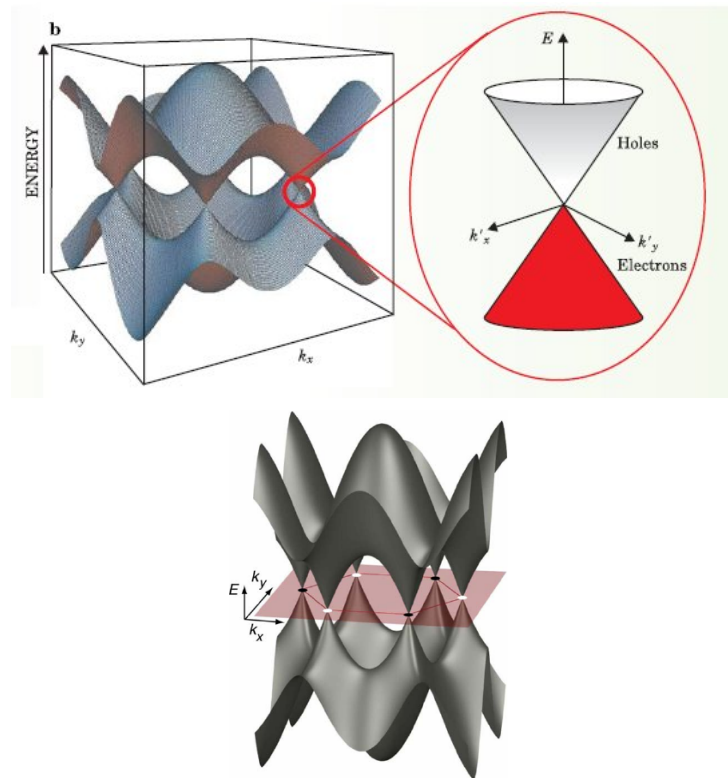


Figure 2.2: The above figures[30, 31] show the location in the Brillouin zone of the six Dirac points, points near which the dispersion relation becomes linear and there is an absence of any band gap. However, it is important to note that only two out of these six points are physically inequivalent, due to symmetry constraints.

The linear dispersion relation implies that the velocity of charge carriers through the lattice is not a function of momentum - rather, it is a constant. This property, when combined with the vanishing mass of the charge carriers, and described under the framework of relativistic quantum mechanics, further implies that the free particle states in graphene are chiral. In the case of spin $1/2$ particles, chirality is equivalent to helicity, which is the projection of the spin of a quantum particle on its momentum.

2.1.3 Graphene's links to quantum electrodynamics

Let us examine then the further links between graphene and quantum electrodynamics. In conventional condensed matter theory, electrons and holes in conduction and valence bands are described by two separate Schrödinger equations, with each type of charge carriers having a different effective mass (as a consequence of the Seitz sum rule[38]). In the case of graphene, the charge carriers are interconnected because of the crystal symmetry of the sublattices, leading to an analogy with charge conjugation symmetry. Chirality itself arises from the fact that, due to the intersecting linear dispersion relation of graphene, an electron with energy E and a hole with energy $-E$ propagating in opposite directions have come from the same branch of the spectrum - implying that both electrons and holes have the same "pseudospin"[39, 40]. This symmetry is what allows the introduction of chirality, (as said above, the projection of a particle's spin on its momentum) which is positive for electrons and negative for holes. This kind of chirality is very similar to the chirality in quantum electrodynamics.

The term "pseudospin" used above might most easily be described by looking at the Dirac equation for the energy of massless, relativistic fermions in quantised fields[41, 42, 43, 44]:

$$E_N = 2e\hbar c_*^2 B \left[N + \frac{1}{2} \pm \frac{1}{2} \right]^{\frac{1}{2}} \quad (2.3)$$

The \pm here refers, in quantum electrodynamics, to the contributions from particles with positive and negative spins. When referring to graphene however, the \pm accounts not for physical spins, but "pseudospin" - which is a result of the crystal structure of the lattice consisting of two identical interlocking sublattices (particles originating from different sublattices have opposite pseudospin). Interestingly, if we look at the $N = 0$ case for the above

equation, we see that the lowest Landau level has zero energy and accommodates only one projection of the pseudospin (in this case, -1); whereas all other levels (i.e. all other $N \neq 0$) contain two. This implies that the degeneracy of the lowest Landau level is half of the degeneracy of any other level. A more succinct way of describing the situation here would be to say that all Landau levels have the same “compound” degeneracy, but the zero-energy Landau level is shared equally between electrons and holes. This peculiar realisation helps describe graphene’s unique half-integer quantum Hall effect. To complement the theory here, the observed anomalous quantum Hall effect in itself could be the most direct evidence for the existence of Dirac fermions acting as charge carriers in graphene systems.

2.1.4 Phenomenon of frequency multiplication in graphene

It is theorised[45, 46, 47] that, in the presence of sufficiently high alternating electromagnetic fields of frequency ω and low temperatures, graphene should begin to emit similar radiative fields with frequencies corresponding to higher (odd) harmonics of the original applied frequency ω . This conclusion follows from the idea that placing a particle with a linear dispersion relation in an external electromagnetic field $E(t) = E_0 \cos \omega t$ will move with momentum calculated using classical mechanics: $\dot{p}(t) = -eE(t)$ giving $\mathbf{p}(t) = -\frac{eE_0}{\omega} \sin \omega t$. The velocity of the particle can then be calculated using $v(t) = \frac{\partial \epsilon}{\partial p}$ where $\epsilon = v_F(p^2)^{1/2}$, giving $v(t) = -v_F \text{sgn}(\sin \omega t)$. This implies that

$$j(t) = en_s v_F \text{sgn}(\sin \omega t) = en_s \frac{4}{\pi} \left\{ \sin \omega t + \frac{1}{3} \sin 3\omega t + \frac{1}{5} \sin 5\omega t + \dots \right\} \quad (2.4)$$

The term on the right is an elementary Fourier series expansion of $\text{sgn}(\sin \omega t)$. One important note is that the amplitudes of each successive harmonic do

not decrease quickly - they only go as $1/m$, where m is the harmonic number 1,3,5.... This is important because of its relevance to the efficiency of producing these higher frequencies with an applied field - implying that a particularly strong field is not necessary for the production of much higher frequencies, thus the aim of generating radiation in the terahertz region may not be difficult.

Mikhailov goes on to discuss this situation in the context of kinetic Boltzmann theory, an approach chosen to take into account the Fermi distribution of charge carriers over the quantum states in the conduction and valence bands in graphene. This frees the restrictions on the amplitude of the applied field $E(t)$, and allows the study of the effects of any $E(t)$ on the system. However, having calculated the intra-band conductivity, it is shown that there are restrictions on the validity of this quasi-classical approach and that higher frequencies can be generated approximately between the frequencies 5 and 10 THz.

2.1.5 Minimum conductivity and the Klein paradox

A further important property of graphene is one that possibly raises the most eyebrows - that even at zero charge carrier density, there remains a positive, finite conductivity[25, 48, 49, 50]. Theorists still struggle to agree on a complete and concise explanation of the exact details of this phenomenon.

More than one value of this minimum conductivity have been predicted, including $4e^2/h$ [48], and e^2/h [40]. All are of the order of e^2/h . One approach that yields a simple, yet not perfectly unambiguous, answer is one involving

the Klein paradox in graphene and Mott's estimation. The argument goes as follows: There is enough disorder in two dimensional systems to give rise to separation of electronic states by barriers with vanishing transparency, leading to Anderson localisation. In graphene, these barriers have a transmission coefficient close to (or equal to) unity, thus not allowing confinement of charge carriers by barriers that are smooth on atomic length scales. In the absence of localisation, it is valid to invoke Mott's assumption that the mean free path cannot be lower than the electronic wavelength. If we then set the mean free path to be of the order of the wavelength, we get

$$\sigma = \left(\frac{e^2}{\hbar}\right) \left(\frac{l}{\lambda}\right) = \left(\frac{e^2}{\hbar}\right) \left(\frac{\lambda}{\lambda}\right) \approx \frac{e^2}{h} \quad (2.5)$$

The Klein paradox is important in the above argument because it accounts for the transmission coefficient in graphene being so high. The Klein paradox itself describes how relativistic particles tunnel through very high potential barriers with probability approaching unity via the notion of conservation of pseudospin (hence the significance of the appearance of chirality) - that is, as a particles approaches the barrier, its antiparticle is created inside the barrier wall whose pseudospin aligns with the incoming particle. This allows the creation of a particle on the opposite outside of the barrier, which propagates away - implying perfect transmission. This is also discussed in the context of Andreev reflections in [51]. For an illustration of this process, see Figure 2.3.

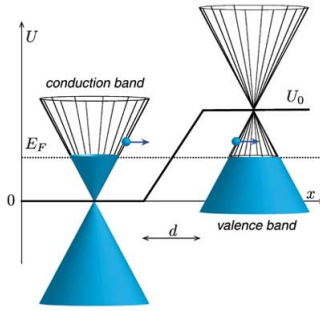


Figure 2.3: Here[32], electron and hole states in graphene's band structure are converted into each other during a process known as Andreev reflection. Charge is conserved in this process by the creation of a Cooper pair.

2.2 Tight-binding model, derivation of linear band structure

2.2.1 Basis Vectors and the Reciprocal Lattice

Graphene is a single two-dimensional layer of graphite, consisting of carbon atoms arranged in a honeycomb structure. This hexagonal arrangement consists more fundamentally of two interlocking triangular Bravais lattices, which we call sublattices "A" and "B", forming a two-point basis (see Figure 2.1).

For the purposes of this investigation, we say that the graphene sheet lies in the $x - y$ plane. "A" sites sit on the sites \vec{R} of the underlying triangular lattice. "B" sites sit at sites $\vec{R} + \vec{d}$, where \vec{d} are the nearest neighbour vectors

defined below. The primitive vectors of the Bravais lattice are

$$\begin{aligned}\vec{a}_1 &= a\hat{x} \\ \vec{a}_2 &= \frac{a}{2}\hat{x} + \frac{\sqrt{3}}{2}a\hat{y}\end{aligned}$$

Let us define the following basis vectors

$$\begin{aligned}\vec{0} \\ d &= \frac{1}{3}(\vec{a}_2 + (\vec{a}_2 - \vec{a}_1)) \\ &= \frac{a}{\sqrt{3}}\hat{y}\end{aligned}$$

The primitive vectors of the reciprocal lattice are

$$\begin{aligned}\vec{b}_1 &= \frac{2\pi}{a}\hat{x} - \frac{2\pi}{\sqrt{3}a}\hat{y} \\ \vec{b}_2 &= \frac{4\pi}{\sqrt{3}a}\hat{y}\end{aligned}$$

The nearest neighbours of site A are displaced from A by nearest neighbour vectors $\vec{d}, \vec{d}' = (\vec{a}_1 - \vec{a}_2) + \vec{d} = \frac{a}{2}\hat{x} - \frac{a}{2\sqrt{3}}\hat{y}$, $\vec{d}'' = -\vec{a}_2 + \vec{d} = -\frac{a}{2}\hat{x} - \frac{a}{2\sqrt{3}}\hat{y}$.

2.2.2 Atomic Orbitals

Atomic carbon has electronic structure $1s^2(\uparrow\downarrow) 2s^2(\uparrow\downarrow) 2p^2(\uparrow\uparrow)$ There are six electrons per carbon atom, with four of those electrons in the outermost $n = 2$ shell. The $1s^2$ electrons have significantly lower energy than the $n = 2$ electrons. When carbon forms the honeycomb structure of graphene, they remain tightly bound to the carbon ion and do not participate in bonding or conduction. Thus we can forget about them from here onwards.

The $2s^2$ and $2p^2$ electrons are very close in energy. When carbon forms the honeycomb structure, these atomic orbitals will mix, or “hybridise”. For car-

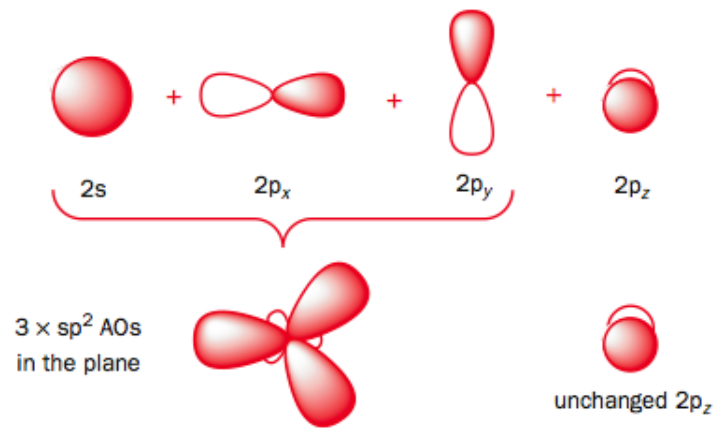


Figure 2.4: Demonstration[33] of how the s orbital hybridises with the two in-plane p orbitals to form sp^2 hybridised orbitals. The p_z orbital, normal to the graphene sheet, remains unchanged.

bon in a 2D honeycomb structure, one finds that the s , p_x and p_y orbitals all mix together roughly equally (these are the orbitals which have significant electron probability density in the $x - y$ plane) while the p_z orbitals remain distinctly separate. The $s - p_x - p_y$ mixed states are called sp^2 hybridised, as one s mixes with two p orbitals.

The sp^2 states give rise to three σ bonding bands and three σ^* antibonding bands. The p_z states give rise to two bands - the π band and the π^* band (making a total of eight bands).

The σ -bonding bands give wavefunctions with electron concentration along the free nearest neighbour bonds between A and B sites in the $x - y$ plane. These are the covalent bonds that hold the honeycomb structure together.

The σ bonding bands have the lowest energy and all lie below the Fermi energy. In the ground state they are completely filled taking six of the eight electrons per BL cell. Since these bands are filled, they play no role in electric

conduction in graphene.

The σ antibonding bands all lie above the Fermi energy. In the ground state they are completely empty, hence we ignore them. (There is a finite energy gap between the minimum energy of the σ^* bands and the Fermi energy).

All the interesting effects concerning conduction there lie with the π and π^* bands. These are essentially between the σ and σ^* bands (though actually the σ band means its maximum overlaps somewhat with the minimum of the π band, and the maximum of the π^* band overlaps somewhat with the minimum of the σ^* band, but these overlapping regions lie well below, or well above, the Fermi energy, and so they play no role in conduction - conduction is determined by electrons in close vicinity of the Fermi energy only).

We will soon see that the π and π^* bands do not overlap. Therefore, in the ground state, with eight electrons per BL cell, six electrons go to completely filling the three σ bands, and two electrons go to completely filling the π band. The σ^* and π^* bands are completely empty. This would be an insulator except we will see that the π and π^* are degenerate (there is no energy gap) at the Fermi surface. We will therefore do a tight-binding calculation involving only the p_z orbital, as a rough calculation for the π and π^* bands.

2.2.3 Tight-binding calculation

If one performs a tight-binding calculation of the band structure from the $n = 2$ shell electrons, one needs to take into account all $2s$, $2p_x$, $2p_y$ and $2p_z$ orbitals. Since there are two atoms per primitive cell of the Bravais lattice

(due to the Bravais lattice having a two-point basis) and there are four atomic orbitals to consider, the Bloch wavefunction is a mixture of eight terms

$$\begin{aligned} \psi_k = \sum_{\vec{R}} \{ & b_{As} \phi_{As} + b_{Ap_x} \phi_{Ap_x} + b_{Ap_y} \phi_{Ap_y} + b_{Ap_z} \phi_{Ap_z} \\ & + b_{Bs} \phi_{Bs} + b_{Bp_x} \phi_{Bp_x} + b_{Bp_y} \phi_{Bp_y} + b_{Bp_z} \phi_{Bp_z} \} \end{aligned}$$

where $\phi_{A(B)s}$, $\phi_{A(B)p_x}$ etc are the atomic orbital wavefunctions centered at site A(B). For each value \vec{k} in the first BZ one then gets eight energies $\epsilon_n(\vec{k})$, that is, eight bands. Let

$$\begin{aligned} \phi_A(\vec{r}) &\equiv \phi(\vec{r}) \\ \phi_B(\vec{r}) &\equiv \phi(\vec{r} - \vec{d}) \end{aligned}$$

where $\phi_{A,B}$ is the p_z orbital centered at site A,B. Our assumed Bloch wavefunction then has the form

$$\psi_k(\vec{r}) = \sum_{\vec{R}} e^{i\vec{k} \cdot \vec{R}} \left\{ b_A \phi_A(\vec{r} - \vec{R}) + b_B \phi_B(\vec{r} - \vec{R}) \right\}; k \in \text{1st BZ}$$

Consider the following

$$\begin{aligned} \langle \phi_A | H | \psi_k \rangle &= \langle \phi_A | H_{at} + \Delta U | \psi_k \rangle \\ &= E \langle \phi_A | \psi_k \rangle + \langle \phi_A | \Delta U | \psi_k \rangle \end{aligned}$$

where E is the energy of the atomic p_z orbital and ΔU is the correction to the atomic potential due to neighbouring atoms. Let us now consider the coefficient

$$\begin{aligned} \langle \phi_A | \psi_k \rangle &= \sum_{\vec{R}} e^{i\vec{k} \cdot \vec{R}} \left\{ b_A \langle \phi_A(\vec{r}) | \phi_A(\vec{r} - \vec{R}) \rangle + b_B \langle \phi_A(\vec{r}) | \phi_B(\vec{r} - \vec{R}) \rangle \right\} \\ &= \sum_{\vec{R}} e^{i\vec{k} \cdot \vec{R}} \left\{ b_A \int d^3r \phi^*(\vec{r}) \phi(\vec{r} - \vec{R}) + b_B \int d^3r \phi^*(\vec{r}) \phi(\vec{r} - \vec{R} - \vec{d}) \right\} \end{aligned}$$

We will assume that all overlaps are negligible except for nearest neighbours - recall that the nearest neighbours of A sites are B sites, and vice-versa. So

in the first term the only \vec{R} we consider is $\vec{R} = 0$, corresponding to the origin. In the second term, we consider only \vec{R} for $\vec{R} + \vec{d} = \{\vec{d}, \vec{d}', \vec{d}''\}$, that is the vectors to the nearest neighbours: $\vec{R} = 0$, $\vec{R} = (\vec{a}_1 - \vec{a}_2)$ and $\vec{R} = -\vec{a}_2$.

$$\langle \phi_A | \psi_k \rangle = b_A + b_B \int d^3r \phi^*(\vec{r}) \phi(\vec{r} - \vec{d}) \left[1 + e^{i\vec{k} \cdot (\vec{a}_1 - \vec{a}_2)} + e^{i\vec{k} \cdot (-\vec{a}_2)} \right]$$

having recalled that

$$\int d^3r \phi^*(\vec{r}) \phi(\vec{r}) = 1 \quad (\text{normalisation})$$

and

$$\begin{aligned} & \int d^3r \phi^*(\vec{r}) \phi(\vec{r} - \vec{d}) \\ &= \int d^3r \phi^*(\vec{r}) \phi(\vec{r} - \vec{d}') \\ &= \int d^3r \phi^*(\vec{r}) \phi(\vec{r} - \vec{d}'') \end{aligned}$$

where the overlap integrals are all equal since ϕ has rotational symmetry about the \hat{z} axis, and

$$|\vec{d}| = |\vec{d}'| = |\vec{d}''|$$

The term in the square brackets is just $\sum e^{i\vec{k} \cdot \vec{R}}$ over the set of $\vec{R} = \{\vec{0}, \vec{a}_1 - \vec{a}_2, -\vec{a}_2\}$ that give the nearest neighbours $\{\vec{d}, \vec{d}', \vec{d}''\}$. The overlap integral $\alpha = \langle \phi(\vec{r}) | \phi(\vec{r} - \vec{d}) \rangle$ is a common factor for all these terms. Therefore we can write

$$\begin{aligned} \langle \phi_A | \psi_k \rangle &= b_A + b_B \alpha \left[1 + e^{i\vec{k} \cdot \vec{a}_1} e^{-i\vec{k} \cdot \vec{a}_2} + e^{-i\vec{k} \cdot \vec{a}_2} \right] \\ &= b_A + b_B \alpha \left[1 + e^{-i\vec{k} \cdot \vec{a}_2} e^{i\vec{k} \cdot \frac{\vec{a}_1}{2}} \left(e^{i\vec{k} \cdot \frac{\vec{a}_1}{2}} + e^{-i\vec{k} \cdot \frac{\vec{a}_1}{2}} \right) \right] \\ &= b_A + b_B \alpha \left[1 + e^{i\vec{k} \cdot \left(\frac{\vec{a}_1}{2} - \vec{a}_2 \right)} 2 \cos \left(\vec{k} \cdot \frac{\vec{a}_1}{2} \right) \right] \end{aligned}$$

Now recall that $\vec{a}_1 = a\hat{x}$, and $\vec{a}_2 = \frac{a}{2}\hat{x} + \frac{\sqrt{3}a}{2}\hat{y}$. Substituting into above yields

$$\langle \phi_A | \psi_k \rangle = b_A + b_B \alpha \left[1 + e^{-i\frac{\sqrt{3}}{2}k_y a} 2 \cos \frac{k_x a}{2} \right] = b_A + (b_B \alpha) f(\vec{k}),$$

calling the term in square brackets $f(\vec{k})$. Now let us calculate

$$\begin{aligned} \langle \phi_A | \Delta U | \phi_B \rangle = & \sum_{\vec{R}} e^{i\vec{k} \cdot \vec{R}} \left\{ b_A \int d^3r \phi^*(\vec{r}) \Delta U(\vec{r}) \phi(\vec{r} - \vec{R}) \right. \\ & \left. + b_B \int d^3r \phi^*(\vec{r}) \Delta U(\vec{r}) \phi(\vec{r} - \vec{R} - \vec{d}) \right\} \end{aligned}$$

Again, keep only nearest neighbour overlaps, so $\vec{R} = 0$ only in the first term, and $\vec{R} = \{\vec{0}, \vec{a}_1 - \vec{a}_2, -\vec{a}_2\}$ in the second term. The conditions concerning the overlap integrals are the same as before, because $\phi(\vec{r})$ is symmetric around the z -axis, and because $\Delta U(\vec{r})$ has rotational symmetry of order three around the z -axis, mapping $\{\vec{d} \mapsto \vec{d}' \mapsto \vec{d}''\}$. Now, defining the following

$$\begin{aligned} \beta &\equiv - \int d^3r \phi^*(\vec{r}) \Delta U(\vec{r}) \phi(\vec{r}) \\ \gamma &\equiv - \int d^3r \phi^*(\vec{r}) \Delta U(\vec{r}) \phi(\vec{r} - \vec{d}) \end{aligned}$$

allows us to write

$$\langle \phi_A | \Delta U | \phi_B \rangle = -b_A \beta (-b_B \gamma) f(\vec{k})$$

We can now write

$$\begin{aligned} (\epsilon_k - E) \left[b_A + (b_B \alpha) f(\vec{k}) \right] + b_A \beta + (b_B \gamma) f(\vec{k}) &= 0 \\ = (\epsilon_k - E + \beta) b_A + [(\epsilon_k - E) \alpha + \gamma] f(\vec{k}) b_B &= 0 \end{aligned} \quad (2.6)$$

Need to now consider the same process to find

$$\langle \phi_B | H | \psi_k \rangle = \epsilon_k \langle \phi_B | \psi_k \rangle = E \langle \phi_B | \psi_k \rangle + \langle \phi_B | \Delta U | \psi_k \rangle$$

Repeating the previous steps we arrive at

$$(\epsilon_k - E + \beta) b_B + [(\epsilon_k - E) \alpha + \gamma] f^*(\vec{k}) b_A = 0, \quad (2.7)$$

where $f^*(\vec{k})$ is the complex conjugate of $f(\vec{k})$. Note that α , β and γ are real, because for the p_z orbital ϕ is real (that is, $\phi = \phi^*$). We can combine equations (2.6) and (2.7) into a set of two homogeneous, linear equations in two

unknowns b_A and b_B . We can therefore write

$$\begin{bmatrix} \epsilon_k - E + \beta & [(\epsilon_k - E)\alpha + \gamma] f(\vec{k}) \\ [(\epsilon_k - E)\alpha + \gamma] f^*(\vec{k}) & \epsilon_k - E + \beta \end{bmatrix} \begin{pmatrix} b_A \\ b_B \end{pmatrix} = \mathbf{M} \begin{pmatrix} b_A \\ b_B \end{pmatrix} = 0.$$

There is a non-trivial solution for b_A and b_B only when $\det \mathbf{M} = 0$. This condition gives a quadratic equation to solve for the two possible values of $\epsilon(\vec{k})$, which we can denote $\epsilon_{\pm}(\vec{k})$. For each \vec{k} there are two solutions: $\epsilon_{-}(\vec{k})$ is the π band, while $\epsilon_{+}(\vec{k})$ is the π^* band. To make the above equation simpler, let us consider the relative magnitudes of α and γ .

$$\begin{aligned} \alpha &\equiv \int d^3r \phi^*(\vec{r}) \phi(\vec{r} - \vec{d}) \\ \gamma &\equiv - \int d^3r \phi^*(\vec{r}) \Delta U(\vec{r}) \phi(\vec{r} - \vec{d}) \end{aligned}$$

Since $\Delta U(\vec{r})$ is large at $(\vec{r} - \vec{d})$, then $|\phi(\vec{r} - \vec{d})| \ll |\Delta U(\vec{r}) \phi(\vec{r} - \vec{d})|$. Therefore we can justify saying that $\alpha \ll \gamma$, and eliminate terms in α from the above equations, leaving

$$\mathbf{M} = \begin{bmatrix} \epsilon_k - E + \beta & \gamma f(\vec{k}) \\ \gamma f^*(\vec{k}) & \epsilon_k - E + \beta \end{bmatrix}$$

allowing $\det \mathbf{M} = 0$ to be solved much more simply:

$$\det \mathbf{M} = (\epsilon_k - E + \beta)^2 - \gamma^2 |f(\vec{k})|^2 = 0$$

Solving for ϵ_k gives

$$\epsilon_{\pm}(\vec{k}) \equiv E - \beta \pm |\gamma| |f(\vec{k})|$$

Note that $|\gamma| |f(\vec{k})| > 0$. This implies the following:

$$\begin{aligned} \epsilon_{+}(\vec{k}) &\geq E - \beta \\ \epsilon_{-}(\vec{k}) &\leq E - \beta \end{aligned}$$

Meaning that the bands do not overlap. That is, the minimum energy of the π^* band is always greater than the maximum energy of the π band:

$$\left(\min \epsilon_+(\vec{k}) \geq \max \epsilon_-(\vec{k}) \right)$$

Consider now

$$f(\vec{k}) = 1 + e^{-i\frac{\sqrt{3}}{2}k_y a} 2 \cos \frac{k_x a}{2}$$

$$|f(\vec{k})| = \left[1 + 4 \cos^2 \frac{k_x a}{2} + 4 \cos \frac{k_x a}{2} \cos \frac{\sqrt{3}}{2} k_y a \right]^{\frac{1}{2}}$$

which is largest when $k_x = k_y = 0$. This implies that $\min \epsilon_+(\vec{k})$ and $\max \epsilon_-(\vec{k})$ both occur at $\vec{k} = 0$. Furthermore, $\epsilon_-(\vec{k})$ (the energy of the π band) increases towards the surface of the first BZ; and conversely $\epsilon_+(\vec{k})$ (the energy of the π^* band) decreases towards the surface of the first BZ.

2.2.4 Linearity near the Dirac points

Near the Dirac points, the energy spectrum becomes increasingly linear. It is possible to make some approximations in this limit - this is known as the low energy approximation. We know that in our basis we have a point of zero energy at $\vec{k}_0 = \left(\frac{2\pi}{3a}, \frac{2\pi}{\sqrt{3}a} \right)$. Let us define a change in basis:

$$k_x = \frac{2\pi}{3a} + \tilde{k}_x$$

$$k_y = \frac{2\pi}{\sqrt{3}a} + \tilde{k}_y$$

and substitute these new variables into $f(\vec{k})$:

$$f(\vec{k}) = 1 + e^{-i\left(\frac{2\pi}{\sqrt{3}a} + \tilde{k}_y\right)\frac{a\sqrt{3}}{2}} 2 \cos \left(\frac{a}{2} \left[\frac{2\pi}{3a} + \tilde{k}_x \right] \right)$$

$$= 1 - e^{-i\frac{a\sqrt{3}}{2}\tilde{k}_y} 2 \cos \left(\frac{a}{2}\tilde{k}_x + \frac{\pi}{3} \right)$$

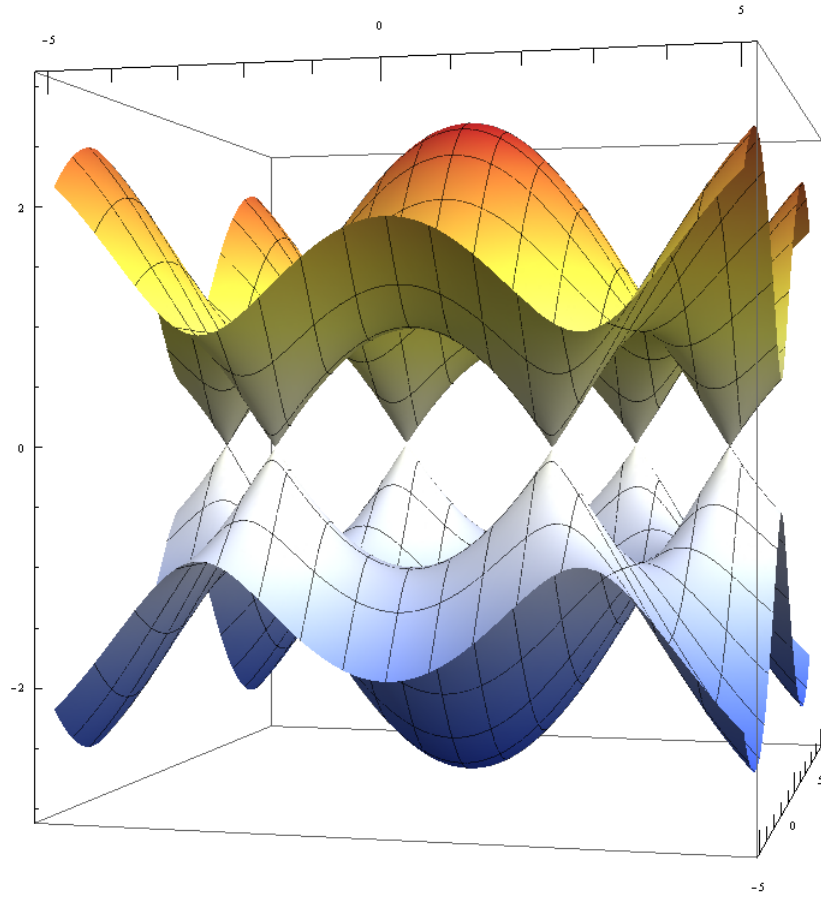


Figure 2.5: Dispersion relation of graphene calculated under the tight-binding model. The six Dirac points bounding the first BZ are shown. Note the linearity of the band structure near these points.

Now, in this new basis, we are interested in positions in k -space close to the Dirac points - corresponding to $\tilde{k}_{x,y} \approx 0$. This justifies Taylor expanding the exponential function around \tilde{k}_y . If we neglect all terms higher than first order in \tilde{k}_y , then $f(\vec{k})$ becomes

$$\begin{aligned} f(\vec{k}) &= 1 - \left(1 - i \frac{a\sqrt{3}}{2} \tilde{k}_y \right) 2 \cos \left(\frac{a\tilde{k}_x}{2} + \frac{\pi}{3} \right) \\ &= 1 - \left(1 - i \frac{a\sqrt{3}}{2} \tilde{k}_y \right) \left(\frac{1}{2} \cos \frac{a\tilde{k}_x}{2} - \frac{\sqrt{3}}{2} \sin \frac{a\tilde{k}_x}{2} \right) \end{aligned}$$

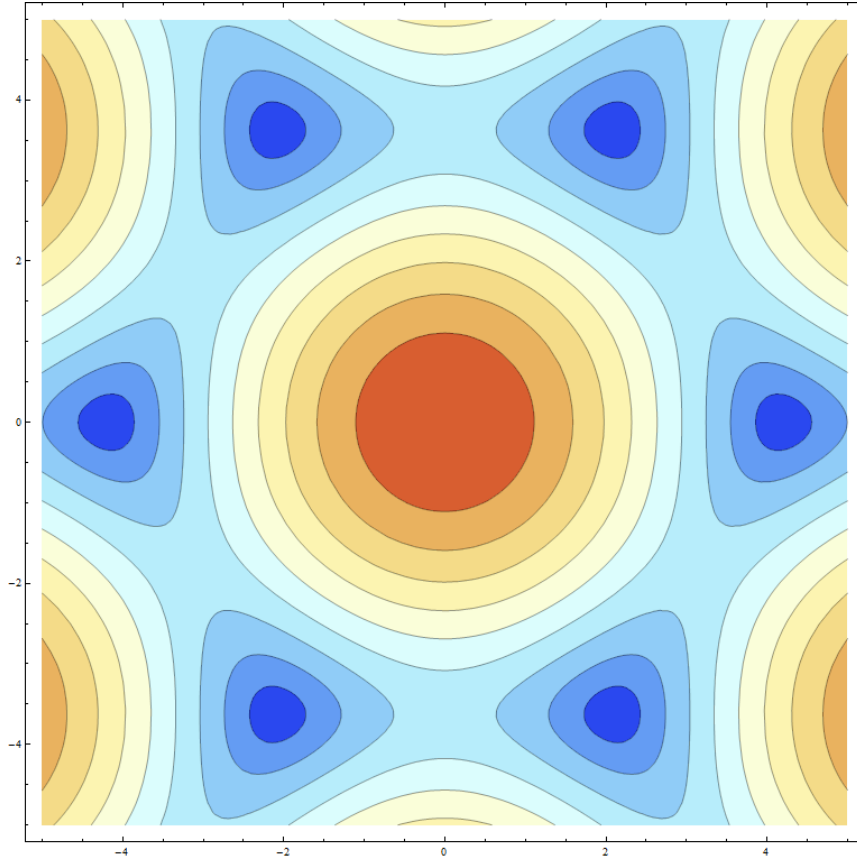


Figure 2.6: A two-dimensional, “top-down” view of the dispersion relation of graphene. The shape and size of the first BZ here are clear, as are the locations of the Dirac points.

and since

$$\begin{aligned}\cos \frac{a\tilde{k}_x}{2} &\approx 1 \\ \sin \frac{a\tilde{k}_x}{2} &\ll 1\end{aligned}$$

near the Dirac points, $f(\vec{k})$ can be simplified further:

$$\begin{aligned}f(\vec{k}) &= 1 - \left(1 - \frac{\sqrt{3}a}{2}\tilde{k}_x - \frac{i\sqrt{3}a}{2}\tilde{k}_y + O(\tilde{k}_x\tilde{k}_y) \dots \right) \\ f(\vec{k}) &= \frac{\sqrt{3}a}{2}\tilde{k}_x + \frac{i\sqrt{3}a}{2}\tilde{k}_y \\ \therefore f^*(\vec{k}) &= \frac{\sqrt{3}a}{2}\tilde{k}_x - \frac{i\sqrt{3}a}{2}\tilde{k}_y\end{aligned}$$

The tight-binding Hamiltonian then becomes

$$H = \gamma \frac{\sqrt{3}}{2} a \begin{bmatrix} 0 & i\tilde{k}_y + \tilde{k}_x \\ -i\tilde{k}_y + \tilde{k}_x & 0 \end{bmatrix}$$

Now we need to take inhomogeneity into account - since electrons scatter when they encounter it. This is done simply by replacing \tilde{k} with its equivalent operator - in this case, since $\vec{p} = \hbar\vec{k}$, we replace \tilde{k} with $\hbar^{-1}\hat{p}$. The Hamiltonian is now

$$\hat{H} = \gamma \frac{\sqrt{3}}{2\hbar} a \begin{bmatrix} 0 & i\hat{p}_y + \hat{p}_x \\ -i\hat{p}_y + \hat{p}_x & 0 \end{bmatrix}$$

where the coefficient $\gamma \frac{\sqrt{3}}{2\hbar} a = v_F$, the Fermi velocity, and finally; this matrix can be separated, transforming the Hamiltonian into

$$\begin{aligned} \hat{H} &= v_F(\sigma_x \cdot \hat{p}_x + \sigma_y \cdot \hat{p}_y) \\ &= v_F(\vec{\sigma} \cdot \vec{p}) \\ &= \hat{H}_D \end{aligned}$$

where \hat{H}_D is the symbol for the Dirac Hamiltonian. To find the eigenvalues of this Hamiltonian, use the characteristic equation $\det \hat{H} - I\lambda = 0$:

$$\begin{vmatrix} -\lambda & i\tilde{k}_y + \tilde{k}_x \\ -i\tilde{k}_y + \tilde{k}_x & -\lambda \end{vmatrix} = 0 \Rightarrow \lambda = \pm \sqrt{\tilde{k}_x^2 + \tilde{k}_y^2}$$

Since $\hat{H}\psi_k = \epsilon_k\psi_k$, we can say that

$$\epsilon_k = \pm \hbar v_F \sqrt{\tilde{k}_x^2 + \tilde{k}_y^2}$$

Chapter 3

Graphene superlattice

Investigation of a material's current-voltage characteristics is a commonplace activity in physics, but what would a purely theoretical enquiry into such characteristics of graphene yield? Esaki and Tsu's paper[1] investigated the properties of semiconductor superlattices, using a path integration method to calculate drift velocity, and predicted the phenomena of Bloch oscillation and negative differential conductivity. Their electronic energy band model of a superlattice (an infinitely long, one-dimensional periodic lattice structure) was a sinusoidal one.

Graphene's dispersion relation is linear, and its band structure consists of intersections of the conduction and valence bands, suggesting that a graphene superlattice would exhibit a periodic but triangular arrangement as shown in Figure 3.1. Our first goal is to use the same method as employed by Esaki and Tsu to investigate the effects of an applied electric field on the drift velocity of charge carriers in graphene, in the context of this unique band structure. A graphene superlattice displaying the same or similar miniband formation

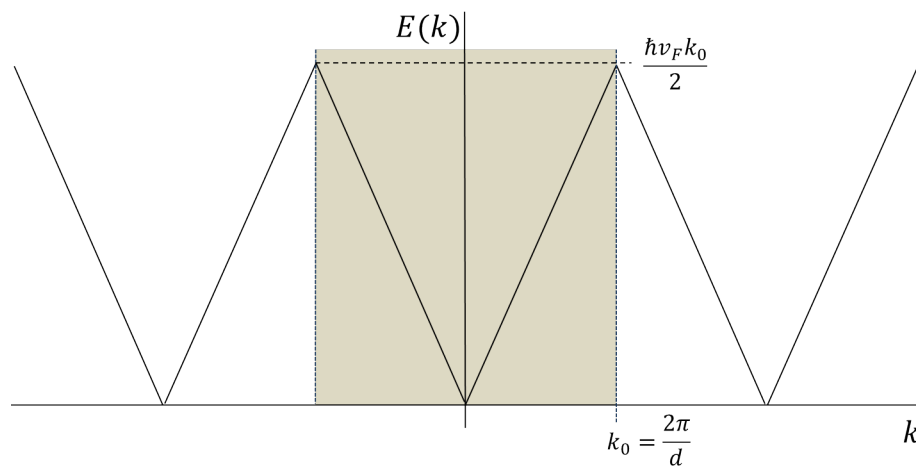


Figure 3.1: This diagram presents our simple model for a graphene superlattice with lattice vector spacing k_0 . This band structure also shows the (relative) directions of propagation of the charge carriers.

might be realised as follows. Consider an insulator or semiconductor substrate patterned with periodically arranged, thin strips of metallic contact material all connected to a voltage source. On this substrate it is feasible to deposit or grow a monatomically thin sheet of graphene. The metallic contacts generate a series of potential barriers of variable height. We suggest that this may be one way of producing a strongly coupled series of quantum wells and barriers in the potential landscape, leading to the formation of minibands. See Figure 3.2 for a diagram of this setup.

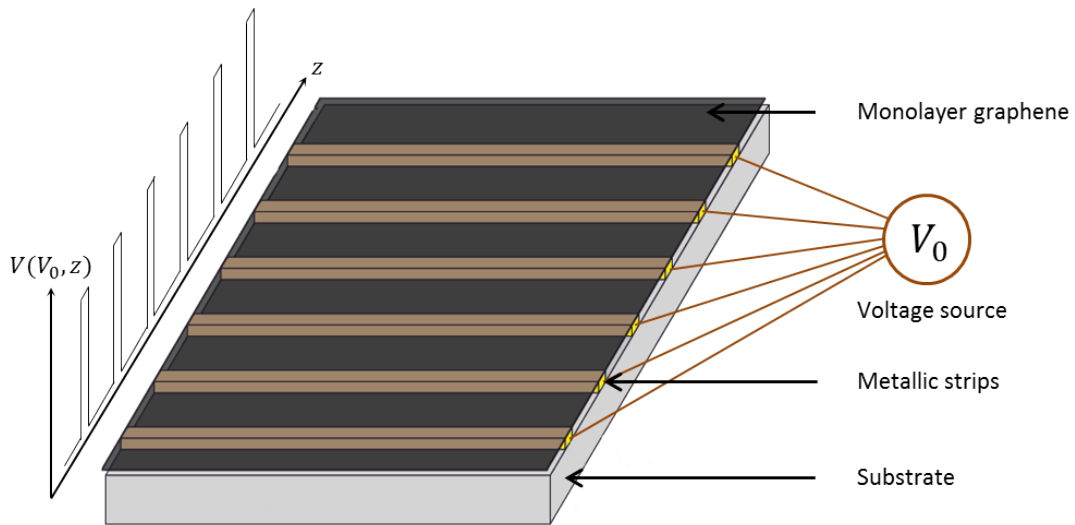


Figure 3.2: This diagram presents our simple model for a graphene superlattice with lattice vector spacing k_0 . This band structure also shows the (relative) directions of propagation of the charge carriers.

3.1 Modelling miniband structure of graphene superlattice

3.1.1 Infinite Fourier series

We know from the study of Fourier analysis that any periodic function can be represented as some finite, or infinite, summation of sinusoidal waveforms. Since the band structure we are dealing with resembles a triangular wave, an accurate mathematical description could be formulated by drawing analogies between the triangular waveform and graphene's periodic/linear band structure, thus allowing us to derive a very specific Fourier series which represents the energy-momentum relation of the superlattice's first miniband.

The Fourier series of a function $f(x)$ is given by:

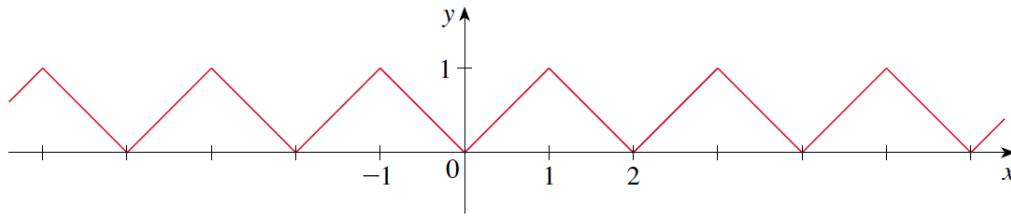
$$f(x) = a_0 + \sum_{n=1}^{\infty} a_n \cos \frac{n\pi x}{L} + b_n \sin \frac{n\pi x}{L} \quad (3.1)$$

$$a_0 = \frac{1}{2L} \int_{-L}^L f(x) dx \quad (3.2)$$

$$a_n = \frac{1}{L} \int_{-L}^L f(x) \cos \frac{n\pi x}{L} dx \quad (3.3)$$

$$b_n = \frac{1}{L} \int_{-L}^L f(x) \sin \frac{n\pi x}{L} dx \quad (3.4)$$

Figure 3.3 is a basic diagram showing this simple arrangement. To draw the



$$f(x) = |x| \quad \text{for } -1 \leq x \leq 1 \text{ and } f(x+2) = f(x) \text{ for all } x.$$

Figure 3.3: This is the model used to begin tailoring a specific Fourier series that represents a graphene superlattice's band structure.

analogies between Figure 3.3 with a graphene superlattice's band structure (Figure 3.1), we see that:

$$x \equiv k \quad (3.5)$$

$$L \equiv \frac{k_0}{2} \quad (3.6)$$

$$f(x) \equiv \hbar v_F |k|; \quad -L \leq k \leq L \quad (3.7)$$

$$(3.8)$$

It is also important to remember $E(k) = E(k + k_0)$ - the periodicity of the

function. The next step is to calculate each of the coefficients a_0 , a_n and b_n .

$$a_0 = \frac{1}{k_0} \int_{-k_0/2}^{k_0/2} \hbar v_F |k| dk \quad (3.9)$$

$$= \frac{\hbar v_F k |k|}{k_0} \Big|_{-k_0/2}^{k_0/2} \quad (3.10)$$

$$= \frac{1}{4} \hbar v_F |k_0| \quad (3.11)$$

$$a_n = \frac{2}{k_0} \int_{-k_0/2}^{k_0/2} \hbar v_F |k| \cos \frac{2n\pi k}{k_0} dk \quad (3.12)$$

$$= \frac{2\hbar v_F}{k_0} \frac{|k|k_0^2}{4n^2\pi^2 k} \left(\cos \frac{2n\pi k}{k_0} + \frac{2n\pi k}{k_0} \sin \frac{2n\pi k}{k_0} \right) \Big|_{-k_0/2}^{k_0/2} \quad (3.13)$$

$$= \frac{\hbar v_F |k_0|}{n^2\pi^2} (\cos n\pi + n\pi \sin n\pi - 1) \quad (3.14)$$

And since $f(k) = |k| \sin \beta k$ is an odd function, we know that

$$b_n = \frac{2}{k_0} \int_{-k_0/2}^{k_0/2} \hbar v_F |k| \sin \frac{2n\pi k}{k_0} dk = 0 \quad (3.15)$$

So all odd terms vanish from the series. Our function then is given by the following:

$$E(k) = \frac{\hbar v_F |k_0|}{4} + \sum_{n=1}^{\infty} \frac{\hbar v_F |k_0|}{n^2\pi^2} (\cos n\pi + n\pi \sin n\pi - 1) \cos \frac{2n\pi k}{k_0} \quad (3.16)$$

Note that $\sin n\pi = 0$, so that term vanishes. The term remaining in brackets is always equal to zero or -2 :

$$(\cos n\pi - 1) = \begin{cases} -2 & n \text{ odd} \\ 0 & n \text{ even} \end{cases} \quad (3.17)$$

Thus the series for $E(k)$ becomes:

$$E(k) = \frac{\hbar v_F k_0}{4} \left(1 - \frac{8}{\pi^2} \sum_{n=1}^{\infty} \frac{1}{(2n-1)^2} \cos(2n-1) \frac{2\pi k}{k_0} \right) \quad (3.18)$$

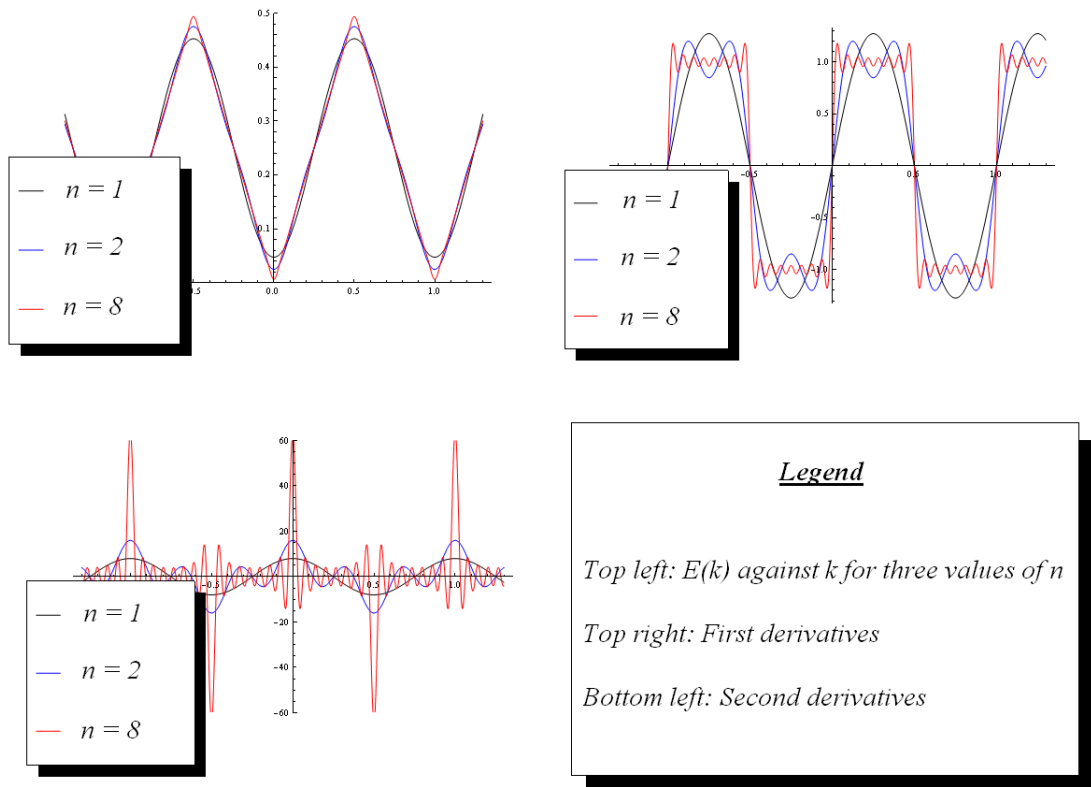


Figure 3.4: These three graphs demonstrate the validity of this Fourier series as used to model a graphene superlattice. Note, when looking at the graph of the second derivative of the series, that as n increases, Dirac delta peaks begin to emerge.

Figure 3.4 displays this series and its derivatives. The next step is to differentiate this equation twice with respect to k , and substitute in $k = eF_0t/\hbar$, since we are considering the simplest case of application of a static field, to get $E(k)$ in terms of t ready for the integration¹. The result is shown below - for full working, please refer to the appendix.

$$\frac{\partial^2 E}{\partial k^2} = \frac{8\hbar v_F}{k_0} \sum_{n=1}^{\infty} \cos(2n-1) \frac{2\pi e F_0 t}{\hbar k_0} \quad (3.19)$$

¹The assumption that $k = eF_0t/\hbar$ implies that at $t = 0$, $k = 0$. This is easily justifiable here, as we are working with a pure (undoped) lattice structure.

The expression for v_d then becomes as follows, and is ready to be integrated:

$$v_d = \frac{eF_0}{\hbar^2} \frac{8\hbar v_F}{k_0} \int_0^\infty dt e^{-t/\tau} \sum_{n=1}^\infty \cos \beta t, \quad (3.20)$$

where $\beta = (2n - 1) \frac{2\pi e F_0}{\hbar k_0}$. This integral requires a minimal amount of mathematical working, as it is a standard integral given by:

$$\int_0^\infty dt e^{-t/\tau} \cos \beta t = \frac{\tau}{1 + (\beta\tau)^2} \quad (3.21)$$

$$= \frac{\tau}{1 + (2n - 1)^2 \left(\frac{2\pi e F_0 \tau}{k_0 \hbar} \right)^2} \quad (3.22)$$

The final step is to compute the summation:

$$v_d = \frac{eF_0}{\hbar} \frac{8v_F}{k_0} \sum_{n=1}^\infty \frac{\tau}{(2n - 1)^2 \left(\frac{2\pi e F_0 \tau}{k_0 \hbar} \right)^2 + 1} \quad (3.23)$$

$$= v_F \tanh \frac{\hbar k_0}{4eF_0\tau} \quad (3.24)$$

The result for the drift velocity in terms of an applied static field F_0 and scattering time τ is given by the following:

$$v_d = v_F \tanh \frac{\hbar k_0}{4eF_0\tau} \quad (3.25)$$

Infinite conductivity appears when an ideal graphene superlattice is subject to a static bias. This result will be investigated further under other mathematical frameworks, and under the influence of more complex applied fields.

A recent paper[56] reports the observation of negative differential resistance in a three-terminal graphene-based device similar to a FET, a device utilising the zero band gap property of graphene.

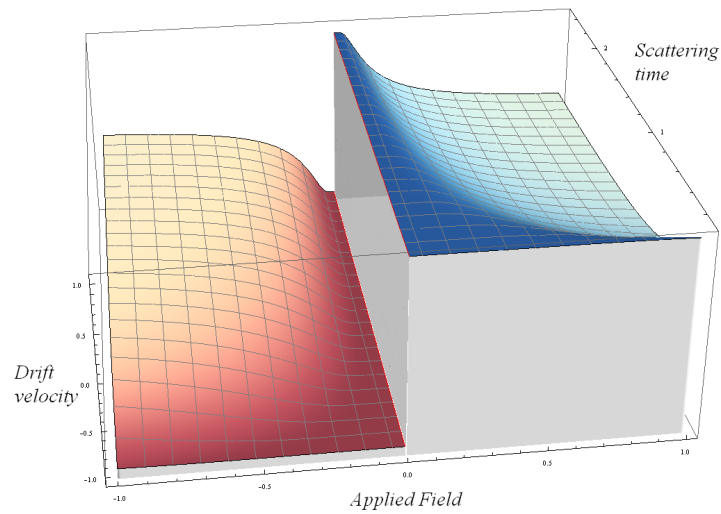


Figure 3.5: This plot demonstrates the appearances of both infinite conductivity and negative differential conductivity, the latter being when the charge-carriers within the graphene superlattice are increasingly localised by the application of a DC field. The former is demonstrated by the discontinuity at zero applied field, and might suggest multistability of current flow, meaning that charge-carriers will propagate at their maximum speed v_F in any direction when no force is applied. This could be a consequence of their quasi-relativistic nature as Dirac quasiparticles.

3.1.2 Formal representation of band structure using Heaviside functions

A particularly formal way of mathematically representing a triangular waveform such as it mimics graphene's band structure is to use products of Heaviside functions to construct a pseudo-piecewise function. The below equation is the result of discussion (and some trial and error work) between Professor

Kusmartsev and myself:

$$E(k) = \sum_{n=-\infty}^{\infty} \left\{ (-1)^n \left(\hbar v_F k - \frac{\hbar v_F k_0 n}{2} \right) + \frac{\hbar v_F k_0}{2} \left(\frac{1 - (-1)^n}{2} \right) \right\} \quad (3.26)$$

$$\Theta \left((n+1) \frac{\hbar v_F k_0}{2} - \hbar v_F k \right) \Theta \left(\hbar v_F k - \frac{\hbar v_F k_0 n}{2} \right) \quad (3.27)$$

The three distinct sections of this equation construct the function as such: The two Heaviside functions “section” the function, that is divide it into sections corresponding to the terms in the summation. The term in curly brackets generates either a positive slope or negative slope in its relevant “section”, and also shifts the line up by a value equal to E_{max} if the slope is negative (because it would originate from the x axis and decrease from there). The result is the function you see.

For simplicity, from hereon the Heaviside and Delta functions that contain the coefficient $(n+1)$ will be denoted with subscript 1, and those functions that contain the coefficient n will be denoted with subscript 0; and the term in curly brackets will be simply called Ψ . That is:

$$E(k) = \sum_{n=-\infty}^{\infty} \Psi \Theta_1 \Theta_0 \quad (3.28)$$

Now this must be differentiated twice with respect to k , as follows

$$\frac{\partial^2 E}{\partial k^2} = \sum_{n=-\infty}^{\infty} \Psi \left(\Theta_1 \frac{\partial^2 \Theta_0}{\partial k^2} + \Theta_0 \frac{\partial^2 \Theta_1}{\partial k^2} + 2 \frac{\partial \Theta_0 \partial \Theta_1}{\partial k^2} \right) \quad (3.29)$$

$$+ \frac{\partial \Psi}{\partial k} \left(\Theta_1 \frac{\partial \Theta_0}{\partial k} + \Theta_0 \frac{\partial \Theta_1}{\partial k} \right) + \Theta_0 \Theta_1 \frac{\partial^2 \Psi}{\partial k^2} \quad (3.30)$$

The last term on the right is zero. Now to substitute in all the derivatives:

$$\frac{\partial^2 E}{\partial k^2} = \sum_{n=-\infty}^{\infty} (\hbar v_F)^2 \Psi (\Theta_1 \delta'_0 + \Theta_0 \delta'_1 - 2 \delta_0 \delta_1) + (-1)^n (\Theta_1 \delta_0 - \Theta_0 \delta_1) \quad (3.31)$$

The next step is to integrate $\frac{\partial^2 E}{\partial k^2} e^{-\frac{t}{\tau}}$ with respect to t , so we need to express $\frac{\partial^2 E}{\partial k^2}$ as a function of t . This is done simply by recalling that $k = e F_0 t / \hbar$, as

calculated using the kinematic and Newton's equations earlier: There are five separate terms in the integrand. These are as follows:

1. $(\hbar v_F)^2 \Psi \Theta_1 \delta'_0 e^{-\frac{t}{\tau}}$
2. $(\hbar v_F)^2 \Psi \Theta_0 \delta'_1 e^{-\frac{t}{\tau}}$
3. $-(\hbar v_F)^2 \Psi \delta_0 \delta_1 e^{-\frac{t}{\tau}}$
4. $-(-1)^n (\hbar v_F)^2 \Theta_0 \delta_1 e^{-\frac{t}{\tau}}$
5. $(-1)^n (\hbar v_F)^2 \Theta_1 \delta_0 e^{-\frac{t}{\tau}}$

Note that integrating number 3 with respect to t will give zero, as there is a product of two delta functions of different arguments. To perform the integrations, some important integral properties of delta functions must be utilised. These are outlined below. The next step is to multiply it by $e^{-t/\tau}$ and integrate with respect to t from zero to infinity. However, we are dealing now with functions that must be integrated carefully, bearing in mind the necessary properties. These are:

$$(i) \quad \int_0^{\infty} f(t) \Theta(b - at) \delta'(ct - d) e^{-t/\tau} dt \quad (3.32)$$

$$= \frac{ae^{-\frac{d}{ct}} \delta\left(b - \frac{ad}{c}\right) f\left(\frac{d}{c}\right) + \frac{1}{\tau} e^{-\frac{d}{ct}} \Theta\left(b - \frac{ad}{c}\right) \left[f\left(\frac{d}{c}\right) - \tau f'\left(\frac{d}{c}\right)\right]}{|c|^2}$$

$$(ii) \quad \int_0^{\infty} f(t) \Theta(at - b) \delta'(d - ct) e^{-t/\tau} dt \quad (3.34)$$

$$= \frac{-ae^{-\frac{d}{ct}} \delta\left(b - \frac{ad}{c}\right) f\left(\frac{d}{c}\right) + \frac{1}{\tau} e^{-\frac{d}{ct}} \Theta\left(\frac{ad}{c} - b\right) \left[f\left(\frac{d}{c}\right) - \tau f'\left(\frac{d}{c}\right)\right]}{|c|^2}$$

$$(3.35)$$

$$(iii) \quad \int_0^{\infty} \Theta(at - b) \delta(d - ct) e^{-t/\tau} dt = \frac{e^{-\frac{d}{ct}} \Theta\left(\frac{d}{c}\right) \Theta\left(\frac{ad}{c} - b\right)}{|c|} \quad (3.36)$$

$$(iv) \quad \int_0^{\infty} \Theta(b - at) \delta(ct - d) e^{-t/\tau} dt = \frac{e^{-\frac{d}{ct}} \Theta\left(\frac{d}{c}\right) \Theta\left(b - \frac{ad}{c}\right)}{|c|} \quad (3.37)$$

There are four terms to integrate, each using one of the integration rules outlined above. Below, the results only are given - please refer to the appendix for the full working. Term 1 uses rule (i), term 2 uses rule (ii), term 4 uses (iii), and 5, (iv); giving the four contributions to v_d . Hence, below is the result for v_d :

$$v_d = \frac{eF_0}{\hbar^2} \sum_{n=0}^{\infty} \left[\frac{\hbar^2}{\tau e^2 |F_0|^2} \left(\left[\frac{1 - (-1)^n}{2} \right] \frac{\hbar v_F k_0}{2} - \tau (-1)^n e v_F F_0 \right) \right] \left(e^{-\frac{\hbar k_0 n}{2eF_0\tau}} + e^{-\frac{\hbar k_0(n+1)}{2eF_0\tau}} \right) \\ + \frac{(-1)^n \hbar^2 v_F}{e |F_0|} \left[\Theta\left(\frac{\hbar k_0 n}{2eF_0}\right) e^{-\frac{\hbar k_0 n}{2eF_0\tau}} - \Theta\left(\frac{\hbar k_0(n+1)}{2eF_0}\right) e^{-\frac{\hbar k_0(n+1)}{2eF_0\tau}} \right]$$

The final step is to calculate the four summations that correspond to the four results just calculated. Once more, please refer to the appendix for the calculation in full. The final result is as follows:

$$v_d = v_F \tanh\left(\frac{\hbar k_0}{4eF\tau}\right) \quad (3.38)$$

Which is precisely the same as calculated using an infinite Fourier series approach, lending credence to the result. Again, this suggest the appearance of infinite conductivity at zero field strength.

3.1.3 Testing results using a parabolic approximation technique

It is possible to use a simple approximation to model the miniband structure of the graphene superlattice. To avoid the discontinuities inherent in the

delta functions' peaks, we “smooth away” the sharp peaks of the triangular energy spectrum into parabolae. Our function then is linear everywhere, like before, except inside small intervals where the discontinuity would normally occur (the peaks and troughs of the spectrum). Below (Figure 3.6) is a diagram of this new, approximated spectrum.

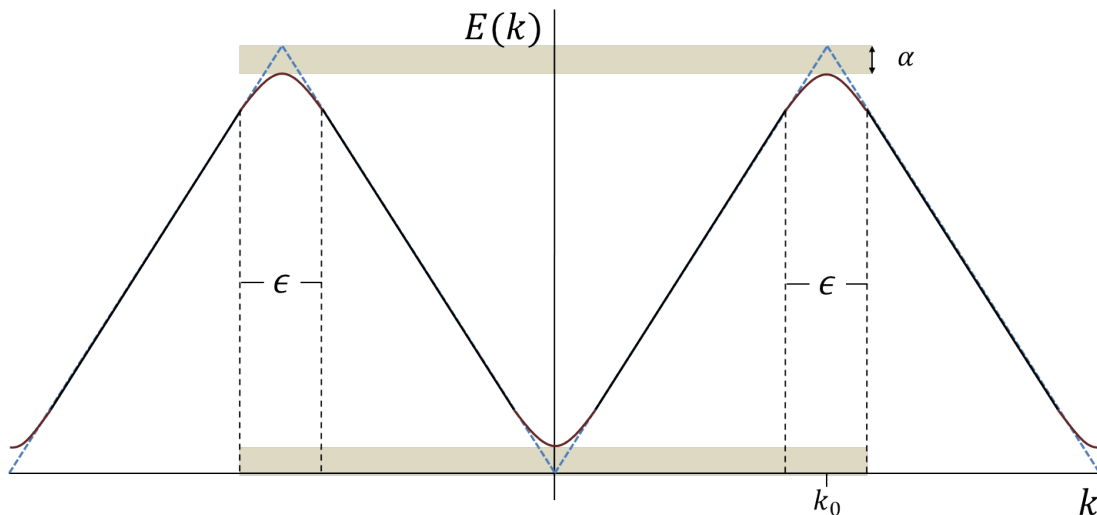


Figure 3.6: The intervals shown here have width ϵ , which is to be taken to zero upon calculation of the final result. The “discrepancy” denoted α is a consequence of this parabolic approximation, and has the effect of reducing the reach of the sharp points up from $E(k) = 0$ to $E(k) + \alpha$ and down from $E(k) = E_{max}$ to $E(k) = E_{max} - \alpha$. As ϵ gets closer and closer to zero, α will likewise disappear. The light blue lines on this diagram indicate where the spectrum originally would have been before the approximation is used.

Some important points to remember as we continue are the following

1. That the curved sections are quadratic parabolae
2. That the nature of the curves means that the peaks and troughs are not

quite as high or low as they were

3. That we must define our new function and its derivative as being continuous as the function crosses from being linear to being parabolic
4. That we must be able to take a limit in such a way that the approximation can become zero
5. When performing the integration, we must bear in mind the necessity of defining new, correct limits
6. That the result we gain might not agree with the results already calculated - this will tell us (assuming the approximation is valid) that the previous results are inaccurate

This approximation is useful in two ways. Firstly, since such effects as corrugation might be the source of the rounding of the otherwise discontinuous spectrum, in this way it may be possible to simply model these effects and discuss how they may relate to the phenomenon of infinite conductivity. Secondly, when the limit $\epsilon \rightarrow 0$ is taken, if it is the same as the two already calculated for this model of a graphene superlattice, it serves to provide further legitimacy.

Remembering the previous formulae that have been derived, and studying the above model diagram, we can say that this piecewise function can be

written as the following:

$$E(k) = \begin{cases} \sum_{n=0}^{\infty} \left[\frac{\hbar^2 k^2}{2m_*} + \alpha \right] (-1)^n + \frac{1 - (-1)^n}{2} \frac{\hbar v_F k_0}{2} & \text{inside the intervals} \\ \sum_{n=0}^{\infty} \left[\hbar v_F k - \frac{\hbar k_0 n}{2} \right] (-1)^n + \frac{1 - (-1)^n}{2} \frac{\hbar v_F k_0}{2} & \text{otherwise,} \end{cases} \quad (3.39)$$

where α is to be determined. An aside: Recall that the dispersion relation for graphene is given by $E(k) = \hbar v_F k$, and the maxima in the spectrum occur at $k = \frac{nk_0}{2}$, $n \in \mathbb{N}$. This means that the amplitude of the spectrum is $E_{max}(k) = \hbar v_F \frac{k_0}{2}$. Now, equate the derivatives of equations 3.39 at a point where they meet (bearing in mind the relevant term in the summation), say at $n = 0 \Rightarrow k = \frac{\epsilon}{2}$. This leaves us with

$$\sum_{n=0}^{\infty} \frac{\hbar^2 k}{m_*} (-1)^n = \sum_{n=0}^{\infty} \hbar v_F (-1)^n \quad (3.40)$$

$$\frac{\hbar^2 k}{m_*} = \hbar v_F \quad (3.41)$$

$$\frac{\hbar \epsilon}{2m_*} = v_F \quad (3.42)$$

$$\epsilon = \frac{2m_* v_F}{\hbar} \quad (3.43)$$

Now equate equations 3.39 on the same boundary, and substitute 3.43 into the result to find α :

$$\frac{\hbar^2 k^2}{2m_*} + \alpha = \hbar v_F k \quad (3.44)$$

$$\frac{\hbar^2 \epsilon^2}{8m_*} + \alpha = \frac{\hbar v_F \epsilon}{2} \quad (3.45)$$

$$\alpha = \frac{\hbar v_F \epsilon}{2} - \frac{\hbar^2 \epsilon^2}{8m_*} \quad (3.46)$$

$$\alpha = \frac{1}{2} m_* v_F^2 \quad (3.47)$$

So now we know $E(k)$ fully, it is expressed as follows:

$$E(k) = \begin{cases} \sum_{n=0}^{\infty} \left[\frac{\hbar^2 k^2}{2m_*} + \frac{1}{2} m v_F^2 \right] (-1)^n + \frac{1 - (-1)^n \hbar v_F k_0}{2} & ; nk_0 - \frac{\epsilon}{2} \leq k \leq nk_0 + \frac{\epsilon}{2} \\ \sum_{n=0}^{\infty} \left[\hbar v_F k - \frac{\hbar k_0 n}{2} \right] (-1)^n + \frac{1 - (-1)^n \hbar v_F k_0}{2} & ; nk_0 + \frac{\epsilon}{2} \leq k \leq (n+1)k_0 - \frac{\epsilon}{2} \end{cases} \quad (3.48)$$

$$\frac{\partial^2 E}{\partial k^2} = \begin{cases} \sum_{n=0}^{\infty} \frac{\hbar^2}{m} (-1)^n & ; nk_0 - \frac{\epsilon}{2} \leq k \leq nk_0 + \frac{\epsilon}{2} \\ 0 & ; nk_0 + \frac{\epsilon}{2} \leq k \leq (n+1)k_0 - \frac{\epsilon}{2} \end{cases} \quad (3.49)$$

$$v_d = \frac{eF}{\hbar^2} \int_0^{\infty} \left\{ \sum_{n=0}^{\infty} \frac{\hbar^2}{m} (-1)^n \right\} e^{-t/\tau} dt \quad (3.50)$$

This equation above is simply the equation for drift velocity, with the non-zero part of $\frac{\partial^2 E}{\partial k^2}$ substituted in. However, it isn't correct, because we need to change the limits quite drastically. Actually, there are an infinite series of integrals, because the function $\frac{\partial^2 E}{\partial k^2}$ is periodically non-zero in the intervals defined before. This means the above equation should look like the following

$$v_d = \frac{eF}{m_*} \sum_{n=0}^{\infty} (-1)^n \left\{ \int_0^{\frac{\epsilon}{2}} e^{-t/\tau} + \int_{k_0 - \frac{\epsilon}{2}}^{k_0 + \frac{\epsilon}{2}} e^{-t/\tau} + \int_{2k_0 - \frac{\epsilon}{2}}^{2k_0 + \frac{\epsilon}{2}} e^{-t/\tau} + \dots \right\} \quad (3.51)$$

We can incorporate the summation outside the brackets into the integration summation - either by alternating +1 and -1 coefficients between each successive term, or perhaps more usefully, by switching the limits of every 2nd term (i.e. each term that would have had a -1 coefficient).

$$v_d = \frac{eF}{m_*} \left\{ \int_0^{\frac{\epsilon}{2}} e^{-t/\tau} + \int_{k_0 + \frac{\epsilon}{2}}^{k_0 - \frac{\epsilon}{2}} e^{-t/\tau} + \int_{2k_0 - \frac{\epsilon}{2}}^{2k_0 + \frac{\epsilon}{2}} e^{-t/\tau} + \dots \right\} \quad (3.52)$$

Computing the integral gives us

$$v_d = -\frac{eF\tau}{m_*} \left\{ e^{-t/\tau} \Big|_0^{\frac{\epsilon}{2}} + e^{-t/\tau} \Big|_{k_0 + \frac{\epsilon}{2}}^{k_0 - \frac{\epsilon}{2}} + e^{-t/\tau} \Big|_{2k_0 - \frac{\epsilon}{2}}^{2k_0 + \frac{\epsilon}{2}} + \dots \right\} \quad (3.53)$$

It is simplest to extract the first term in the curly brackets above, then we can formulate what remains in the bracket as an infinite series.

$$v_d = -\frac{eF\tau}{m_*} \left(e^{\epsilon\hbar/2eF\tau} - 1 \right) - \frac{eF\tau}{m_*} \left\{ e^{-t/\tau} \begin{bmatrix} k_0 - \frac{\epsilon}{2} \\ k_0 + \frac{\epsilon}{2} \end{bmatrix} + e^{-t/\tau} \begin{bmatrix} 2k_0 + \frac{\epsilon}{2} \\ 2k_0 - \frac{\epsilon}{2} \end{bmatrix} + \dots \right\} \quad (3.54)$$

The infinite series of terms in the curly brackets can be expressed most simply as two summations:

$$\sum_{n=1}^{\infty} (-1)^n e^{-\alpha \left(\frac{nk_0}{2} + \beta \right)} + \sum_{n=1}^{\infty} (-1)^{n-1} e^{-\alpha \left(\frac{nk_0}{2} - \beta \right)} \quad (3.55)$$

where $\alpha = \hbar k_0 / 2eF\tau$ and $\beta = \epsilon / 2$. Calculating these two summations, and recalling that $m_* = \hbar\epsilon / 2v_F$ gives:

$$v_d = \left(\frac{-2v_F eF\tau}{\hbar\epsilon} \right) \left[\left(e^{-\frac{\hbar\epsilon}{2eF\tau}} - 1 \right) + \sum_{n=1}^{\infty} (-1)^n e^{-\alpha \left(\frac{nk_0}{2} + \beta \right)} + \sum_{n=1}^{\infty} (-1)^{n-1} e^{-\alpha \left(\frac{nk_0}{2} - \beta \right)} \right] \quad (3.56)$$

$$= \left(\frac{-2v_F eF\tau}{\hbar\epsilon} \right) \left[\left(e^{-\frac{\hbar\epsilon}{2eF\tau}} - 1 \right) + \frac{(e^{\alpha\beta} - e^{-\alpha\beta})}{1 + e^{\frac{k_0\alpha}{2}}} \right] \quad (3.57)$$

$$= \frac{2eFv_F\tau}{\hbar\epsilon} \left(1 - e^{-\frac{\epsilon\hbar}{2eF\tau}} - \frac{2 \sinh \left\{ \frac{\epsilon\hbar}{2eF\tau} \right\}}{e^{\frac{\hbar k_0}{2eF\tau}} + 1} \right) \quad (3.58)$$

Figures 3.7 and 3.8 display what effect the value of ϵ has on the relationship between the drift velocity v_d and the applied field F .

$$\lim_{\epsilon \rightarrow 0} \frac{2eFv_F\tau}{\hbar\epsilon} \left(1 - e^{-\frac{\epsilon\hbar}{2eF\tau}} - \frac{2 \sinh \left\{ \frac{\epsilon\hbar}{2eF\tau} \right\}}{e^{\frac{\hbar k_0}{2eF\tau}} + 1} \right) \quad (3.59)$$

$$= v_F \left\{ \frac{e^{\frac{\hbar k_0}{2eF\tau}} - 1}{e^{\frac{\hbar k_0}{2eF\tau}} + 1} \right\} \quad (3.60)$$

$$v_d = v_F \tanh \frac{\hbar k_0}{4eF\tau} \quad (3.61)$$

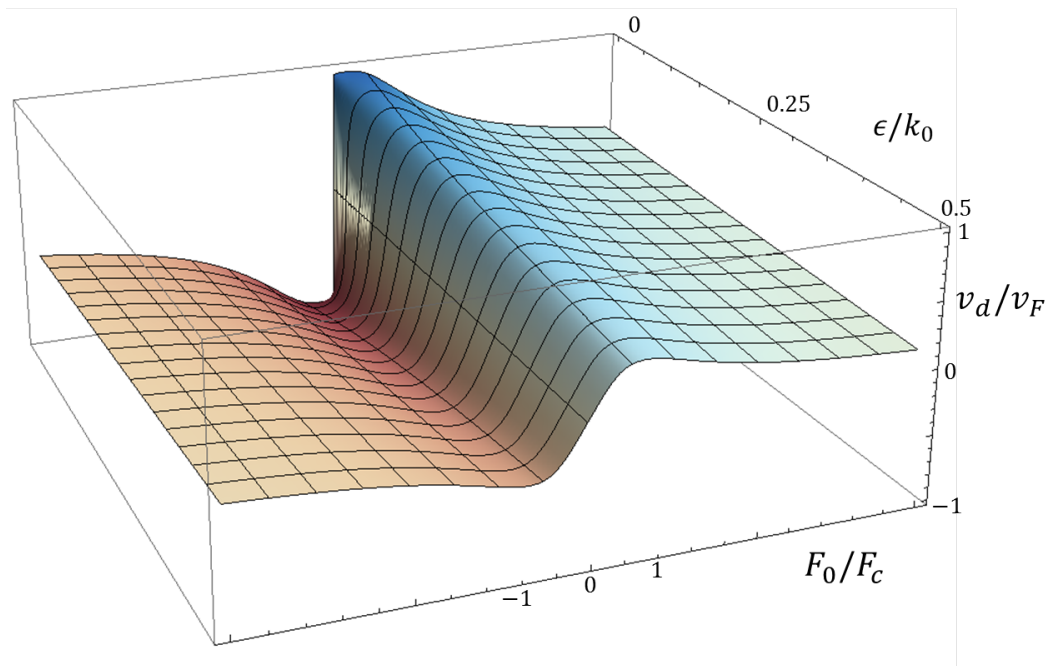


Figure 3.7: This 3D plot helps demonstrate how the maximal values that drift velocity takes, and the corresponding values of the applied field for which they occur, change with the scale of the smoothing - represented by the quantity ϵ .

which is in perfect agreement with the result calculated when the band structure was expressed as an infinite Fourier series.

Further analysis of charge-carrier behaviour in graphene superlattices was written for a paper to be submitted for publication, and is contained within Appendix B as a preprint version.

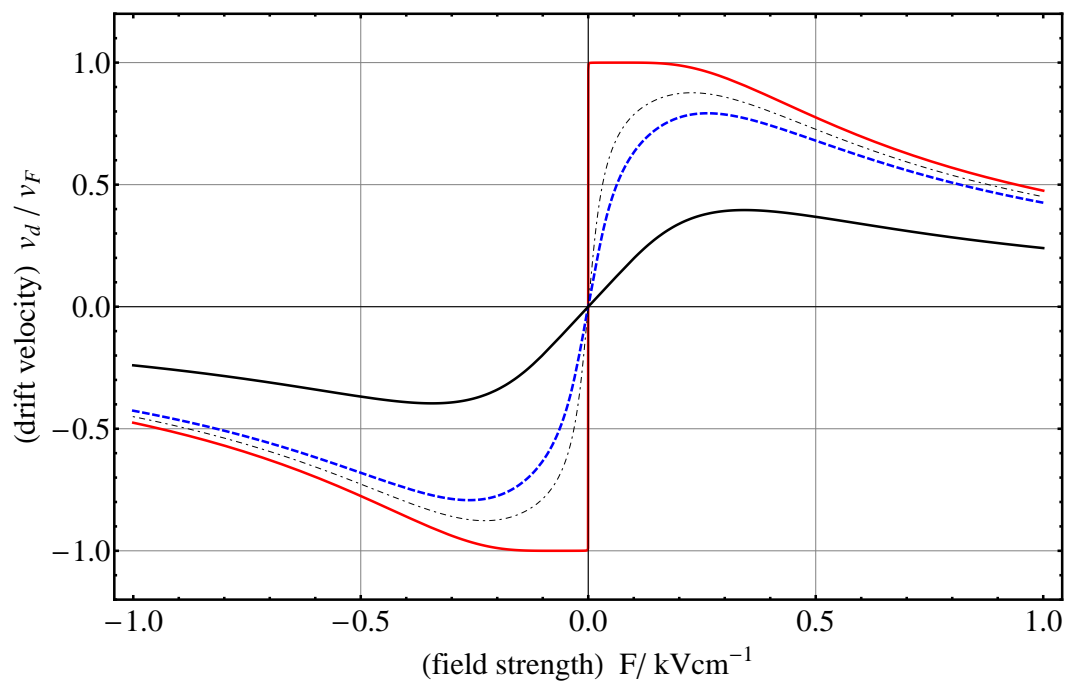


Figure 3.8: This graph helps to show how decreasing the value of ϵ forces the curve to tend to a hyperbolic tangent curve in $1/F$.

Chapter 4

Suggestions and further work

There remain several relatively unexplored avenues of interest closely related to the research in this thesis. Investigation, both theoretical and experimental, into the field of semiconductor superlattices, has never really slowed since 1970. Indeed, since the advent of graphene-related research, interest in superlattice systems has seen yet another surge. The unity of these two topics motivated my own interest into the possibility of using graphene, or another material with similar properties (specifically, the linear relation between energy and momentum), as the fundamental constituent of a superlattice. This idea forms the basis of our paper (see supplementary materials at the end of this thesis for a preprint version), which we are to submit to PRL in the near future.

The topic of effects of magnetic fields applied to superlattices is notably absent in this work. This area is being looked at by colleagues of mine at Loughborough University and has formed the basis of several theses by research students at the University Of Nottingham [53, 54, 55]. All effort expended for this work has been put into examining current-voltage and charge density characteristics and how they change under different, increasingly complex, applied external biases.

Certain circumstances seem to indicate that superlattices can be forced into a so called "active region", in which all interesting phenomena occur. These include NDV, Bloch oscillations, gain effects [7, 8], and absolute negative conductivity [52] due to multistability. The majority of this research turned towards the possibility of using superlattices to generate radiation, particularly in the Terahertz range. More accurately, the work focusses on tunability of the system under different applied field configurations: that is, how the applied fields can be altered in order to manipulate the shape of the drift velocity - field characteristics. In this way, it seems possible to find multiple

ways of localising the charge-carriers in the superlattice as they propagate, thus causing them to accelerate, and ultimately radiate. The frequency of the radiation, in the same way as the behaviour of the current-voltage relation, appears to be tunable.

Graphene has been the subject of an immense amount of interest, especially since Geim and Novoselov won the Nobel Prize in Physics for its discovery in 2010. Its applications to electronics and nanotechnology notwithstanding, the discovery of stable, monolayer graphene, and its fascinating properties, created an opportunity to direct my superlattice research towards the properties that a superlattice made from graphene might have. As far as possible, I have aimed to maintain an analytical approach to the investigation of current-voltage characteristics of a superlattice constructed from graphene or other materials which exhibit the rare linear energy-momentum relation, bearing in mind the possibilities for generating emitted radiation using these superlattice systems. In this way I hope to have provided a transparent foundation for further work in this direction - perhaps for an investigation into applying alternating fields to the graphene superlattice in the same way as was done for the semiconductor superlattice.

Appendix A

Mathematics

A.1 Calculation of $\frac{\partial^2 E(k)}{\partial k^2}$ for Fourier series model

$$E(k) = \frac{\hbar v_F k_0}{4} - \frac{2\hbar v_F k_0}{\pi^2} \sum_{n=1}^{\infty} \frac{1}{(2n-1)^2} \cos(2n-1) \frac{2\pi k}{k_0} \quad (\text{A.1})$$

$$\frac{\partial E}{\partial k} = + \frac{2\hbar v_F k_0}{\pi^2} \sum_{n=1}^{\infty} \frac{2\pi}{k_0(2n-1)} \sin(2n-1) \frac{2\pi k}{k_0} \quad (\text{A.2})$$

$$\frac{\partial^2 E}{\partial k^2} = \frac{2\hbar v_F k_0}{\pi^2} \sum_{n=1}^{\infty} \frac{4\pi^2}{k_0^2} \cos(2n-1) \frac{2\pi k}{k_0} \quad (\text{A.3})$$

$$= \frac{8\hbar v_F}{k_0} \sum_{n=1}^{\infty} \cos(2n-1) \frac{2\pi k}{k_0} \quad (\text{A.4})$$

$$= \frac{8\hbar v_F}{k_0} \sum_{n=1}^{\infty} \cos(2n-1) \frac{2\pi e F t}{\hbar k_0} \quad (\text{A.5})$$

A.2 Integration using properties of Heaviside, Dirac, and Dirac prime functions

A.2.1 Integrating term 1 using rule (i)

$$\text{Term 1} = \psi \Theta_1 \delta'_0 e^{-t/\tau} (\hbar v_F)^2 \quad (\text{A.6})$$

$$a = e v_F F_0 \quad (\text{A.7})$$

$$b = \frac{\hbar v_F k_0}{2} (n+1) \quad (\text{A.8})$$

$$c = e v_F F_0 \quad (\text{A.9})$$

$$d = \frac{\hbar v_F k_0}{2} n \quad (\text{A.10})$$

$$\psi = f(t) = (-1)^n \left[(e v_F F_0) t - \frac{\hbar v_F k_0}{2} n \right] + \frac{\hbar v_F k_0}{2} \left(\frac{1 - (-1)^n}{2} \right) \quad (\text{A.11})$$

Substituting everything into rule (i) gives:

$$\Rightarrow \frac{1}{ev_F F_0} e^{-\frac{\hbar k_0 n}{2eF_0 \tau}} \delta\left(\frac{\hbar v_F k_0}{2}\right) \psi\left(t = \frac{\hbar v_F k_0 n}{2ev_F F_0}\right) \quad (\text{A.12})$$

$$+ \frac{1}{\tau (ev_F F_0)^2} e^{-\frac{\hbar k_0 n}{2eF_0 \tau}} \Theta\left(\frac{\hbar v_F k_0}{2}\right) \left[\psi\left(t = \frac{\hbar v_F k_0 n}{2ev_F F_0}\right) - \tau \psi'\left(t = \frac{\hbar v_F k_0 n}{2ev_F F_0}\right) \right] \quad (\text{A.13})$$

$$= e^{-\frac{\hbar k_0 n}{2eF_0 \tau}} \left\{ \frac{1}{\tau (ev_F F_0)^2} \left(\frac{\hbar v_F k_0}{2} \frac{1 - (-1)^n}{2} - \tau (-1)^n ev_F F_0 \right) \right\} \quad (\text{A.14})$$

Since $\delta(x, x \neq 0) = 0$ and using $\Theta(x \geq 0) = 1$. Therefore the result is

$$= \frac{\hbar^2 e^{-\frac{\hbar k_0 n}{2eF_0 \tau}}}{\tau e^2 F_0^2} \left(\frac{\hbar v_F k_0}{2} \frac{1 - (-1)^n}{2} - \tau (-1)^n ev_F F_0 \right) \quad (\text{A.15})$$

A.2.2 Integrating term 2 using rule (ii)

Very similar to previous process.

$$\text{Term 2} = \psi \Theta_0 \delta_1' e^{-t/\tau} (\hbar v_F)^2 \quad (\text{A.16})$$

$$a = ev_F F_0 \quad (\text{A.17})$$

$$b = \frac{\hbar v_F k_0}{2} n \quad (\text{A.18})$$

$$c = ev_F F_0 \quad (\text{A.19})$$

$$d = \frac{\hbar v_F k_0}{2} (n + 1) \quad (\text{A.20})$$

$$\psi = f(t) = (-1)^n \left[(ev_F F_0)t - \frac{\hbar v_F k_0}{2} n \right] + \frac{\hbar v_F k_0}{2} \left(\frac{1 - (-1)^n}{2} \right) \quad (\text{A.21})$$

Substituting everything into rule (ii) gives:

$$\Rightarrow \frac{1}{ev_F F_0^2} \left\{ \frac{1}{\tau} e^{-\frac{\hbar k_0 (n+1)}{2eF_0 \tau}} \left[\psi\left(t = \frac{\hbar v_F k_0 (n+1)}{2ev_F F_0}\right) - \tau \psi'\left(t = \frac{\hbar v_F k_0 (n+1)}{2ev_F F_0}\right) \right] \right\} \quad (\text{A.22})$$

Thus the result is

$$= \hbar^2 v_F^2 \frac{1}{ev_F F_0^2} \left\{ \frac{1}{\tau} e^{-\frac{\hbar k_0 (n+1)}{2eF_0 \tau}} \left[\frac{1 - (-1)^n}{2} \frac{\hbar v_F k_0}{2} - \tau (-1)^n ev_F F_0 \right] \right\} \quad (\text{A.23})$$

A.2.3 Integrating term 4 using rule (iii)

$$\text{Term 4} = -(-1)^n \Theta_0 \delta_1 e^{-t/\tau} \hbar^2 v_F^2 \quad (\text{A.24})$$

$$a = ev_F F_0 \quad (\text{A.25})$$

$$b = \frac{\hbar v_F k_0}{2} n \quad (\text{A.26})$$

$$c = ev_F F_0 \quad (\text{A.27})$$

$$d = \frac{\hbar v_F k_0}{2} (n + 1) \quad (\text{A.28})$$

Substituting everything into rule (iii) gives:

$$\Rightarrow -\hbar^2 v_F^2 (-1)^n \frac{1}{ev_F F_0} e^{-\frac{\hbar k_0 (n+1)}{2eF_0 \tau}} \Theta \left(\frac{\hbar k_0 (n+1)}{eF_0} \right) \quad (\text{A.29})$$

$$= \frac{-(-1)^n \hbar^2 v_F}{eF_0} e^{-\frac{\hbar k_0 (n+1)}{2eF_0 \tau}} \Theta \left(\frac{\hbar k_0 (n+1)}{eF_0} \right) \quad (\text{A.30})$$

A.2.4 Integrating term 5 using rule (iv)

Finally, in a process similar to the one above:

$$\text{Term 5} = (-1)^n \Theta_1 \delta_0 e^{-t/\tau} \hbar^2 v_F^2 \quad (\text{A.31})$$

$$a = ev_F F_0 \quad (\text{A.32})$$

$$b = \frac{\hbar v_F k_0}{2} (n + 1) \quad (\text{A.33})$$

$$c = ev_F F_0 \quad (\text{A.34})$$

$$d = \frac{\hbar v_F k_0}{2} n \quad (\text{A.35})$$

Substituting everything into rule (iv) gives:

$$\Rightarrow -\hbar^2 v_F^2 (-1)^n \frac{1}{ev_F F_0} e^{-\frac{\hbar k_0 n}{2eF_0 \tau}} \Theta \left(\frac{\hbar k_0 n}{eF_0} \right) = \frac{(-1)^n \hbar^2 v_F}{eF_0} e^{-\frac{\hbar k_0 n}{2eF_0 \tau}} \Theta \left(\frac{\hbar k_0 n}{eF_0} \right) \quad (\text{A.36})$$

A.3 Final calculation of v_d for Heaviside model

The expression for drift velocity is now:

$$v_d = \frac{eF_0}{\hbar^2} \sum_{n=0}^{\infty} (\text{Sum of the 4 contributions})$$

As calculated in Appendix B. Therefore:

$$v_d = \frac{eF_0}{\hbar^2} \left\{ \right. \quad (A.37)$$

$$\frac{1}{e\tau F_0} \sum_{n=-\infty}^{\infty} \left(\left(\frac{1 - (-1)^n}{2} \right) \frac{\hbar v_F k_0}{2} - (-1)^n \tau e v_F F_0 \right) e^{-\frac{\hbar k_0 n}{2eF_0\tau}} \quad (A.38)$$

$$\frac{1}{e\tau F_0} \sum_{n=-\infty}^{\infty} \left(\left(\frac{1 - (-1)^n}{2} \right) \frac{\hbar v_F k_0}{2} - (-1)^n \tau e v_F F_0 \right) e^{-\frac{\hbar k_0 (n+1)}{2eF_0\tau}} \quad (A.39)$$

$$v_F \sum_{n=-\infty}^{\infty} (-1)^n \Theta \left(\frac{\hbar k_0 n}{2eF_0} \right) e^{-\frac{\hbar k_0 n}{2eF_0\tau}} \quad (A.40)$$

$$-v_F \sum_{n=-\infty}^{\infty} (-1)^n \Theta \left(\frac{\hbar k_0 (n+1)}{2eF_0} \right) e^{-\frac{\hbar k_0 (n+1)}{2eF_0\tau}} \left. \right\} \quad (A.41)$$

The four summations are calculated to be:

$$0 \quad (A.42)$$

$$0 \quad (A.43)$$

$$v_F \left[\frac{1}{2} - \frac{1}{e^x + 1} \right] \quad (A.44)$$

$$v_F \left[\frac{1}{2} - \frac{1}{e^x + 1} \right] \quad (A.45)$$

$$(A.46)$$

Therefore, the expression for drift velocity now is as follows:

$$v_d = v_F \left[1 - \frac{2}{e^x + 1} \right] \quad (\text{A.47})$$

$$= v_F \left[\frac{e^x + 1}{e^x + 1} - \frac{2}{e^x + 1} \right] \quad (\text{A.48})$$

$$= v_F \left[\frac{e^x - 1}{e^x + 1} \right] \quad (\text{A.49})$$

$$= v_F \tanh \frac{x}{2} = v_F \tanh \frac{\hbar k_0}{4eF_0\tau} \quad (\text{A.50})$$

Absolute negative differential conductivity in graphene-like superlattices

P. A. Dakers and F. V. Kusmartsev

Department Of Physics, Loughborough University, Leics, UK

Abstract

We describe a new type of superlattice with a linear Dirac spectrum which has many of the special properties of graphene. Such superlattices can be made from graphene and/or various semiconductors using electronic band-structure engineering. Electronic transport in such graphene-like superlattices has been described taking into account both a high level of disorder and possible formation of a miniband gap in the Dirac spectrum. Limiting electron motion to the first miniband we find an exact analytic equation for the current-voltage characteristics of the graphene-like superlattice, which exhibit negative differential conductivity. We estimate the value of the critical field F_c required for onset of Bloch oscillations and predict that such a superlattice can enter its active region for a significantly lower critical field strength than conventional semiconductor superlattices, reducing the possibility of Zener tunnelling to higher minibands. The frequency of the Bloch oscillations depends on the bias, Fermi velocity and the miniband gap width. We show that for all described structures the miniband gap in the Dirac spectrum can be precisely determined from direct electrical measurements of their current-voltage characteristics.

INTRODUCTION

A highly influential paper, published in 1970 by Esaki and Tsu[1], investigated the current-voltage properties of semiconductor superlattices. They used a path integration method and the scattering time approximation within the Boltzmann transport approach to calculate the relationship between the strength of a voltage bias (or electric field) and the drift velocity (average current) of the charge-carriers. They described a semiconductor superlattice consisting of a regular array of square potential wells separated by square barriers as a single miniband tight binding model with an associated cosinusoidal electronic energy-momentum relation. This approach allows the calculation of both charge-carrier displacement and drift velocity when a static electric field F is applied and the prediction of quantum phenomena known as negative differential conductivity and electron localisation due to Bloch oscillations.

Here we introduce a new class of superlattices which have a Dirac-like miniband electron spectrum and therefore have advanced electrical properties similar to pristine graphene, the name given to a single layer of carbon atoms arranged in a hexagonal lattice. Graphene exhibits semi-metallic behaviour and a linear Dirac energy-momentum spectrum. Originally it was shown that two-dimensional electrons with such a gapless spectrum have very high mobility and conductivity when the temperature decreases[2]. The high mobility of the charge carriers in graphene can be used in various devices and superlattices if the Dirac spectrum with a small, or controllable, miniband gap is engineered. Then they may work both as amplifiers and transistors. Indeed, modern technology has developed advanced methods of electronic band-structure engineering[3] where materials and superlattices may be constructed with any needed electronic energy-momentum relation such as the Dirac-like spectrum. For example, when in the semiconductor superlattice consisting of GaAs/AlAs layers a very thin InAs layer is inserted the position of the miniband shifts while its width changes[4]. Thus, the presence of the subnanometer thick InAs layer in the central plane of each GaAs quantum well allows control of the electron injection into the superlattice and facilitates single miniband transport. Here we would like to consider properties of a superlattice where the lowest miniband has the Dirac-like spectrum (as in the Tomonaga model[5]) which may be built up with electronic band-structure engineering. Graphene is a good candidate for construction of such devices and in general for development of graphene-

based electronic technology. One of the analogous devices - an array of antidots - has been recently developed and its properties investigated[6]. The graphene-like superlattice (GSL) with the Dirac-like miniband spectrum can be also made from graphene or graphene nanoribbons or in general from structures made of multilayered semiconductors, while their miniband structure may be designed with electron-band engineering[3].

In the first case, to make such a GSL from graphene, for example, the graphene sheets should be decomposed into nanoribbons and then deposited on a semiconductor or insulator substrate. These ribbons are narrow and straight-edged strips of graphene. They are predicted to exhibit electronic properties that make them attractive for the fabrication of nanoscale electronic devices. The nanoribbon formation can open up a miniband gap whose value depends on the width of the nanoribbon. Moreover, more general practical devices and circuits will require the production of dense arrays of ordered nanoribbons, which can be done by electron lithography of graphene deposited on a substrate or on copper foils[10]. Devices made from nanoribbons deposited on a substrate usually exhibit very strong disorder, which is associated with the defects in the substrate. As a consequence these devices have very low driving currents[7–9] and therefore to describe the electronic transport there the approach used in the original paper by Esaki and Tsu[1] is applicable.

A superlattice of graphene nanoribbons deposited on a substrate will have a miniband structure where the majority of the Brillouin zone has a linear energy-momentum relation, similar to graphene. Due to this linear energy-momentum relation its electron-hole transport dynamics are very interesting[2]. As derived under the tight-binding model, graphene's dispersion relation is given by the following[11]

$$|\varepsilon(k_x, k_y)| = \hbar v_F \left(1 + 4 \cos^2 \frac{k_x a}{2} + 4 \cos \frac{k_x a}{2} \cos \frac{\sqrt{3} k_y a}{2} \right)$$

where a is the interatomic $C - C$ spacing, and $k_{x,y}$ are the reciprocal lattice vectors. It is linear near the Dirac points, which are situated on the Fermi level; therefore only charge-carriers around these points contribute to conduction. As in the Tomonaga model[5, 12] the miniband structure of a GSL can be periodically linear (resembling a triangular waveform), assuming that the Brillouin zone, of width $k_0 = \pi/d$, is sufficiently narrow. This assumption will take into account the main feature of GSLs, namely the linear Dirac spectrum, and simultaneously allow us to find an exact solution for electron transport in very disordered superlattices even when a miniband gap arises in the Dirac spectrum. The proposed

miniband structure may be considered as an approximation of the original spectrum of a superlattice of square potential wells induced in two dimensional graphene[13]. However, such a spectrum allows us to produce analytic calculation of the effects of applied fields on charge-carrier dynamics and investigate the nature of the Bloch oscillations. That is, we focus our studies of the GSL with an effective period d long enough to ensure that the energy-momentum relation remains effectively linear within $|k| \leq \pi/d$.

We would like to study the properties of such novel devices which may be made, for example, from an array of nanoribbons deposited on a substrate as those discussed in the paper[7] or multilayer composition made from various semiconductors. We expect that this new class of graphene-like superlattices (GSL) we introduce here, with the Dirac miniband spectrum, can be made by MBI both from graphene and various semiconductors.

We make use of the path integration method as used by Esaki and Tsu to calculate the transport properties of a graphene-like superlattice. Such a GSL should exhibit miniband structure as seen in Figure 1. Various ideas for construction of GSLs have been already

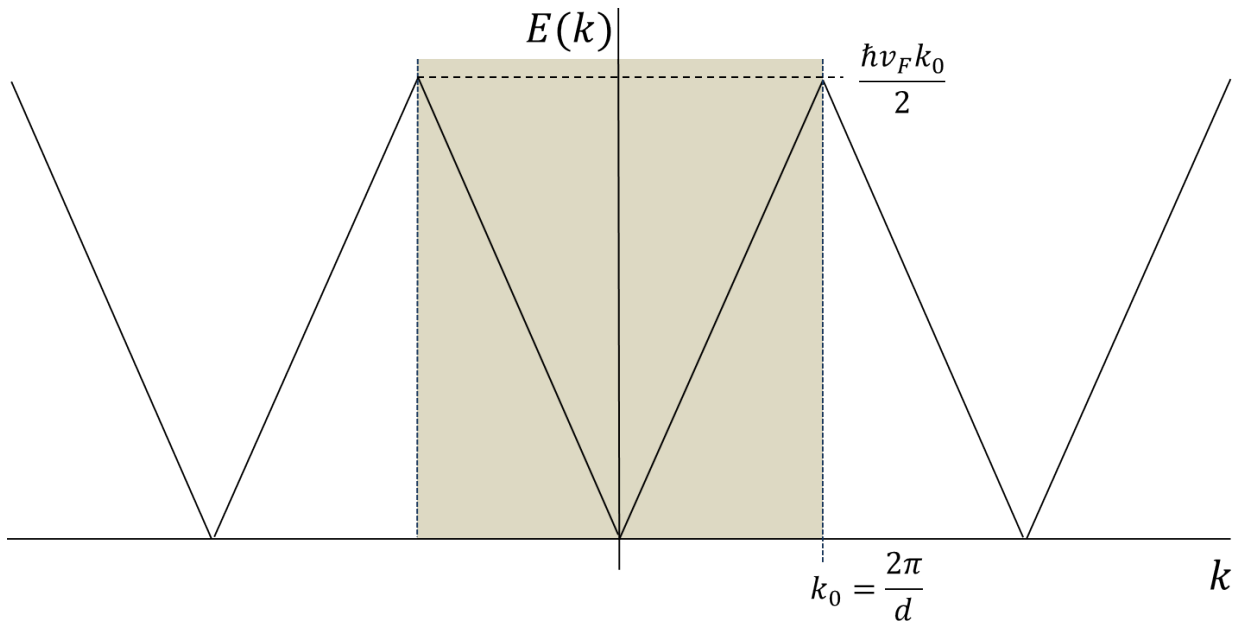


FIG. 1. This diagram presents a simple model for a graphene-like superlattice whose first Brillouin zone lies within $|k_0| \leq 2\pi/d$, that generalizes a Tomonaga model spectrum[5] to that of a superlattice energy-momentum relation associated with the first miniband.

discussed in the literature [14–16]. The transport properties of such device can be studied

using the Kronig-Penney[13, 17, 18] model of periodic potential barriers embedded on the graphene sheet.

PARABOLIC APPROXIMATION FOR A MINIBAND-GAP FORMATION

We use a simple approximation to model the periodic $E(k)$ relation associated with the superlattice. Due to a semiconductor or insulator substrate as SiO_2 there in the Dirac spectrum may arise a miniband gap, equal to $\Delta = 2\alpha$ described in the Ref. [23]. The formation of the miniband gap allows us to avoid the discontinuities present at $|k| = nk_0/2, n \in \mathbb{N}^0$. Therefore we “smooth away” the sharp peaks of the triangular energy spectrum of the Tomonaga model into parabolae. The function then is linear everywhere, as before, except inside intervals where the discontinuity would normally occur (the peaks and troughs of the spectrum). Figure 2 demonstrates this new, approximated spectrum. As the piecewise

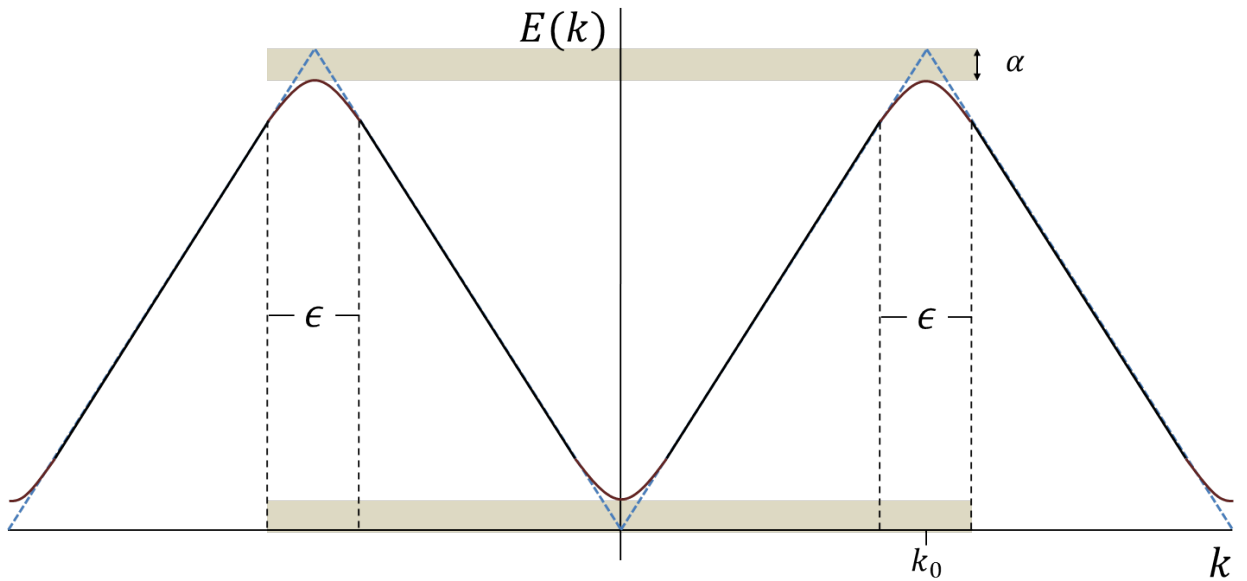


FIG. 2. The intervals shown here have width ϵ , the limit of which can be taken to zero upon calculation of the final result. The “discrepancy” denoted α is a consequence of this parabolic approximation, and has the effect of reducing the reach of the sharp points up from $E(k) = 0$ to $E(k) + \alpha$ and down from $E(k) = E_{\max}$ to $E(k) = E_{\max} - \alpha$. As ϵ gets closer and closer to zero, α will likewise tend to zero.

equation which describes this model is generated, the following must be taken into account:

That the curved sections are quadratic parabolae, that the nature of the curves means that the peaks and troughs of the spectrum are not as high or low as they were (this discrepancy is defined and quantified below), that we must define our new function and its derivative as being continuous as the function crosses from being linear to being parabolic, and that we must be able to take a limit in such a way that the approximation can become zero; corresponding to a periodically linear miniband.

This approximation is useful in two ways. Firstly, impurities and defects in the lattice, the surface corrugation, and the disorder arising due to a lattice mismatch with a substrate might all be the source of the rounding of the otherwise discontinuous spectrum. In this way it may be possible to model these effects and how they affect the I-V curves of GSLs and relate to the phenomena of NDV and Bloch oscillation. Secondly, when the limit as $\epsilon \rightarrow 0$ is taken, the behaviour of a “perfect” GSL miniband may be examined. Studying the model schematic in Figure 2, we can say that the piecewise function describing the the first Brillouin Zone of the miniband may be written as follows:

$$E(k) = \begin{cases} \sum_{n=0}^{\infty} \left[\frac{\hbar^2 k^2}{2m_*} + \frac{1}{2} m v_F^2 \right] (-1)^n + \frac{1 - (-1)^n}{2} \frac{\hbar v_F k_0}{2} & ; \quad nk_0 - \frac{\epsilon}{2} \leq k \leq nk_0 + \frac{\epsilon}{2} \\ \sum_{n=0}^{\infty} \left[\hbar v_F k - \frac{\hbar k_0 n}{2} \right] (-1)^n + \frac{1 - (-1)^n}{2} \frac{\hbar v_F k_0}{2} & ; \quad nk_0 + \frac{\epsilon}{2} \leq k \leq (n+1)k_0 - \frac{\epsilon}{2} \end{cases} \quad (1)$$

where ϵ can vary from zero to $k_0/2$. The quantity α corresponds to a half of the miniband gap. The effective mass m_* is related to the interval width ϵ via $m_* = \hbar\epsilon/2v_F$, and the miniband gap Δ via $\Delta = m_* v_F^2$.

Using Esaki and Tsu’s method[1], the drift velocity-field characteristic is calculated via a path integration method using the equation

$$v_d(F(t), \tau) = \frac{1}{\tau} \int_0^{\infty} v_g(F(t), t) e^{-\frac{t}{\tau}} dt \quad (2)$$

When the DC field only case $F(t) = F$ is considered, the group velocity is given by $v_g(t) = \hbar^{-1} \partial E(k) / \partial k$, and the quasimomentum $k(t)$ is found by solving Newton’s equation $k'(t) = eF/\hbar$ giving $k(t) = eFt/\hbar$. The constant of integration is assumed to be zero, corresponding to zero initial quasimomentum. Equation (2) becomes

$$v_d = \frac{eF\tau}{m_*} \left(1 - 2e^{-\frac{\epsilon\hbar}{2eF\tau}} + \frac{4 \sinh \left\{ \frac{\epsilon\hbar}{2eF\tau} \right\}}{e^{\frac{\hbar k_0}{eF\tau}} - 1} \right) \quad (3)$$

See the Appendix for details. Figure 3 displays what effect the value of Δ has on the relationship between the drift velocity v_d and the applied field strength F .

Esaki and Tsu received a similar result for a band structure made up of parabolae of opposite curvature, meeting at an inflection point k_i defined as a fraction of the Brillouin zone size k_d . For $k_i = k_d/2$, and taking $\epsilon = k_0/2$ in our model, a direct comparison can be made:

$$\frac{v_d}{v_d^{ET}} = \frac{m(0)}{m_*} = \frac{8\hbar v_F}{E_1 \pi d} \quad (4)$$

where the superscript ET denotes the Esaki-Tsu characteristic, $m(0) = 2\hbar^2/\Delta d^2$ is the effective mass of a charge-carrier at the bottom of a semiconductor superlattice miniband, v_F the Fermi velocity of a charge-carrier propagating in graphene, and $v_0 = E_1 d/2\hbar$ the maximum drift velocity of a charge-carrier propagating within a semiconductor superlattice as implemented in Esaki and Tsu's cosinusoidal model (corresponding to the charge experiencing a static field of strength $F_c = \hbar/ed\tau$ and propagating through a miniband of width E_1). For a typical semiconductor superlattice made mainly of GaAs-GaAlAs, and a graphene-like superlattice of effective period $d = 100\text{\AA}$, this ratio is

$$\frac{v_d}{v_d^{ET}} \approx 5.6$$

In the limit of zero ϵ (or Δ), the equation for drift velocity becomes:

$$v_d = v_F \tanh \frac{\hbar k_0}{4eF\tau} \quad (5)$$

corresponding to a perfectly linear miniband structure. A discontinuity in the current-voltage curve manifests as a jump from $v_d = -v_F$ to $v_d = v_F$ at zero field strength; an infinite gradient, and since the DC conductivity $\sigma_{DC} = en \frac{dv_d}{dF}$ is directly proportional to the gradient, this suggests an instability within the electronic behaviour of the graphene system leading to spontaneous current generation and extremely high conductivity. Recall that $m_* \propto \epsilon$, so as the interval size decreases and the miniband becomes more linear, the effective mass of the charge-carrier vanishes. The zero effective mass of charge-carriers in graphene is broadly discussed and is related to their relativistic behaviour as Dirac fermions[20–22].

MINIBAND GAP

The model for GSL has been introduced where the energy-momentum relation has been defined as a piecewise function. This model is used to calculate the I-V curves or the drift

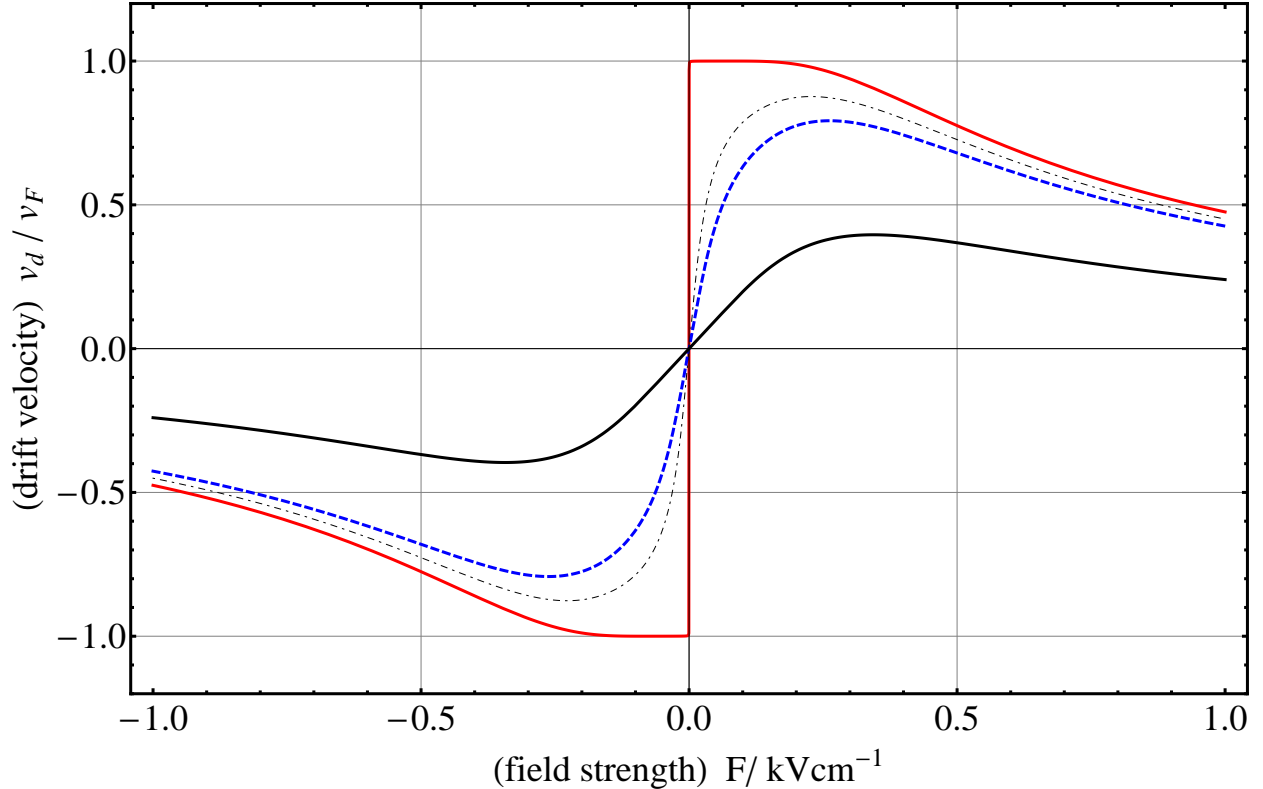


FIG. 3. The above plot displays current-voltage characteristics for three values of the miniband gap $\Delta = \Delta_{max} \approx 50\text{meV}$ (thin, black), $\Delta = 10\text{meV}$ (dashed, blue), $\Delta = 5\text{meV}$ (dot-dashed, black) and 0.01meV (solid, red) as given by equation (8). The following values are used: $\tau = 1\text{ps}$, $d = 100\text{\AA}$, $v_F = 10^6\text{ms}^{-1}$. As the miniband gap decreases, the critical field which defines the active region threshold also decreases. Furthermore, the peak drift velocity increases with decreasing band gap, implying that the larger the linear sections of the miniband get, the higher peak velocity that a charge-carrier propagating through the miniband can attain. These results are remarkably similar to those calculated for a suspended graphene nanoribbon of varying width[19].

velocity-field characteristics of such a superlattice. The appearance of NDC resembles the result derived by Esaki and Tsu. In a specific case ($\epsilon = k_0/2$, $k_d/k_i = 2$), there exists a basis for direct comparison of the I-V characteristics for semiconductor and graphene superlattices. In the limit of small ϵ , the drift velocity can be expressed to first order as

$$v_d \approx v_F \left(1 - \frac{2}{1 + e^{\frac{\hbar k_0}{eF\tau}}} - \frac{\hbar\epsilon}{4eF\tau} \right) \quad (6)$$

for which the maximum drift velocity occurs for the critical field

$$F_c(\Delta) = \frac{\pi \hbar}{ed\tau \ln \left(\frac{2\pi \hbar v_F}{\Delta d} - 1 \pm \frac{\sqrt{2\hbar v_F}}{\Delta} \sqrt{\frac{2\pi^2}{d^2} - \frac{2\pi \Delta}{d\hbar v_F}} \right)} \quad (7)$$

(where $\Delta = 2\alpha$ is the size of the miniband gap) which converges upon zero for vanishing ϵ and

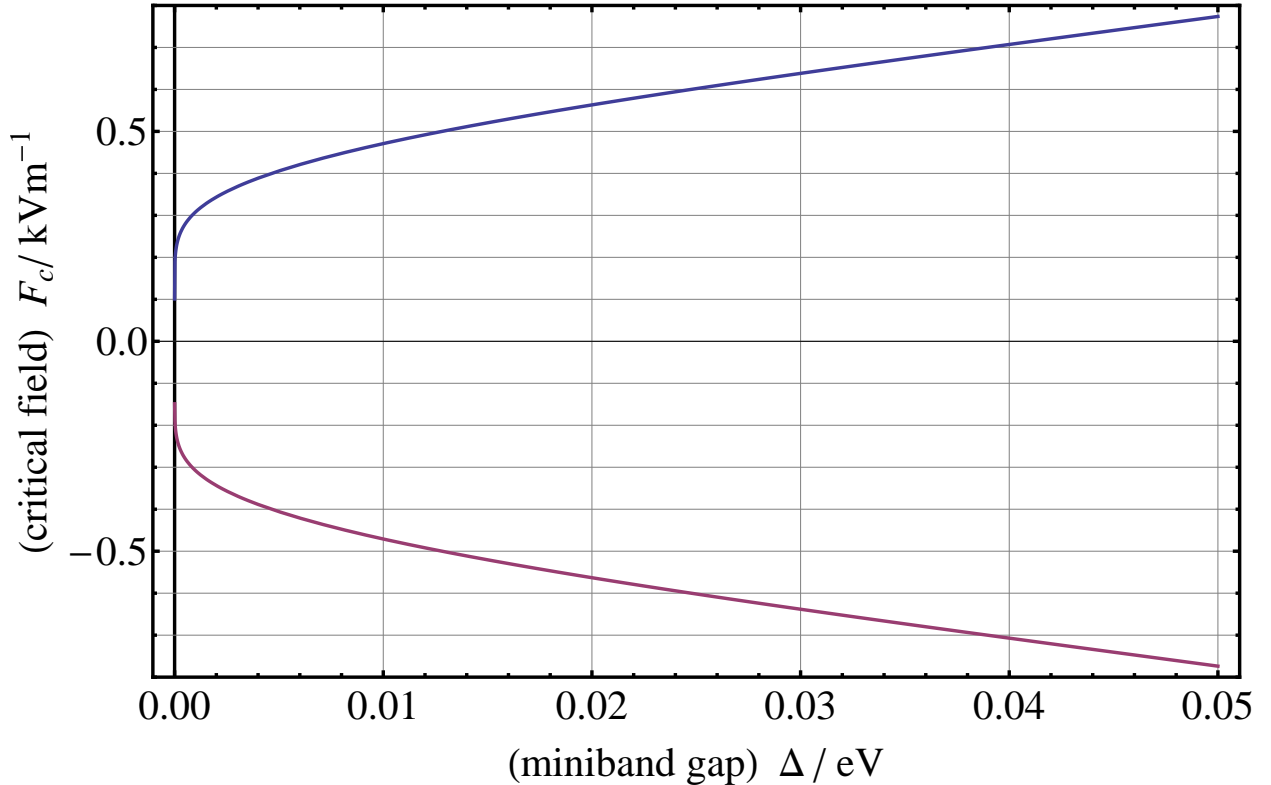


FIG. 4. Critical field dependence on miniband gap $\Delta = 2\alpha$ according to equation (7), where both (\pm) solutions are presented, corresponding to NDV regions occurring in the current-voltage curve for positive and negative applied field. The maximum value Δ can assume within this model relates directly to the maximal interval width $\epsilon = k_0/2$, and is approximately equal to 50meV when the superlattice period is equal to $d = 10$ nm.

Δ , implying that as the interval width ϵ or miniband gap Δ defined within this approximation is reduced, the current-voltage curve tends toward $\tanh F^{-1}$ behaviour, implying that, effectively, the critical field F_c required to force the charge-carriers into performing Bloch oscillations reduces (from $F_c = \hbar/(ed\tau)$) to zero in that limit. Therefore the onset of Bloch oscillations should occur in a linear miniband structure given the application of a static bias of minimal strength. Furthermore, it is important to point out that all interesting features

of superlattice dynamics occur within the negative differential portion of the current-voltage characteristics. This region is known as the active region. The results discussed here suggest that a superlattice exhibiting a linear miniband structure as shown in our model will enter its active region for a lower critical value of applied field strength. By reducing this value, the possibility of charge-carriers gaining enough energy from the applied field and undergoing Zener tunnelling, thus destroying the NDV characteristics, will also be reduced. This will increase the possibility of observing Bloch oscillation, thus increasing the possible range of radiation frequency emission in comparison to the original Esaki-Tsu results.

The miniband gap Δ , is directly related to the interval width from equations (9) and (10), allowing the drift velocity to be expressed as a function of the size of the miniband gap:

$$v_d(\Delta) = \frac{eF\tau v_F^2}{\Delta} \left(1 - 2e^{-\frac{\Delta}{eF\tau v_F}} + \frac{4 \sinh \left\{ \frac{\Delta}{2eF\tau v_F} \right\}}{e^{\frac{\hbar k_0}{eF\tau}} - 1} \right) \quad (8)$$

In our phenomenological model Δ can vary from zero to $\hbar v_F \pi / 4d \approx 51 \text{meV}$. In this way, by introducing some rounding to the linearity of the superlattice energy-momentum relation, it is possible to create a miniband gap up to a value of roughly 50meV, around one half of that when considering the energy spectrum of corrugated graphene in two dimensions[23].

Equation (8) and Figure 3 demonstrates the dependence of drift velocity on miniband gap size. This dependence resembles the effect that a suspended graphene nanoribbon's width has on its own current-voltage characteristics as calculated by Betti et al[19]. Increasing the width of the GNR increases the peak velocity of the charge-carriers and decreases the critical field strength required to enter the superlattice's active region.

Electronic mobility μ can be calculated when the drift velocity is known using the simple formula $\mu = v_d/F$: Figure 5 supports the analogy between our investigation regarding the effect of miniband gap width on electronic transport and the effect of GNR width on GNR transport characteristics, as discussed in [19]. Furthermore, a miniband gap can appear in graphene's band structure when an electronic defect is present, such as a missing interatomic bond [24].

In summary we have described a class of superlattices which, like graphene, have a Dirac like miniband spectra. Such superlattices with a Dirac-like electronic spectrum can be made from layers of different semiconductors or graphene with the use of modern technology methods of band-structure engineering. Such graphene-like superlattice structures may also

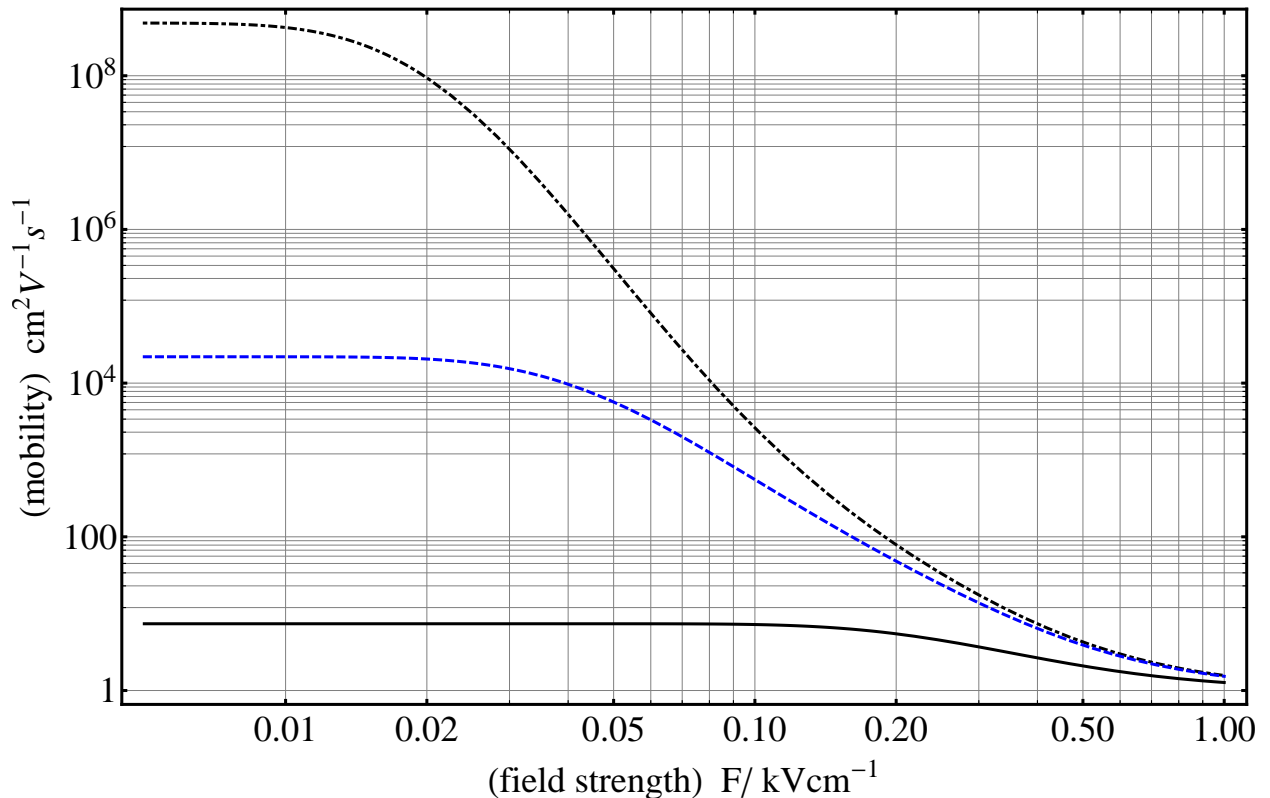


FIG. 5. Corresponding mobility of charge-carriers $\mu = v_d/F$ for $\Delta = \Delta_{max} \approx 50\text{meV}$ (thin, black), $\Delta = 10\text{meV}$ (dashed, blue), and $\Delta = 5\text{meV}$ (dot-dashed, black). It is clear that mobility reaches its maximum for at zero field, and that the mobility depends very strongly on the miniband gap width. This implies that the ability of an electronic device constructed from graphene to exhibit a huge electronic mobility is very quickly reduced in the presence of disorder.

be created in supercooled gases. This was discussed in great detail in a recent paper [25]. Due to the linear energy-momentum relation there exists a high electronic mobility, arises absolute negative conductivity in a very broad range of applied voltage bias and in some cases there may arise a spontaneous persistent current as the one discussed in recent work[26, 27]. We suggest that our phenomenological approach creates a framework under which it is possible to estimate the size of a miniband gap within the energy-momentum spectrum of a GSL, or GNR, by examining the drift velocity dependence on an applied static bias. All these properties can make such graphene-like superlattice to be an outstanding candidate for a development of new devices, the graphene-like technology, which can be built up with

the use of conventional semiconductors as well as from graphene.

-
- [1] L. Esaki and R. Tsu, *IBM J. Res. Dev.*, (1970).
 - [2] F.V. Kusmartsev, A.M. Tselick, *Sov. Phys.- JETP Lett.* **42**, 257 (1986).
 - [3] M. Shen, W. Cao, *Materials Science and Engineering*, **B103** 122 (2003).
 - [4] A. Patane, D. Sherwood, L. Eaves, T. M. Fromhold, M. Henini, and P. C. Main, G. Hill, *Appl. Phys. Lett.*, **81**, 661 (2002).
 - [5] S. Tomonaga, *Progr. Theoret. Phys. (Kyoto)* **5**, 544 (1950).
 - [6] J. Bai, et al, *Nature Nanotechnol.* **5(3)**, 190194. (2010).
 - [7] H. Sevincli, M. Topsakal and S. Ciraci *Phys. Rev. B* **78**, 245402 (2008)
 - [8] L.Y. Jiao et al. *Nature*, **458**, 7240, (2009)
 - [9] J. Bai J, X. Duan and Y. Huang *Nano Lett*, **9**, (5), (2009)
 - [10] X. Li et al. *Science* **5**. (2009)
 - [11] V.P. Gusynin, S.G. Sharapov and J.P. Carbotte, *Int. J. Mod. Phys. B*, **21**, 4611-58 (2007)
 - [12] H. Gutfreund et al., *Phys. Rev.*, **168**, 418 (1968)
 - [13] M.R. Masir, P. Vasilopoulos and F.M. Peeters, *New. J. Phys.*, **11**, 095009 (2009).
 - [14] Cheol-Hwan Park et al., *Nature Physics*, **4**, 213-7 (2008).
 - [15] Cheol-Hwan Park et al., *Phys. Rev. Lett.*, **101**, 126804 (2008).
 - [16] R.P. Tiwari and D. Stroud, *Phys. Rev. B*, **79**, 205435 (2009).
 - [17] M. Barbier, P. Vasilopoulos and F.M. Peeters, *Phys. Rev. B*, **80**, 205415 (2009).
 - [18] S. Gattenlöhner, W. Belzig and M. Titov, *Phys. Rev. B*, **82**, 155417 (2010).
 - [19] A. Betti, G. Fiori and G. Iannaccone, *arXiv:1108.2146v2* (2011)
 - [20] K.S. Novoselov, A.K. Geim et al., *Nature*, **438**, 197-200 (2005).
 - [21] M.I. Katsnelson, K.S. Novoselov and A. K. Geim, *Nature Physics*, **2**, 620-5 (2006).
 - [22] K. Nomura and A.H. MacDonald, *Phys. Rev. Lett.*, **98**, 076602 (2007).
 - [23] A. O'Hare, F.V. Kusmartsev and K.I. Kugel, *Physica B*, (2012) (in press)
 - [24] D. Huang, G. Gumbs and O. Roslyak, *Phys. Rev. B*, **83**, 115405 (2011)
 - [25] L. Nadvornik et al, *arXiv:1104.5427v3*.
 - [26] K.N. Alekseev et al., *Phys. Rev. Lett.* **80**, 2669 (1998)
 - [27] E. H. Cannon et al., *Phys. Rev. Lett.* **85**, 1302-1305 (2000)

APPENDIX

Parabolic approximation mathematics

Recall that the dispersion relation for graphene in the proximity of the Dirac points, to first order, is given by $E(k) = \hbar v_F |k|$, and the maxima (and minima) in the spectrum occur at $|k| = nk_0/2$, $n \in \mathbb{N}^0$. This means that the amplitude of the spectrum is $E_{max}(k) = \hbar v_F k_0/2$. Now, equate the derivatives of equation (1) at a point where they meet, bearing in mind the relevant term in the summation, say at $n = 0 \Rightarrow k = \epsilon/2$. This leaves us with

$$\epsilon = \frac{2m_*v_F}{\hbar} \quad (9)$$

Now equate equations (1) on the same boundary, and substitute (9) into the result to find α :

$$\alpha = \frac{1}{2}m_*v_F^2 \quad (10)$$

The piecewise representation for $E(k)$ is now fully known, and it is expressed as follows:

$$E(k) = \begin{cases} \sum_{n=0}^{\infty} \left[\frac{\hbar^2 k^2}{2m_*} + \frac{1}{2}m v_F^2 \right] (-1)^n + \frac{1 - (-1)^n}{2} \frac{\hbar v_F k_0}{2} \\ \sum_{n=0}^{\infty} \left[\hbar v_F k - \frac{\hbar k_0 n}{2} \right] (-1)^n + \frac{1 - (-1)^n}{2} \frac{\hbar v_F k_0}{2} \end{cases} \quad (11)$$

$$\frac{\partial^2 E}{\partial k^2} = \begin{cases} \sum_{n=0}^{\infty} \frac{\hbar^2}{m} (-1)^n \\ 0 \end{cases} \quad (12)$$

Inside the regions defined by $nk_0 - \frac{\epsilon}{2} \leq k \leq nk_0 + \frac{\epsilon}{2}$ and $nk_0 + \frac{\epsilon}{2} \leq k \leq (n+1)k_0 - \frac{\epsilon}{2}$, respectively.

$$v_d = \frac{eF}{\hbar^2} \int_0^{\infty} \frac{\partial^2 E}{\partial k^2} e^{-\frac{t}{\tau}} dt \quad (13)$$

$$= \frac{eF}{\hbar^2} \int_0^{\infty} \left\{ \sum_{n=0}^{\infty} \frac{\hbar^2}{m} (-1)^n \right\} e^{-\frac{t}{\tau}} dt \quad (14)$$

Equation (14) above is simply the equation for drift velocity, with the non-zero part of $\frac{\partial^2 E}{\partial k^2}$ from equation (12) substituted in. However, it isn't correct, because the limits must be changed to reflect the piecewise behaviour of the integrand. In actuality, there are an infinite series of integrals, because the function $\frac{\partial^2 E}{\partial k^2}$ is periodically non-zero in the intervals

defined in equation (11). We can incorporate the summation outside the brackets into the integration summation - either by alternating +1 and -1 coefficients between each successive term, or perhaps more pragmatically, by switching the limits of every 2nd term (i.e. each term that would have had a -1 coefficient).

$$v_d = \frac{eF}{m_*} \left\{ \int_0^{\frac{\epsilon}{2}} e^{-\frac{t}{\tau}} dt + \int_{k_0 + \frac{\epsilon}{2}}^{k_0 - \frac{\epsilon}{2}} e^{-\frac{t}{\tau}} dt + \dots \right\}$$

Computing the integral gives us

$$v_d = -\frac{eF\tau}{m_*} \left\{ e^{-\frac{t}{\tau}} \Big|_0^{\frac{\epsilon}{2}} + e^{-\frac{t}{\tau}} \Big|_{k_0 + \frac{\epsilon}{2}}^{k_0 - \frac{\epsilon}{2}} + \dots \right\}$$

Upon extracting the first term in the curly brackets above, what remains inside the brackets is an infinite series, which converges to the following result for the drift velocity:

$$v_d = \frac{eF\tau}{m_*} \left(1 - e^{-\frac{\epsilon\hbar}{2eF\tau}} - \frac{2 \sinh \left\{ \frac{\epsilon\hbar}{2eF\tau} \right\}}{e^{\frac{\hbar k_0}{2eF\tau}} + 1} \right) \quad (15)$$

$$= \frac{eF\tau}{m_*} \left(1 - 2e^{-\frac{\epsilon\hbar}{2eF\tau}} + \frac{4 \sinh \left\{ \frac{\epsilon\hbar}{2eF\tau} \right\}}{e^{\frac{\hbar k_0}{eF\tau}} - 1} \right) \quad (16)$$

The former (15) becomes the latter (16) after some algebraic rearrangement. Recalling how the effective mass m_* is related to the interval width ϵ in equation (9), figure 3 displays what effect the value of ϵ has on the relationship between the drift velocity v_d and the applied field strength F . In the limit of zero ϵ :

$$\begin{aligned} \lim_{\epsilon \rightarrow 0} \frac{2eFv_F\tau}{\hbar\epsilon} \left(1 - e^{-\frac{\epsilon\hbar}{2eF\tau}} - \frac{2 \sinh \left\{ \frac{\epsilon\hbar}{2eF\tau} \right\}}{e^{\frac{\hbar k_0}{2eF\tau}} + 1} \right) \\ = v_F \left\{ \frac{e^{\frac{\hbar k_0}{2eF\tau}} - 1}{e^{\frac{\hbar k_0}{2eF\tau}} + 1} \right\} \\ v_d = v_F \tanh \frac{\hbar k_0}{4eF\tau} \end{aligned} \quad (17)$$

Heaviside function representation

The linear, periodic energy-momentum relation of the first miniband may also be described by the following equation:

$$E(k) = \sum_{n=-\infty}^{\infty} \Psi(n) \Theta_1(n) \Theta_0(n) \quad (18)$$

where

$$\begin{aligned}\Psi(n) &= (-1)^n \left(\hbar v_F k - \frac{\hbar v_F k_0 n}{2} \right) + \frac{\hbar v_F k_0}{2} \left(\frac{1 - (-1)^n}{2} \right) \\ \Theta_1(n) &= \Theta \left((n+1) \frac{\hbar v_F k_0}{2} - \hbar v_F k \right) \\ \Theta_0(n) &= \Theta \left(\hbar v_F k - \frac{\hbar v_F k_0 n}{2} \right)\end{aligned}$$

This equation generates the linear miniband piece by piece for increasing n . The two Heaviside functions “section” the equation, that is, divide it into sections corresponding to the terms in the summation. $\Psi(n)$ generates either a positive slope or negative slope in the relevant section, and also shifts the line up by a value equal to E_{max} if the slope is negative (since it originates from the x axis and decreases from there). Equation (18) is to be differentiated, substituted into equation (13), and integrated using the relevant delta and delta-prime function properties, to get

$$\begin{aligned}v_d = \frac{eF}{\hbar^2} \sum_{n=-\infty}^{\infty} \left\{ \frac{\hbar^2}{\tau e^2 |F|^2} \left(\left[\frac{1 - (-1)^n}{2} \right] \frac{\hbar v_F k_0}{2} - \tau (-1)^n e v_F F \right) \right\} & \left(e^{-\frac{\hbar k_0 n}{2eF\tau}} + e^{-\frac{\hbar k_0 (n+1)}{2eF\tau}} \right) \\ + \frac{(-1)^n \hbar^2 v_F}{e|F|} \left[\Theta \left(\frac{\hbar k_0 n}{2eF} \right) e^{-\frac{\hbar k_0 n}{2eF\tau}} - \Theta \left(\frac{\hbar k_0 (n+1)}{2eF} \right) e^{-\frac{\hbar k_0 (n+1)}{2eF\tau}} \right] & \left. \right\}\end{aligned}$$

This summation is convergent, and yields the equation

$$v_d = v_F \tanh \frac{\hbar k_0}{4eF\tau}$$

Consolidating the previous result calculated in the limit of zero ϵ in equation (17).

Bibliography

- [1] L.Esaki and R.Tsu, *IBM J. Res. Dev.*, (1970)
- [2] H.T.Grahn *et al*, "*Semiconductor Superlattices: Growth and Electronic Properties*", **World Scientific**, (1995).
- [3] C.Wasche *et al.*, *Phys. Rev. Lett.*, **70**, 21 (1993).
- [4] J.Ziman, *Principles Of The Theory Of Solids*, p**116**, (1964)
- [5] G.D.Mahan, *Many Particle Physics*, p**593**, (1981)
- [6] R.Ferreira *et al*, *App. Phys. Expr.* **2**, (2009).
- [7] K.N.Alekseev *et al*, *Phys. Rev. B*, **54** 15, (1996).
- [8] T.Hyart *et al*, *Phys. Rev. B*, 77(16), (2008).
- [9] G.L.Carr *et al*, *Nature*, **420**, pp153-6, (2002).
- [10] L.Ozyuzer *et al*, *Science*, **318**, pp1291-3, (2007).

- [11] H.B.Wang *et al*, *Phys. Rev. Lett.*, **10**, (2001).
- [12] M.Tachiki *et al*, *Phys. Rev. B*, **71**, (2005).
- [13] A.M.Bouchard and M.Luban, *Phys. Rev. B*, **47**, (1993).
- [14] Y.Shimada *et al*, *Phys. Rev. Lett.*, **90**, (2003).
- [15] J.F.Federici *et al*, *Semicond. Sci. Technol.*, **20**, S266-S280 (2005).
- [16] E.R.Mueller, <http://www.aip.org/tip/INPHEA/vol-9/iss-4/p27.pdf>,(2003).
- [17] <http://www.rohm.co.jp/news/111121.html> (2011).
- [18] K.Ishigaki *et al*, *Electronics Letters*, **48** (10), pp 582-3 (2012).
- [19] N. W. Ashcroft and N. D. Mermin, *Solid State Physics*, Saunders College Publishing (1976).
- [20] W.Pauli, *Pauli Lectures On Physics Volume 4: Statistical Mechanics*, p111, Republished (2000)
- [21] A.Ignatov and Y.A.Romanov, *Sci-Ref. Inst. of Radiophysics*, **21**, 1, pp132-8 (1978).
- [22] A.Ignatov *et al*, *Z. Phys. B* **98**, pp187-915 (1995).
- [23] Mouras *et al*, *Revue de Chimie Minerale* **24** 572 (1987).

- [24] P.R.Wallace, *Phys. Rev.* **71** 9 (1947).
- [25] K.S.Novoselov, A.K.Geim *et al*, *Nature*, **438**, 197-200 (2005).
- [26] K.S.Novoselov, A.K.Geim *et al*, *Science*, **306** 5696, pp 666-9 (2004).
- [27] K.S.Novoselov *et al.*, *Science*, **306**, (2004).
- [28] K.S.Novoselov *et al.*, *Nature*, **438** 10, (2005).
- [29] ''<http://nanoprobes.aist-nt.com/apps/HOPG%20info.files/image001.jpg>''
- [30] ''http://www.lps.u-psud.fr/IMG/jpg_axe_I_N8_fig.jpg''
- [31] ''http://ej.iop.org/images/0034-4885/75/5/056501/Full/rpp342429f06_online.jpg''
- [32] ''http://ll.a.5d6d.com/userdirs/4/4/phys/attachments/month_0811/20081123_ccb9c2161162cc7d8912ikluE5qTpbuf.jpg''
- [33] ''<http://osxs.ch.liv.ac.uk/~ng/external/images/sp2hybrids.png>''
- [34] J.C.Slonczewski and P.R.Weiss, *Phys. Rev.*, **109** 272 (1958).
- [35] G.W.Semenoff, *Phys. Rev. Lett.*, **53**, pp2449-52 (1984).
- [36] F.D.M.Haldane, *Phys. Rev. Lett.*, **61**, pp2015-18 (1988).

- [37] M.I.Katsnelson and K.S.Novoselov, *Solid State Communications*, (2007).
- [38] S.V.Vonsovsky and M.I.Katsnelson, *Springer, Berlin*, **4.6.6**, (1989).
- [39] M.I.Katsnelson, K.S.Novoselov and A.K.Geim, *Nature Physics*, **2**, pp620-25 (2006).
- [40] M.I.Katsnelson, *Eur. Phys. J. B*, **51**, pp157-160 (2006).
- [41] V.P.Gusynin and S.G.Sharapov, *Phys. Rev. B*, **71**, (2005).
- [42] V.P.Gusynin and S.G.Sharapov, *cond-mat*, **0506575**.
- [43] N.M.R.Peres *et al*, *cond-mat*, **0506709**.
- [44] T.Zheng and T.Ando, *Phys. Rev. B*, **65**, (2002).
- [45] S.A.Mikhailov and K.Ziegler, *Phys. Rev. Lett.*, **99**, (2004).
- [46] S.A.Mikhailov and K.Ziegler, *J. Phys. Cond. Mat.*, **20**, (2008).
- [47] S.A.Mikhailov, *Physica E*, **40** 7, p2629 (2007).
- [48] S.Adam *et al*, *PNAS*, **104** 47, pp18392-97 (2007).
- [49] M.Trushin and J.Schliemann, *Phys. Rev. Lett.*, **99**, (2007).
- [50] Y.W.Tan *et al*, *Phys. Rev. Lett.*, **99**, (2007).

-
- [51] C.W.J.Beenakker, *Mod. Phys. Rev.*, **80**, (2008).
- [52] E.H.Cannon *et al*, *Phys. Rev. Lett* **85** 6, (2000).
- [53] M.T.Greenaway, "*Single particle and collective dynamics in periodic potentials*", University of Nottingham, (2010).
- [54] D.Hardwick, "*Quantum and semiclassical calculations of electron transport through a stochastic system*", University of Nottingham, (2007).
- [55] S.Naylor, "*Stochastic dynamics in periodic potentials*", University of Nottingham, (2006).
- [56] Y.Wu *et al*, *ACS Nano.*, **2012**, 6 (3), pp 2610-2616, (2012).